UNIVERSITY OF SOUTHAMPTON

FACULTY OF ENGINEERING, SCIENCE & MATHEMATICS

School of Chemistry

EMITFSI - an Ionic Liquid Electrolyte for Lithium Batteries

by

Yasuaki Wakizaka

Thesis submitted for the degree of Doctor of Philosophy

November 2007

UNIVERSITY OF SOUTHAMPTON

ABSTRACT

FACULTY OF ENGINEERING, SCIENCE & MATHEMATICS
SCHOOL OF CHEMISTRY

Doctor of Philosophy

EMITFSI – AN IONIC LIQUID ELECTROLYTE FOR LITHIUM BATTERIES

by Yasuaki Wakizaka

The ionic liquid, 1-Ethyl-3-methylimidazolium bis- (trifluoromethylsulfonyl)-imide (EMITFSI) was studied as an electrolyte for rechargeable lithium batteries. This work focused on two main topics: cathodic stability and lithium ion transport.

The ionic liquid was synthesised and purified until Br < 40 wtppm, H_2O < 2 ppm. Effects of water on the cathodic stability limit were studied using a platinum microdisc electrode and a gold microdisc electrode array. The response of the cathodic current on the water concentration suggests catalytic decomposition of EMI^+ with moisture. The cathodic potential limit shifted negative with addition of lithium salt, especially on a nickel microelectrode, so that deposition and stripping current for lithium was observed. This is attributed to the formation of a solid electrolyte interface (SEI). Evidence for the formation of a SEI was also found from cyclic voltammograms and impedance spectra for lithium metal electrodes as well as open circuit cell potentials.

Addition of LiTFSI to EMITFSI resulted in a decrease in the conductivity (e.g., from 10.5 to 5.6 mS cm^{-1} for 0.47 mol dm^{-3}) and the lithium ion diffusion coefficient was found to be 1.2 x 10^{-7} cm^2 s^{-1} for 0.47 mol dm^{-3} added Li salt. The transference number for lithium ions) in LiTFSI / EMITFSI was found to be proportional to the concentration of the lithium salt. The measured value of 0.04 for 0.47 mol dm^{-3} is significantly higher than that of $LiBF_4$ / $EMIBF_4$ at the same concentration and temperature. This may be explained with two factors; the differences in size and dissociation level of the anions.

The charge / discharge rate performance of $LiFePO_4$ carbon composite electrodes with various thicknesses in different concentrations of LiTFSI / EMITFSI electrolytes was studied using 3-electrode cells. At fast charge or discharge rates, discharge capacities were approximately inversely proportional to C-rate, suggesting that the capacities were controlled by lithium ion diffusion in the pores of the composite electrode. Differences in rate performance were found between charge and discharge and for different concentrations of lithium salt in the ionic liquid. Two models are proposed to explain above phenomena; a transmission circuit to represent electrolyte resistance, and a salt depletion model simplified by the assumption of a compact discharge front.

An optimised cell was designed and constructed according to the above findings, using a 14 μm $LiFePO_4$ positive electrode, 0.47 mol dm^{-3} LiTFSI / EMITFSI and a lithium negative electrode. The cell gave a discharge capacity of more than 100 mAh g^{-1} over 850 cycles.

Table of Contents

Acknowledgements

I would like to thank who helped me with my work. Firstly, Professor John Owen has been giving me brilliant experimental ideas, great suggestions, and interpretations for experimental results. He, moreover, kindly corrected my English. I also would like to thank Dr. Guy Denuault who gave me important comments on my every quarterly report.

Furthermore, I really appreciate the help of members of the Owen Group. I couldn't have survived without Mr Mathew Roberts's help about life in England. Dr Girts Vitins showed me practice of lithium batteries and gave me excellent theoretical background. Dr. Thierry Le Gall provided much advice on every experiment with organic compounds. I also thank Mr Ken Reinman who gave me suggestion about general electrochemistry. Both Mr Philip Johns and Miss Hannah Alcock kindly helped me lots with English.

Table of Abbreviations

EMITFSI	1-ethyl-3-methylimidazolium bis(trifluoromethanesulfonyl)imide
LiTFSI	lithium bis(trifluoromethanesulfonyl)imide
EMIBr	1-ethyl-3-methylimidazolium bromide
PC	propylene carbonate
EC	ethylene carbonate
VC	vinylene carbonate
EMC	ethylmethyl carbonate
DMC	dimethyl carbonate
CV	cyclic voltammograms
LSV	linear sweep voltammograms
OCV	open circuit voltage
wtppm	weight part per million

Chapter 1. Introduction

1. Introduction

1.1. Lithium rechargeable batteries

Lithium has the lowest molar mass and lowest electrochemical potential of all metals. Also Lithium is the element that makes the largest numbers of known insertion compounds. Taking those advantages, batteries with lithium and its compounds have been developed and commercialised through minor and major changes on their systems in their electrodes and electrolyte.

One of the first studies appeared in a PhD thesis by Harris 1958[1]. He reported that lithium was stable in some organic solvents, cyclic esters, and investigated the electrochemistry of lithium in mainly propylene carbonate.

In the 1980s, investigations were accelerated and brought many attempts to develop a rechargeable lithium battery. An effort was inhibited by difficulties recharging the metallic double-bladed lithium anode, which has a high energy density. The reactivity occasionally caused cell venting and flaming especially with high surface area electrodeposited lithium. In order to avoid a violent reaction between water and lithium, primary and secondary lithium batteries use non-aqueous electrolytes, which are inherently orders of magnitude less conductive than aqueous electrolyte. The reactions of the lithium electrode were studied extensively and the investigations included a number of strategies to modify the reactivity of the Li-solution interface and thus improve its utility and safety.

Regarding positive electrodes, a host structure led to the development of rechargeable batteries during late 1970s and 1980s using lithium insertion compounds. After the era of transition metal chalcogenides came the higher voltage metal oxide [2], $LiMO_2$ which is used as positive electrode of common commercialised lithium ion batteries. The concept of host material was also accepted at the negative electrode, thus eliminating the use of a metallic lithium anode[3]. Subsequently, lower potential lithium insertion electrode, LiC_6 was applied to lithium ion batteries by Dey et al in 1970 [4]. With two

insertion electrodes, the lithium ion batteries finally obtain the similar system as we know today and commercially released by Sony, in 1991.

The commercialised lithium (ion) battery is the most important development in portable energy storage for 100 years. It has the potential to combat global warming with an efficient energy management system, power implanted medical devices and a number of other applications. Particularly, demands on energy suppliers for mobile electric products are still growing. Although lithium batteries have already been used practically for years, many of the mechanisms used in them and other phenomena in them are unclear and controversial areas still remain. Moreover, some problems about safety have been found in these years.

1.2. Safety issue of the batteries

A lithium ion battery made by Sony exploded at a conference in Japan on 21 June, 2006[5]. The accident was broadcast widely on the internet, so that the company was forced to recall 9.6 million of batteries. The recall cost £215 million and was the biggest in the history of the consumer electronics industry at that time. It was reported that the batteries might have overheated because microscopic nickel particles became trapped inside them during production; accordingly the particles made a short-circuit. The batteries used cobalt oxide, which is a strong oxidant and can undergo thermal runaway: a process where once it reaches a certain temperature it begins to self heat. Moreover, a volatile and flammable organic solvent is contained in them; therefore, the mechanism possibly could continue until the batteries catches fire.

In July 2007, a 22-year old Chinese welder was killed after a mobile phone battery residing in his pocket exploded because of a high temperature from the working condition. The eruption broke a rib and drove the remnants of the pack into his heart [6].

In August 2007, Nokia also announced that a battery produced by Matsushita caused a minor property damage and the company has identified that in very rare cases the affected batteries could potentially experience over heating initiated by a short circuit while charging, causing the battery to be recalled [7]. In this case, Matsushita reported a

defect at the separator caused the short circuit and they recalled 46 million of batteries [8]. The cases of accidents were different in these cases; however, if non-flammable electrolytes had been used for the lithium batteries, the issue would not be a matter of safety.

1.3. Aims of the thesis

The low volatility and non-flammability of the ionic liquid EMITFSI (1-ethyl-3-methylimidazolium bis-(trifluoromethanesulfonyl)-imide) make it an ideal candidate as an electrolyte for lithium ion batteries since the fire accidents due to the batteries have been a serious concern for users and makers.

However, there are two main problems to use the ionic liquid as an electrolyte for lithium batteries. The first is its poor stability at negative potentials. The poor stability can be affected by impurities, such as moisture from atmosphere, lithium and bromide ions from the starting materials. Hence, the effects of impurities on the cathodic potential limit of the ionic liquid have been studied. Although only few solvents such as trialkylamines are thermodynamically stable at the potential of lithium deposition, they are still able to be used as the electrolyte for lithium batteries, due to the formation of a solid electrolyte interface. Therefore, a proper interface may be also formed at the surface of electrodes with the ionic liquid and the properties of the interface have been studied.

The second problem is lithium ion transfer in the ionic liquid. The conductivity, 11 mS cm^{-1}, is acceptably high but low transference numbers for the lithium ion are a matter for concern. Therefore, work includes a detailed study of the lithium ion mobility in the ionic liquid as a function of lithium salt concentration and temperature. The effects of the mobility on the charge / discharge rates in composite electrodes with EMITFSI have been further investigated.

The final aim of this study is to demonstrate a lithium rechargeable battery containing the ionic liquid, achieving many charge / discharge cycles. A preliminary study for the cell with a polymer electrolyte plasticised by the ionic liquid will be also shown.

1.4. Ionic Liquids

1.4.1. General properties

Ionic liquids have aroused interest as new electrolytes for lithium batteries due their interesting properties listed below [9,10,11,12];

1) They are non-flammable and have a negligible vapour pressure at room temperature. The risk of burning and/or explosion of a misused battery is significantly reduced; the safety of the battery is strongly improved.
2) They are stable and liquid in a wide temperature range. The battery can be used more wide temperature range, even under harsh condition, such as in bonnets of cars.
3) Some ionic liquids have been reported to have a wide electrochemical stability range, allowing the use of high potential material as positive electrodes.
4) A high conductivity has been reported for some ionic liquids

1.4.2. EMI-TFSI

Ionic liquids based on 1-ethyl-3-methylimidazolium (EMI) and, particularly, the bis(trifluoromethanesulfonyl)imide (EMITFSI) salts, have several desirable properties such as: hydrophobicity, relatively low viscosity and higher conductivity than other ionic liquids. However, poor electrochemical stability at cathodic potentials currently prevents reversible lithium deposition. Similarly, on a graphite surface, imidazolium cations tend to be reduced at the electrode/electrolyte interface before lithium insertion occurs. However this is true for many organic solvents; with some exception such as solutions containing ethylene carbonate (EC). On the other hand, under well dehydrated conditions, successful charge/discharge was described up to 100 cycles, with a lithium metallic anode. [13]. The latter study was the only successful result found in the literature, and the study was limited to slow cell cycling rates such as C/8. The present work aims to derive a with deeper understanding of the electrolyte with respect to its cathodic

stability, transport properties and how these factors will affect the performance of cells under a variety of operating conditions.

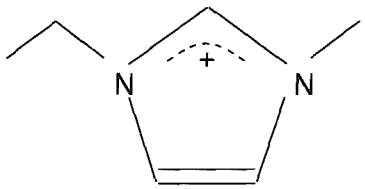

EMI^+
1-ethyl-3-methylimidazolium

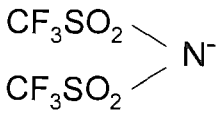

$TFSI^-$
bis(trifluoromethanesulfonyl)imide

Fig.1.1 EMI-TFSI

1.4.3. Other ionic liquids

Ionic liquids with tetraalkyl ammonium, pyrrolidinium and piperidinium cations, such as TMHA-TFSI (trimethylhexylammonium bis-(trifluoromethanesulfonyl)-imide)[14] and PP13-TFSI (N-methyl-N-propylpiperidinium bis-(trifluoromethanesulfonyl) -imide) [15] have been reported to have a wider electrochemical stable potential range than EMITFSI and a negative limit of almost 0 V *vs* Li^+/Li. Li deposition was observed in some of cases without the use of additives. For commercial applications, lithium metal is, however, not advantageous. The problem associated to it is its potential hazard which is due to the high reactivity of its surface, above all at elevated temperatures. These ionic liquids also need the addition of additives such as organic carbonates to form the lithium intercalated graphite electrochemically.

One exception of lithium intercalation into graphite without any additives is the system of ionic liquids based on aluminium chloride. These are, however, difficult to prepare and strongly moisture-sensitive due to $AlCl_3$ [16,17,18,19]. Studies concerning lithium intercalation into graphite in these ionic liquids are so far quite preliminary. Optimization of these ionic liquid systems and the electrolyte additives has not yet been subject to thorough investigation.

1.5. Important properties of lithium battery electrolytes

1.5.1. Ionic conductivity and diffusivity

Liquid electrolytes commonly used in ambient-temperature rechargeable lithium and/or lithium-ion batteries comprise solutions of lithium salts in non-aqueous organic solvents, such as mixtures of ethylene carbonate EC, propylene carbonate PC, and tetrahydrofuran THF, 2-methyltetrahydrofuran 2- MeTHF. Given that these have ionic conductivities in the range 10^{-3} to 10^{-2} S cm^{-1}, alternative electrolytes, such as ionic liquids or polymers, are expected to have conductivities approaching or beyond 10^{-3} S cm^{-1} at ambient temperature.

1.5.1.1. Diffusion coefficient and conductivity

The concept of mobility arose from the observation that small particles, including ions and molecules, move at a constant velocity in a fluid in response to an applied gradient of potential energy. The rate and direction of movement is described by the following equation which defines the mobility:

$$v_i = b_i\left(\frac{d\mu_i}{dx}\right) \qquad \text{eq.1.1}$$

Where v_i is the velocity, b_i is the mobility and μ_i is the chemical potential of particle i in the fluid.

Multiplying the equation by concentration we obtain the flux, J_i.

$$J_i = c_i v_i = c_i b_i\left(\frac{d\mu_i}{dx}\right) \qquad \text{eq.1.2}$$

If the flux is due to diffusion, Fick's first law can be derived by expressing the chemical potential in terms of the concentration:

$$\mu_i = \mu_0 + RT \ln a \qquad \text{eq.1.3}$$

$$\frac{d\mu_i}{dx} = RT\left(\frac{d\ln a_i}{dx}\right) = RT\left(\frac{d\ln a_i}{d\ln c_i}\right)\left(\frac{d\ln c_i}{dx}\right) = \frac{RT}{c_i}\left(\frac{d\ln a_i}{d\ln c_i}\right)\left(\frac{dc_i}{dx}\right) \qquad \text{eq.1.4}$$

From eq.1.2 and eq.1.4

$$J_i = RTb_i\left(\frac{d\ln a_i}{d\ln c_i}\right)\left(\frac{dc_i}{dx}\right) \qquad \text{eq.1.5}$$

On the other hand, Chemical diffusion coefficient $\tilde{D}$ is defined by Fick's first law

$$J_i = \tilde{D}\frac{dc_i}{dx}$$

Therefore,

$$\tilde{D} = RTb_i\left(\frac{d\ln a_i}{d\ln c_i}\right) \quad \text{or} \quad \left(b = \frac{RT}{\tilde{D}}RT\left(\frac{d\ln a_i}{d\ln c_i}\right) \right) \qquad \text{eq.1.6}$$

In ideal solutions, $d\ln a/d\ln c = 1$ and $\tilde{D}$ becomes equal to the diffusivity or self diffusion coefficient D

$$D = RTb_i \qquad \text{eq.1.7}$$

For a flux due to electrical migration, we can use the electrical mobility, u_i

$$u_i = zFb_i \qquad \text{eq.1.8}$$

where z is the charge number, F is the Faraday constant.

$$v_i = u_i\left(\frac{d\phi}{dx}\right) \qquad \text{eq.1.9}$$

where $d\phi/dx$ is the electrical potential field.

This leads to a current density, j

$$j_i = Fu_ic_i\left(\frac{d\phi}{dx}\right) \qquad \text{eq.1.10}$$

An expression for conductivity σ is (from eq.1.8 and eq.1.10)

$$\sigma_i = j_i\left(\frac{d\phi}{dx}\right) = z_iFu_ic_i = z^2F^2b_ic_i \qquad \text{eq.1.11}$$

Therefore,

$$\sigma_i = \frac{z^2 F^2 D c_i}{RT} \qquad \text{eq.1.12}$$

This is the Nernst-Einstein equation which relates the partial conductivity of a single ion to its self-diffusion coefficient.

The total conductivity σ arises from the combined current from all ions and the ratio σ_i/σ is called the transport number.

1.5.1.2. Walden's rule

The earliest and simplest rule for the relationship between conductivity and electrolyte viscosity was reported in 1893 by Walden [27].

$$Const = \sigma\eta \qquad \text{eq.1.13}$$

Where σ is the conductivity of the solution and η is the viscosity of the solution.

1.5.1.3. Stokes Einstein equation

The Stokes Einstein equation relates the mobility of ions to the frictional force and the mobility to the diffusion coefficient.

$$D = \frac{k_B T}{6\pi\eta r} \qquad \text{eq.1.14}$$

Where D is the diffusion constant, k_B is the Bolzmann's hydrodynamic constant, T is the temperature, η is the dynamic viscosity of the fluid and r is the radius of the particle.

This equation with the Nernst-Einstein equation explains the Walden's rule and evaluates the constant. Therefore, the general mobility applies to diffusion, conduction and viscosity.

1.5.1.4. VTF equation

Vogel-Tamman-Fulcher (VTF) equation [28] was originally proposed to describe the property of super cooled liquid electrolyte

$$\eta^{-1}(T) = A \exp[- B / R (T - T_0)] \qquad \text{eq.1.15}$$

Where A,B,T_0 are fitting parameters, A is assumed to be proportional to the number of carrier ions and B has dimensions of energy.

Armand et al. [29] observed that the conductivity collected over a wide temperature range on amorphous polymer salt complexes is accurately represented by the equation. To explain conductive properties of ionic liquids, the equation is also applied to the studies [30].

1.5.2. Transference number

Usually, conductivity measurements are implemented to estimate the transport properties of an electrolyte at first; however, they provide information only on the total transport of charge. Especially for ionic liquids as a lithium battery electrolyte, this information is not as important as the transport of lithium ions, which have an essential role in the lithium batteries.

It is desirable that the transference number of lithium ions approaches unity in an electrolyte system. Many existing electrolyte systems, either liquid or polymeric, have transference numbers less than 0.5, *i.e.*, no more than half of the ionic charge is transported *via* the movement of lithium ions [20,21,22]. A large transference number can reduce concentration polarization of electrolytes during charge–discharge steps, and thus produce higher power density.

1.5.3. Definition of transference number

A transference number refers to the proportion of the current carried by a constituent of the salt [31]. For example, MX salt which is composed of the basic constituents M^+ and

X^-, then when dissolved in the solvent the X^- constituent exists as an X^- species but also as part of the $[M_2X]^+$ cation and $[MX_2]^-$ anion triples. The constituent is also present in the $[MX]_0$ ion pair; however, this does not influence the transference number. The X^- constituent is transported by all three charged species. They in turn carry the charge on the constituent around the cell. For the passage of one Faraday of charge across the cell, the net number of Faradays carried by the X^- constituent is its transference number. The sum of the cation and anion transference number is equal to unity. For a salt dissociating fully into species M^+ and X^-, the transference numbers for cations and anions are identical to transport numbers.

1.5.4. Transference number in various electrolytes

Several techniques can be applied to measure transference numbers as shown in Table 1.1. Theoretically, for a fully dissociated salt, all measurements show the same value for the same electrochemical system; however, values obtained for the transference numbers by different methods are generally different. For example, $LiCF_3SO_3$ in polyethylene oxide values vary from 0.34 to 0.7 as shown in Table 1.2. Bruce reported [32] the differences tend to be significant between values from different groups as shown in Table 1.1.

Table 1.1 Method for the measurement of transport in electrolytes [32]

I	II	III
Hittorf Tubandt	radiotracer	dc polarisation
Concentration cell	PFG NMR	ac method
Centrifugal	Cottrell	

Table 1.2 Variation of transference numbers for $LiCF_3SO_3$ in polyethylene oxide

Concentration cell	PFG-NMR	dc polarisation
0.7 [33]	0.34 [34]	0.46 [35]

$LiPF_6$ in organic solvents is one of the most common electrolytes, which is used for lithium ion batteries. Valoen reviewed [36] and measured the transference number for lithium ions; the value is reported as ca. 0.4 and not significantly varied with the concentration of the salt and different solvents.

For ionic liquid electrolyte, Hayamizu *et al.* have reported that the transference number is varied with lithium salt concentration. [30] For 0.25 mol dm^{-3} $LiBF_4$ / $EMIF_4$ the value was obtained as 0.01 and at the highest concentration, 1.5 mol dm^{-3}, 0.045, which is still notably small compared to those in polymer or organic solvents.

1.6. Solid Electrolyte Interface in lithium batteries

1.6.1. General aspects

The surface films on both electrodes in lithium batteries have important roles in their stability and their operation. This discussion about SEI lays the groundwork for the rest of the investigations of materials in lithium batteries, such as anode cathode solvent, salt or polymer electrolyte into perspective with regard to their reactivity and passivation, reaction kinetics and cell operation. Development of new electrolytes, anodes and cathodes must take this reactivity into account, otherwise some new and promising electrode materials may continuously lose capacity due to their inability of passivating with the electrolyte employed. The discussion of reactivity among materials behaviour of electrodes, solute and salts, will decide whether we can apply a new possible material such as ionic liquids for electrolyte of lithium batteries.

Therefore, a key factor to improve characters of lithium (ion) batteries is the nature of the interfaces between electrolytes and electrodes. Especially to use ionic liquids, which are thermodynamically less stable at negative potentials, we must investigate the interface. Various kinds of interfaces in lithium (ion) batteries have been classified according to their materials as follows.

1.6.2. SEI on positive electrodes

Interfaces (SEI) at carbon negative electrodes have been deeply investigated. On the other hand those on positive electrodes and on alternative negative (non-carbon) electrodes have not been investigated so extensively. About 10% of investigations into the Solid Electrolyte Interface cover interfaces between positive electrodes and electrolytes. Several positive electrodes have been studied as detailed below.

1.6.2.1. $LiCoO_2$

This material is most commonly used as positive electrodes at lithium ion batteries. During first charge-discharge cycle, some compounds are found on surface of $LiCoO_2$, which are supposed to be formed with decomposition of the electrolyte at the interface. Those films were examined by SEM[37], XAFS, TOF-SIMS and XPS[38], and it was shown that the structure and composition both depended on the electrolytes used. The films were characterised with the above equipment, hence some general models were proposed to reflect characteristics of the various systems[39]. However, it was not obvious whether those films have a good effect on lithium (ion) batteries or not. Some beneficial effects have been suggested. First, the film could help to preserve the morphology of $LiCoO_2$ while lithium insertion and extraction occurs. Second, blocking electron transfer while allowing Li^+ to pass, can prevent electrolyte decomposition during battery cycling. More investigations of SEI on $LiCoO_2$ are needed and the investigations could encourage the discovery of appropriate solvents and electrolytes.

1.6.2.2. $LiMn_2O_4$, $LiNiO_2$, $LiFePO_4$ and their mixture compounds

There have been several other investigations on positive electrode materials. Each of these materials and their mixtures thereof are commonly used as positive electrode next to $LiCoO_2$ and the SEIs at these materials have been studied. The Films on manganese and nickel compounds were analyzed using FT-IR[40,41], Raman[40,41], XPS[39,41] and SEM[37,41]. In these cases, the films structure and compounds depended on solvents, salt and additives. Wursig *et al.*[37] investigated the SEI at $LiNi_2O_4$, $LiMn_2O_4$ and $LiCoO_2$

with many kinds of electrolytes using FE-SEM. The SEIs were observed at all investigated oxides with PC-based electrolytes but most obvious in the case of $LiNiO_2$. Only thin films were detected in the case of electrolytes containing EC and DMC as solvent. VC addition strongly affects the shape of SEI and gave porous structures.

Jang *et al.*[42], showed one of the reason for the poor cyclability of $LiMn_2O_4$ compared with $LiCoO_2$. That was the difference of the surface chemistry of the electrode-electrolyte interface. In the case of Mn compounds, Mn was lost from the spinel electrode surface into the electrolyte *via* the disproportionation of trivalent Mn (Hunter reaction). Edstrom *et al.*[39] proposed a structure and the composition of the films on $LiMn_2O_4$, $LiCoO_2$, $LiNi_{0.8}Co_{0.2}O_2$ and $LiFePO_4$ using information from XPS depth profile. The organic species formed on the electrode were more or less similar, varying more in their amount than in their precise chemical compounds.

However, the ionic compounds formed there were more dependent on the electrode material type. For example, in the case of carbon coated $LiFePO_4$, no solvent decomposition products (*e.g.*. polycarbonate, semicarbonate and Li_2CO_3) were detected on the surface, indicating that the phosphate group did not react with the solvents. Hence $LiFePO_4$ was different from the other cathode products that they examined.

Aurbach *et al.*[40], demonstrated that the electrochemical behaviour of $LiNiO_2$ and $LiMn_2O_4$ strongly depended on their surface chemistry in solutions, using electrolyte of EC:DMC (1:1 by volume) with three different salts respectively: $LiAsF_6$ 1M, $LiPF_6$ 1M, LiTFSI 0.75M. It was shown that the active cathode material particles were initially covered with pristine surface films comprised of Li_2CO_3 as the major component. During charging, this film was replaced by solution-related surface species comprised of varieties of compounds, including ROLi, $ROCO_2$-Li, polycarbonates and electrolyte reduction products which could include LiF, containing As-F, P-F and sulphuric compounds as corresponding with kinds of salt. Although they could not prove the exact mechanisms for the formation of these surface films, they assumed that one source could be possible nucleophilic reactions of the $LiMO_x$ species with the alkyl carbonate solvents which are strong electrophiles. They also supposed the acidic contaminants in

the electrolyte might play an important role in the formation of the films since the contaminants would act to catalyse the polymerisation of the alkyl carbonate at the SEI. Impedance of $LiNiO_2$ electrodes was higher than that of $LiMn_2O_4$ electrodes, therefore they presumed the former material was more reactive, nucleophilic and basic. The impedance of the electrodes in the three salts solutions was measured and that in $LiAsF_6$ was the lowest and it seemed that the surface chemistry in the solution was the most stable.

1.6.3. Negative Electrodes

1.6.3.1. Lithium

Lithium metal is suitable for negative electrode material because of its very low electrochemical potential and high specific charge, however it typically deposits as dendrites during cycles. Dendrites are covered with SEIs, therefore problems on the SEI must be solved before practical usage. Many investigations have been undertaken, yet a revolutionary solution like the ethylene carbonate for the graphite anode, has not been discovered.

SEIs at lithium metal have two layers, the inorganic layer and the organic layer[49] and the composition is depending on the electrolyte[44]. The inorganic one is formed on lithium metal directly and it is thinner, more compact and better at lithium ion transfer than the organic one, which is formed on the inorganic one. The organic layer is more porous and the surfaces of dendrites with SEI are not uniform; therefore, the surface of electrode tends to partly inactive. Hence, the battery using lithium metal as negative electrode has difficulties with charge and discharge cycle. Many kinds of examinations were made focusing on improving the character of the SEI at lithium metal. These approaches were examined by screening liquid electrolyte[44], polymer electrolyte[45], scavengers[46], surface treatment reagents [47], lithium-ion conductive membrane on metal electrode [48] and the other additives.

1.6.3.2. Carbon

Since the SEI is believed to be essential to reversible lithium insertion into carbon negative electrodes, most of the studies on the SEI are those of its formation. Negative electrodes are of several types including lithium metal intercalation compounds and alloys.

Some theories of lithium insertion into carbon materials have appeared recently. Many carbon samples used for practical lithium ion batteries commonly contain both graphitic and non-graphitic structures. Hence it is a little difficult to distinguish clearly whether the influence is from graphitic or non-graphitic nature. However, the mechanism of lithium ion insertion into the carbon and SEI strongly depend on their structure, graphitic or non-graphitic. In the case of graphite, lithium graphite intercalation compound, Li_xC_6 were formed. However, commercial products have already achieved theoretical capacities, 339 Ah/kg[49] and there is little space for improvement of this system. Therefore emphasis of investigations shall be placed on the other SEIs. If the electrolyte is intercalated with the lithium ion into the graphite, an expansion of the gap between layers happens, causing the deterioration of the graphite. As a result, this decreases charge capacities. EC based electrolyte[50] prevented that since decomposed compounds of the electrolyte formed a film at SEI, which prevented the penetration of the solvent and preserved the gap between layers of graphite, not to be expanded.

In the case of non-graphite, [43] much higher capacities have been obtained with hard carbons made by calcinations of organic polymers at temperatures near 1000 ℃. These form of carbons consist of predominantly single-layer carbon sheets linked together in a random fashion. The voids located between the carbon sheets are sites where lithium ions can be adsorbed. This implies that specific capacity (per unit mass) of these materials could ultimately be twice that of graphite. However, the capacity depends on the sizes and shapes of these voids and pores. If the pore sizes are large enough that organic electrolytes can easily access these pores and form SEI layer on the entire surface (internal and external) of the carbon sheets and direct surface adsorption of lithium ions is prevented.

1.6.3.3. Sn compounds

As Sn compounds[51,52] have very high capacities, nearly 1000 mA g^{-1}, attention has focussed on these as negative electrode of lithium ion battery. Choi *et al.*[53], investigated SEI at Sn-Li alloy electrode using TEM, SEM, FT-IR. They suggested the formation of the SEI had a similar mechanism to that of graphite electrode, even though a volume of the compounds changes much more when lithium ions are inserted. The thickness of the SEI layer was larger than that on carbon black. Generally SEI layers are non-crystalline and homogeneous but the SEI at Sn alloy electrode has a poorly aligned structure and is inhomogeneous. They did not find out if this SEI has good influence on charge and discharge cycle or not. Cu-plated Ni_3Sn_4[54] and SnSbC[55] were studied as negative electrode material. SEI formations were suggested in both of the cases since large initial irreversible capacities were lost.

1.6.3.4. Si, and the other compounds

In Si compounds like porous silicon[56], nanocomposite of Si/C[57] and graphite-silicon mixtures encapsulated in a Si-O network[58] were investigated as the negative electrode material for lithium ion battery. These compounds have large specific capacities; however decrease of capacities during charge/discharge cycles is a serious problem, which is same in the case of Sn compounds. SEIs at these compounds have not been mentioned yet. For graphite, Si compounds have potential as a high performance anode when combined with appropriate SEI.

Zn_4Sb_3[59] and Co_3O_4[60] etc. were recently examined as negative electrode, however the SEIs have not yet been researched.

1.6.4. SEI with ionic liquids

Formations of SEIs using ionic liquid as solvent have been investigated for several systems of salt. Generally, to insert lithium ion to graphite, ethylene carbonate (EC) or vinylene carbonate (VC) must be added to ionic liquid [61,62,,63,64]. In this case the SEI

formed at the negative carbon electrode is supposed to be similar to that with common organic electrolytes, such as EC/DMC. On the other hand, the SEI on positive electrodes, such as $LiCoO_2$, has not been investigated so intensively. Cathodic decomposition mechanism on $LiCoO_2$ was studied using EMITFSI 1M $LiPF_6$ as electrolyte. It was shown that VC addition was detrimental to charge-discharge cycle. Holzapfel *et al.*[62,64] successfully presented the lithium intercalation into an artificial graphite in 1 M solution of $LiPF_6$ in 1-ethyl-3-methyl imidazolium bis(trifluoromethylsulfonyl) imide (EMI-TFSI) containing 5 wt% of VC as an additive. A reversible capacity around 350 mAh/g was obtained with a satisfactory cyclability. The approach of stabilising lithiated graphite electrodes in lithium-ion batteries by the admixture of small amounts of highly active film forming additives is interesting because it offers a protection against the continuing reduction of the electrolyte itself.

1.6.5. SEI with polymer electrolytes

As mentioned previously, the cyclability of lithium batteries with metallic lithium negative electrode depends on the passivating layer[65] and dendrite formed at the interface. A polymer or gel component in the electrolyte has been known to give two possible factors for the negative electrode/electrolyte interface. Firstly, it may suppress dendrite growth[65]. These electrolytes do not have pores which ordinary separators have, therefore restrict the dendrite growth more effectively than separators. Secondly, the polymer can reduce the reactivity by immobilising reaction products at the interface with carbonaceous anodes and lithium[66,67]. Zhang *et al.*[68] studied the electrochemical impedance on the first lithium intercalation kinetics of mesocarbon microbeads (MCMB) as the lithium intercalation electrode in a gel electrolyte. They found the resistance of SEI film formed in the electrolyte was relatively higher compared with that in liquid electrolytes.

A few investigations have been made for interfaces on the positive electrodes with polymer electrolytes. Uchimoto *et al.*[69] studied on the charge-transfer reaction rate following lithium intercalation/de-intercalation at the $LiMn_2O_4$ cathode/polymer

electrolyte interface. The reaction rate was evaluated with the surface-conductivity of the charge-transfer reaction calculated by impedance measurements and it was found that the charge-transfer reaction rate at the interface was inversely proportional to the viscosity.

1.7. Experimental techniques used in experiments

1.7.1. Microelectrode technique

Microelectrode technique has become widespread in the past 30 years and is one of the most actively pursued fields in electroanalytical chemistry[70]. The diameter of electrode should be less than 50 μm, to make a characteristic surface dimension smaller than the thickness of the diffusion layer on the timescale of the electrochemical experiment [71]. Mainly, four advantages have been found to use the technique for this investigation on the ionic liquid:

a) Size of the electrode:

The amount of sample can be reduced [72] because of the size, so that a fresh sample always can be used and an expensive ionic liquid sample is not wasted.

b) Mass transport regime:

From Fick's second law, a current transient for a spherical electrode is given by

$$I_L = \frac{nFAD^{1/2}c^{\infty}}{\pi^{1/2}t^{1/2}} + \frac{nFADc^{\infty}}{r} \qquad \text{eq.1.16}$$

When r is small enough and t is large enough, current flow is dominated by the steady state (the latter term); therefore, the diffusion coefficient can be determined. For ionic liquids, diffusion coefficients have been reported to be small; hence long time is necessary to reach the steady state. However, the time can be reduced by a microelectrode.

c) Insignificant double layer charge:

The surface area of a microelectrode is small, so that a full capacitance of double layer is diminished.

d) Decreased IR drop:

Ionic liquids have larger resistance than aqueous electrolytes; therefore, the voltammograms can be disturbed by an IR drop. However, total current flow between the working electrode and the counter electrode can be diminished and the potential field between the working electrode and the reference electrode is not affected significantly.

1.7.2. Restricted diffusion method[74] – Potential relaxation

This method was developed by Onsager *et al.* in 1945[73]. The diffusion length was restricted using a cell of finite geometry. They monitored the decay of concentration gradients by conductivity measurements with time. Ma *et al.* devised the technique to measure the diffusion coefficient of sodium ions in polymer electrolyte [76]. In their case, potential relaxation after a constant current pulse was monitored.

For a dilute, constant-property solution, Fick's second law in one dimension takes the form

$$\frac{\partial c}{\partial t} = D\frac{\partial^2 c}{\partial y^2} \qquad \text{eq.1.17}$$

and the boundary condition for a rectangular cell, which have electrode distance ℓ

$$\frac{\partial c}{\partial y} = 0 \qquad \text{at } y = 0 \text{ and } y = \ell \qquad \text{eq.1.18}$$

Standard separation of variables applied to eq.1.17 leads to

$$c = c^{\infty} + \sum_{n=1}^{\infty} A_n \exp\left(-\frac{n^2\pi^2 Dt}{\ell^2}\right)\cos\frac{n\pi y}{\ell} \qquad \text{eq.1.19}$$

where D is the diffusion coefficient, y is the distance from the bottom of the cell, t is time, and c^{∞} is the uniform solute concentration at infinite time. The A_n depend on the initial distribution of solute in the cell.

This series converges with time and gives the following relationship after sufficient time[75]

$$\ln(\Delta c) = -\frac{Dt\pi^2}{\ell^2} + \ln B \qquad \text{eq.1.20}$$

For a small value of $\Delta\phi$,

$$\Delta\phi = \Delta c \cdot \frac{\partial E}{\partial c} \qquad \text{eq.1.21}$$

From the Nernst equation

$$\Delta\phi = \frac{RT}{F}\left(\frac{\Delta c}{c}\right) \qquad \text{eq.1.22}$$

$$\ln\Delta\phi = \ln\frac{RT}{F} - \ln c + \ln\Delta c \qquad \text{eq.1.23}$$

From eq.1.20 and eq.1.23,

$$\ln\Delta\phi = \ln\frac{RT}{F} - \ln c + \ln B - \left(\frac{\pi}{L}\right)^2 Dt \qquad \text{eq.1.24}$$

Hence

$$\frac{\ln(\Delta\phi)}{t} = -\frac{D\pi^2}{\ell^2} + B' \qquad \text{eq.1.25}$$

Therefore, diffusion coefficients are evaluated from a relaxation potential profile between non-blocking electrodes.[76]

1.8. Following chapters

It is suggested that two main problems prevent the use of ionic liquid as an electrolyte for lithium batteries. The first is its poor stability at negative potentials. The poor stability can be affected by impurities and additives. The effects will be shown in Chapter 2. The second problem is lithium ion transport in the ionic liquid. The conductivity is high but low transference numbers for the lithium ion can be a problem. Therefore, these transport properties of lithium ions in the ionic liquid will be studied in Chapter 3. The effects of these properties on discharge capacities under variable charge / discharge rates in composite electrodes with EMITFSI have been further investigated with a proposed model in Chapter 4. Studies on many charge / discharge cycles using an optimised cell containing the ionic liquid will be shown in Chapter 5, which include an investigation on the cell with a polymer electrolyte plasticised by the ionic liquid.

References

1. W.S. Harris, *Ph.D. Thesis UCRL-8381*, University of California, Berkeley (1958).

2. K. Mizunuma, P.C. Jones, P.J. Wiseman and J.B. Goodenough, *Mat. Rds. Bull.*, **15**, 783 (1980).

3. M. Lazzari and B. Scrosati, *J. Electrochem. Soc.*, **127**, 773 (1980).

4. A. N. Dey and B. P. Sullivan, *J. Electrochem. Soc.*, 117, 222 (1970).

5. 15/8/2006, *Times*

6. http://www.engadget.com/2007/07/05/chinese-welder-killed-by-exploding-cellphone-battery/

7. http://batteryreplacement.nokia.com/batteryreplacement/en/

8. 14/8/2007, *Times*

9. L.A. Blanchard, D. Hancu, E.J. Beckman and J.F. Brennecke, *Nature*, **399**, 28 (1999).

10. J.G. Huddleston, H.D. Willauer, R.P. Swatloski, A.E. Visser and R.D. Rogers, *Chem. Comm.*, 1765 (1998),

11. T. Welton, *Chem Rev.*, **99**, 2071 (1999).

12. W. Xu and C.A. Angell, *Science*, **302**, 422 (2003).

13. S. Seki, Y. Kobayashi, H. Miyashiro, Y. Ohno, A. Usami, Y. Mita, N. Kihara, M. Watanabe and N. Terada, *J. Phys. Chem. B*, **110**, 10228 (2006).

14. H. Zheng, H. Zhang, Y. Fu, T. Abe and Z. Ogumi, *J. Phys. Chem. B*, **109**, 13676 (2005).

15. H. Sakaebe and H. Matsumoto, *Electrochem. Comm.*, **5**, 594 (2003).

16. R.T. Carlin, J. Fuller and M. Hedenskoog, *J. Electrochem. Soc.*, **141**, L21 (1994).

17. J. Fuller, R.A. Osteryoung and R.T. Carlin, *J. Electrochem. Soc.*, **142**, 3632 (1995).

18. N. Koura, K. Etoh, Y. Idemoto and F. Matsumoto, *Chem. Lett.* 1320 (2001).

19. D.L. Boxall and R.A. Osteryoung, *J. Electrochem. Soc.*, **149**, E185 (2002).

20. J. Evans, C.A. Vincent, P.G. Bruce, *Polymer*, **28**, 2324 (1987).

21. P.G. Bruce, M.T. Hardgrave, C.A. Vincent, *Solid State Ionics.*, **53**, 1087 (1992).

22. I.I. Olsen, R. Koksbang, E. Skou, *Electrochim. Acta*, **40**, 1701 (1995)

23. A. Mittasch, *Adv. Catal.* **2**, 81 (1950).

24. E. Reddington, A. Sapienza, B. Gurau, R. Viswanathan, S. Sarangapani, E.S. Smotkin and T.E. Mallouk, *Science*, **280**, 1735 (1998).

25. M.D. Fleicshauer, T.D. Hatchard, G.P. Rockwell, J.M. Topple, S. Trussler, S.K. Jericho, M.H. Jericho and J. R. Dahn, *J. Electrochem. Soc.*, **150**, A1465 (2003).

26. A.D. Spong, G. Vitins and J.R. Owen, *J. Electrochem. Soc.*, **152**, A2376 (2005).

27. P. Walden, *Chem. Ber.* **26**, 210, (1893),

28. H. Vogel, *Phys. A.*, **22**, 645 (1921)

29. M. Armand, J.M. Chabagno, M.J. Duclot, in *Fast Ion Transport in Solids*, eds. P. Vashishita, J.N. Mundy, G.K. Shenoy , Elsevier, New York, 1979, p. 131

30. K. Hayamizu, Y. Aihara, H. Nakagawa, T. Nukuda and W. S. Price, *J. Phys. Chem. B*, **108**, 19527 (2004).

31. M. Spiro, in Physical Methods of Chemistry, *Electrochemical. Methods*. eds. A. WEISSBERGER. and B. W. ROSSITER. Parts IIA Ch.IV Wiley-Interscience, New York, (1971)

32. P.G. Bruce, *Solid State Electrochemistry*, Cambridge University Press p154. (1995)

33. W. C. Yu,W. W. Callahan, D. F. Dwiggins, H. M. Fisher, M. W. Geiger, W. J. Schell; North Am. Membrane Soc. Conf. Breckenridge, Co. (1994)

34. D. Zuckerbrod, R.T. Giovannoni, K.R. Grossman, in: *Proceedings of the 34th International Power Sources Symposium*, NT, 1990, p. 172.

35. R. Spotnitz, M. Ferebee, Rcallahan, K. Nguyen, W.-C. Yu, C. Dwiggins, H. Fisher, D. Hoffman, in: *Proceedings of the Twelfth International Seminar on Primary and Secondary Battery Technology and Applications*, Florida, 1995.

36. O. Valoen and J. N. Reimers, *J. Electrochem. Soc.*, **152**, A882 (2005).

37. A. Wursig, H. Buqa, M. Holzapfel, F. Krumeich and P. Novak, *Electrochem. Solid State Lett.*, **8**, A34 (2005).

38. H. Ota, T. Akai, H. Namita, S. Yamaguchi and M. Nomura, *J. Power Sources*, **119**, 567 (2003).

39. K. Edstrom, T. Gustafsson and J.O. Thomas, *Electrochim. Acta*, **50**, 397 (2004).

40. D. Aurbach, K. Gamolsky, B. Markovsky, G. Salitra, Y. Gofer, U. Heider, R. Oesten, M. Schmidt, *J. Electrochem. Soc.* **147**, 1322 (2000).

41. T. Eriksson, A.M. Andersson, A.G. Bishop, C. Gejke, T. Gustafsson and J. O. Thomas, *J. Electrochem. Soc.*, **149**, A69 (2002).

42. D.H. Jang and S.M. Oh, *J. Electrochem. Soc.*, **144**, 3342 (1997).

43. J.S. Xue and J.R. Dahn, *J. Electrochem. Soc.*, **142**, 3668 (1995).

44. E. Peled, D. Golodnitsky and G. Ardel, *J. Electrochem. Soc.*, **144**, L208 (1997).

45. T. Matsui and K. Takeyama, *Electrochim. Acta*, **40**, 2165 (1995).

46. M. Hughes, N. A. Hampson and S. A. G. R. Karunathilaka, *J. Power Sources*, **12** 83 (1984)

47. E. Eweka, J. R. Owen and A. Ritchie, *J. Power Sources*, **65**, 247 (1997).

48. C. Liebenow and K. Luhder, *J. Appl. Electrochem.*, **26**, 689 (1996).

49. M. Winter, O Juegen, O. Besenhard, M. E. Spahr and P. Novak, *Adv. Mater.* **10**, 725 (1998).

50. R. Fong, U. Vonsacken and J.R. Dahn, *J. Electrochem. Soc.*, **137**, 2009 (1990).

51. I.A. Courtney and J.R. Dahn, *J. Electrochem. Soc.*, **144**, 2045 (1997).

52. A.H. Whitehead, J.M. Elliott and J.R. Owen, *J. Power Sources*, **82**, 33 (1999).

53. W. Choi, J. Y. Lee, B.H. Jung and H.S. Lim, *J. Power Sources*, **136**, 154 (2004).

54. X.Q. Cheng and P.F. Shi, *J. Alloy. Compd.*, **391**, 241 (2005).

55. X.D. Wu, Z.X. Wang, L.Q. Chen and X.J. Huang, *Carbon*, **42**, 1965 (2004).

56. H.C. Shin, J.A. Corno, J.L. Gole and M.L. Liu, *J. Power Sources*, **139**, 314 (2005).

57. I.S. Kim and P. N. Kumta, *J. Power Sources*, **136**, 145 (2004).

58. S.B. Ng, J.Y. Lee and Z.L. Liu, *J. Power Sources*, **94**, 63 (2001).

59. X.B. Zhao and G.S. Cao, *Electrochim. Acta*, **46**, 891 (2001).

60. Y.M. Kang, M.S. Song, J.H. Kim, H.S. Kim, M.S. Park, J.Y. Lee, H.K. Liu and S.X. Dou, *Electrochim. Acta*, **50**, 3667 (2005).

61. T. Sato, T. Maruo, S. Marukane and K. Takagi, *J. Power Sources*, **138**, 253 (2004).

62. M. Holzapfel, C. Jost and P. Novak, *Chem. Commun.*, 2098 (2004).

63. Y. Katayama, M. Yukumoto, T. Miura, *Electrochem. Solid State Lett.*, **6** A96 (2003).

64. M. Holzapfel, C. Jost, A. Prodi-Schwab, F. Krumeich, A. Wursig, H. Buqa and P. Novak, *Carbon*, **43**, 1488 (2005).

65. A, Teyssot, M. Rosso, R. Bouchet, S. Lascaud, *Solid State Ionics*, **177**, 141 (2006).

66. S. Megahed, B. Scrosati, *Interface*, **4**, 34 (1995).

67. J.Y. Song, Y.Y. Wang and C.C. Wan, *J Power Sources*, 77, 183 (1999).

68. S. Zhang and P. Shi, *Electrochim. Acta* **49**, 1475 (2004).

69. Y. Uchimoto, K. Anezawa, T. Furushita, M. Wakihara, I. Taniguchi, *Solid State Ionics*, **176**, 2377 (2005)

70. A. M. Bond, *Analyst*, 119, R1 (1994)

71. M. D. Imisides, R. John, G. G. Wallace, *CHEMTECH*, **26**, 19 (1996)

72. R. M. Wightman, *Anal. Chem.*, **53**, 125A (1981)

73. L. Onsager, *Annals New York Acad. Sci.*, **46**, 267 ()1945

74. J. Newman and T. W. Chapman, *AIChE J.* **19**, 343 (1973)

75. H. K. Shepard, T. J. Wilson, T. P. Moody, J. O. Wooll and T. M. Laue, *Eur. Biophys. J.*, **25**, 481 (1997).

76. Y. P. Ma, M. Doyle, T. F. Fuller, M. M. Doeff, L. C. Dejonghe and J. Newman, *J. Electrochem. Soc.*, **142**, 1859 (1995).

Chapter 2. Stability of the Ionic Liquid

2.1. Introduction

Although it is often claimed that one of the advantages of ionic liquids is to be stable at a wide range of potentials, the property of stability is not general for all ionic liquids. Certain cations, EMI^+ and anions, $TFSI^-$ were chosen for this thesis and several studies have been reported about the instability of EMITFSI, especially at negative potentials. The potential range which we can use as an electrolyte without decomposition is called "Potential window". However, there are mainly two reasons which cause uncertainty of the values. Firstly, the decomposition current increases exponentially as a function of overpotential according to Butler-Volmer equation; therefore the decomposition potential limit is an arbitrary definition. Secondly, the reaction mechanism may be influenced by a catalytic mechanism depending on the material of the electrodes and impurities. In this investigation, various impurities, such as water from the atmosphere or bromine from the synthesis reagent, were introduced into the electrolyte and their effects were studied quantitatively.

2.2. Experimental

2.2.1. Synthesis

a) Synthesis of EMITFSI and LiTFSI/EMITFSI

1-Ethyl-3-methylimidazolium bis-(trifluoromethylsulfonyl)-imide (EMITFSI) was synthesised by an ion exchange reaction, according to the procedure described in earlier publications[1]. 0.128 mol of 1-ethyl-3-methylimidazolium bromide (EMIBr purum, ≥97.0% Fluka) and an equivalent amount of bis-(trifluoromethylsulfonyl)-imide lithium salt (LiTFSI puriss., ≥99.0% Fluka) were respectively dissolved in some aliquots of water then mixed to give a milky liquid. The mixture was then heated at 80 °C for 8 hours and formed two liquid layers. The EMITFSI was extracted into dichloromethane and washed with its own volume of water three times. After removing the water layer, it

was dried for 48 hours at 10 Pa, 120 °C with a vacuum ssytem, shown in Fig. 2.1. To obtain a highly dehydrated condition, a trap filled with molecular sieves and a cold trap cooled with liquid nitrogen were applied. The distance, *d* between the container .and the trap was minimised. The synthesised EMITFSI was checked for its impurities using Electrospray Ionisation Mass Spectra (ESI-MS), 1H-NMR, 13C-NMR and Karl Fischer measurement and stored in a glove box.

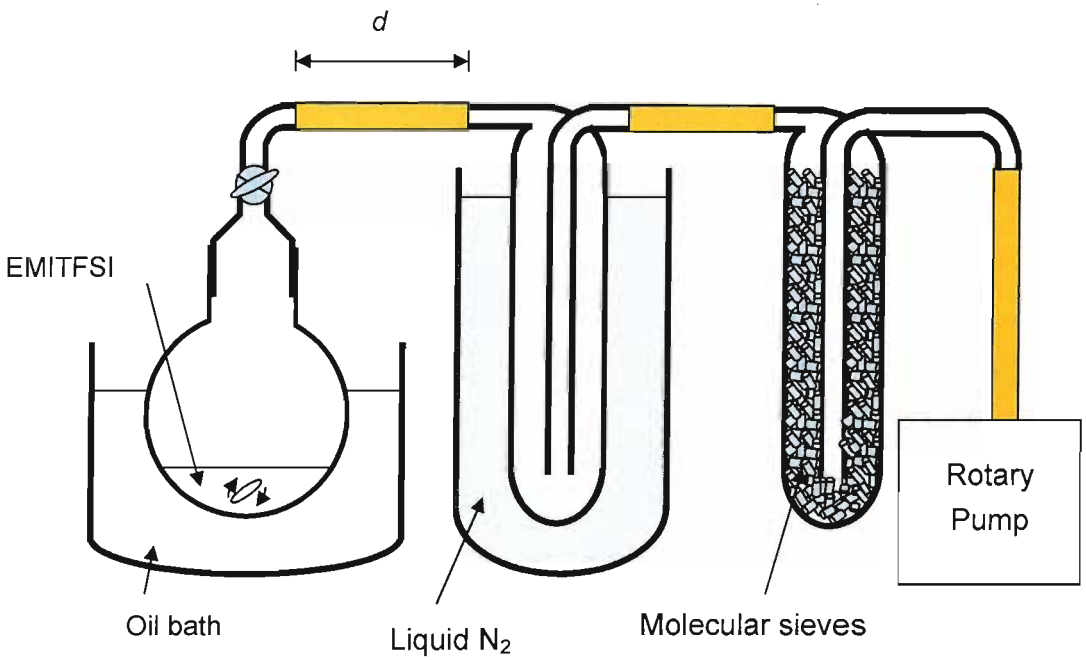

Fig. 2.1 Schematic illustration of the vacuum system, used for the dehydration of the ionic liquid.

After LiTFSI was dissolved to EMITFSI at a concentration of 0.9 mol kg^{-1} (=1.4 mol dm^{-3}), the whole liquid was dehydrated by the same method and diluted to appropriate concentrations before use.

b) Synthesis of a 5:1 mixture of $Li_1Mn_2O_4$ and $Li_2Mn_2O_4$

LiI and $LiMn_2O_4$ (Carus) dehydrated at 0.2 mbar, 120 °C for 15 hours were ground at the stoichiometric ratio Li:Mn = 1.2:2 in the glove box, placed into a Buchi furnace tube

and evacuated to 0.2 mbar. After being sealed, the container was heated at 180 °C for 15 hours to perform the reaction ($LiMn_2O_4 + LiI \rightarrow Li_2Mn_2O_4 + 1/2\ I_2$, the $Li_{1.2}Mn_2O_4$. The product, (a 5:1 mixture of $LiMn_2O_4 + Li_2Mn_2O_4$) was washed with acetonitrile and dried under vacuum. The electrochemical potential was measured against a Li metal electrode in 1 mol dm^{-3} EC/DME electrolyte and found to be 2.90 V.

The following data were mainly measured with this reference electrode but the potential was converted and shown as potential vs Li, to make them comparable with other investigations for lithium batteries.

2.2.2. Electrochemical measurement

a) Microelectrode cell

A two electrode cell was used for electrochemical measurement to investigate the effect of impurities. A platinum microelectrode (diameter = 25 μm) was used as a working electrode, as shown in Fig. 2.2. A $Li_{1.2}Mn_2O_4$ carbon composite electrode, containing 70 wt% of active material, 20 wt% of acetylene black and 10 wt% of PVdF, was dip-coated on a Pt wire and immersed in 10 mmol dm^{-3} LiTFSI / EMITFSI solution. This was separated from the electrolyte with a glass frit and was used as the common reference and counter electrode.

The dry electrolytes for study of LiBr addition were prepared in the glove box ($O_2 < 0.1$ ppm, $H_2O < 0.1$ ppm) and the cell was assembled. Those for the water addition studies were prepared by mixing in septum sealed vials, which were transferred to the glove box and syringed into the cell after assembly. Linear sweep voltammetry or cyclic voltammetry was performed on the platinum microdisc. Both anodic behaviour and cathodic behaviour were investigated. To study the effect of O_2, a cell was assembled in the glove box and dehydrated O_2 was bubbled into the electrolyte for 10 minutes.

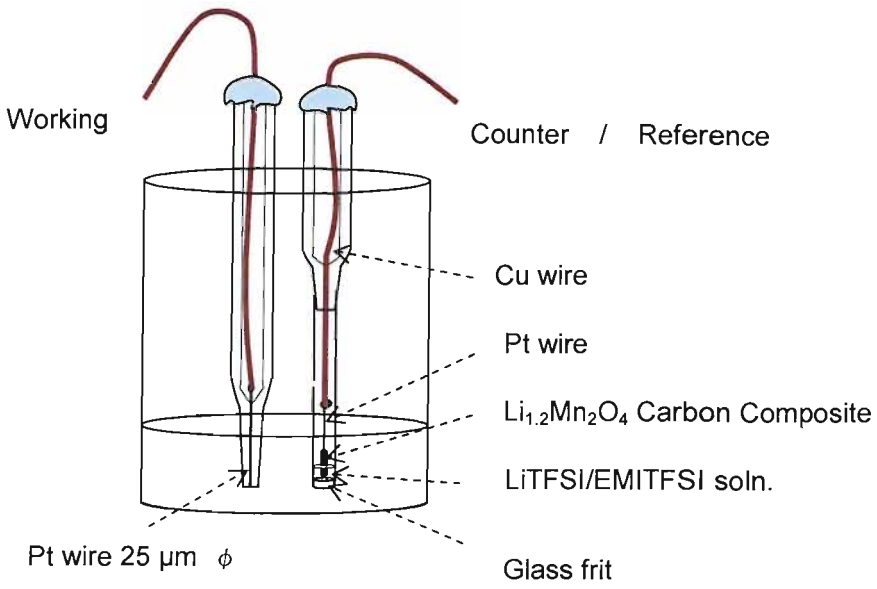

Fig. 2.2 Schematic illustration of the glass cell, used for measurement to investigate the effect of additives and lithium insertion study on a tin electrode

b) Gold microelectrode array

An array of gold microelectrodes with 14 channels was made from an integrated circuit[2] (Motorola SN74LS00N) by polishing carefully, as shown in Fig. 2.3. To prevent exposure of metal parts, such as legs and leads, the electrode unit was covered with an epoxy resin (Struers) except for the surface of the micro gold electrodes.

A three electrode cell was used to determine the surface areas of the microelectrodes. A Pt mesh electrode was used for the counter electrode and a saturated calomel electrode was used for the reference electrode. The areas were determined from the diffusion limited currents of cyclic voltammograms in an aqueous solution including 250 mmol dm^{-3} of $K_4Fe(CN)_6$, 25 mmol dm^{-3} of $K_3Fe(CN)_6$ and 500 mmol dm^{-3} of KCl. The diffusion coefficient has been published as 7.1 x 10^{-6} cm^2 s^{-1}[13]. The effective radii were calculated and varied from 19.1 μm up to 29.2 μm. The variation implies some gold

wires are not built vertically in the integrated circuit chip. The ratio of the maximum and minimum radiuses 0.64, may represent the tilt $\cos^{-1}\theta$, where θ is 49°.

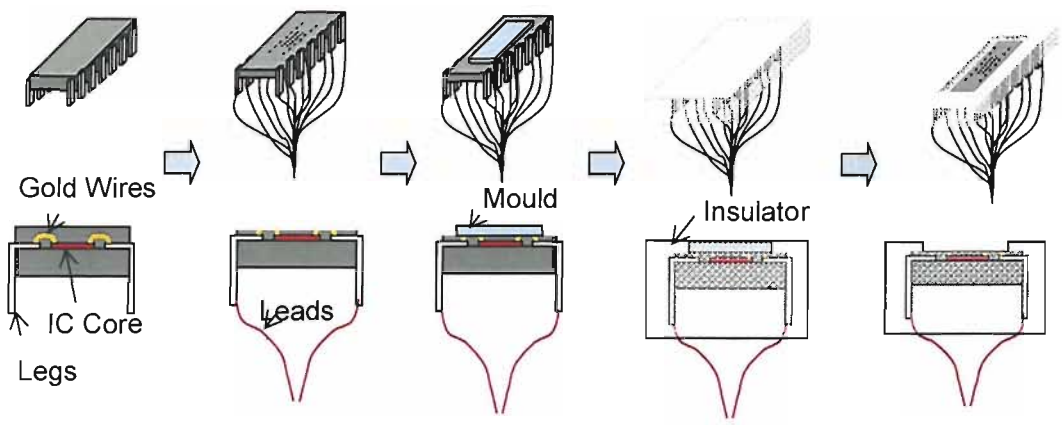

Fig. 2.3 a schematic showing the assembly of an array of gold microelectrodes

Table 2.1 Radii of gold microelectrodes in the array

Ch.	1	2	3	4	5	6	7	8	9	10	11	12	13	14
radius /μm	26.7	26.7	24.1	21.4	24.1	29.2	28.5	19.1	25.3	23.5	20.2	24.5	25.9	18.8

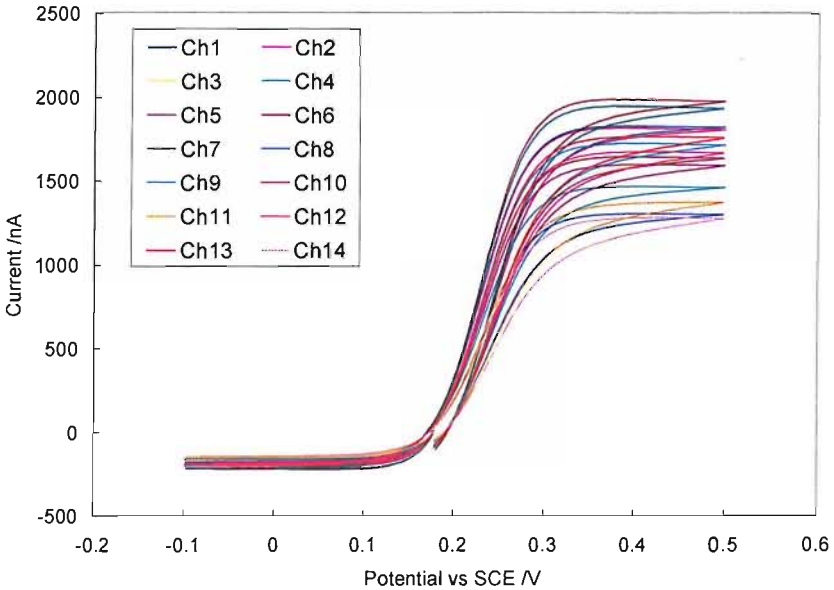

Fig. 2.4 Cyclic voltammograms of 250 mmol dm^{-3} $K_4Fe(CN)_6$, 25 mmol dm^{-3} $K_3Fe(CN)_6$ and 500 mmol dm^{-3} KCl solution on the microelectrode array.

c) Lithium electrode cell

To study deposition and stripping of lithium and a solid electrolyte interface in LiTFSI/EMITFSI, a lithium metal electrode was used as working electrode. A poly-ethylene film was used to insulate the material and limit the surface area to 1 mm^2.A large piece of lithium was used for the counter electrode and $Li_{1.2}Mn_2O_4$ carbon composite electrode was used as the reference electrode. An impedance measurement and cyclic voltammetries were implemented.

2.2.3. Lithium insertion into a tin and a graphite electrode

A three electrode cell was used for deposition of tin on a Pt microdisc and a Cu disc. 0.6 mol dm^{-3} sulphuric acid solutions containing a tin sulphate at 0.15 mol dm^{-3} were used as an electroplating bath. A Pt mesh electrode was used as the counter electrode and a mercurous sulphate electrode in saturated K_2SO_4 solution was used as the reference electrode. The electrodepositon was performed under constant current at 10 mA cm^{-2} and the amount of a deposit by electro-stripping in the same cell was estimated, except for using 0.1 mol dm^{-3} hydrochloric acid as electrolyte.

For investigation of the lithium insertion behaviour on a deposited tin and graphite, a three electrode cell was used. For the graphite electrode, a 1 mm graphite rod (Goodfellow) was sealed into a glass tube using epoxy resin (Struers). The same reference electrode was used for the investigation of lithium insertion and extraction as shown in Fig. 2.3 and a $LiFePO_4$ carbon composite electrode (active material : acetylene black : PTFE = 75 : 15 : 5) used as the counter electrode to allow a large current flow in the electrochemical system. Cyclic voltammetry and constant current charge and discharge were performed on the working electrode and the lithium insertion capacity was evaluated with the integration of the current.

2.3. Results and discussion

2.3.2. Neat EMITFSI

The investigations start with the neat ionic liquid without lithium salts, which corresponds to a solvent of electrolytes for lithium ion batteries. The ionic liquid can be used for capacitors although the use was not studied specially in this thesis.

2.3.2.1. Impurities

The yield of EMITFSI was 90 % of its expected amount. The 1H and 13C NMR of the EMITFSI showed no peaks other than those which can be attributed to functional groups in EMITFSI and water, which could have originated from the solvent used for measuring NMR, d-acetone.

Found M/Z	Species	Calculated M/Z	Intensity
111.0	EMI^+	111.1	100
112.1	EMI^+(^{13}C or ^{14}N Isotope)	112.1	20.9
502.2	$[EMI_2TFSI]^+$	502.1	10.6
503.3	$[EMI_2TFSI]^+$ (^{13}C or ^{14}N Isotope)	503.1	1.5

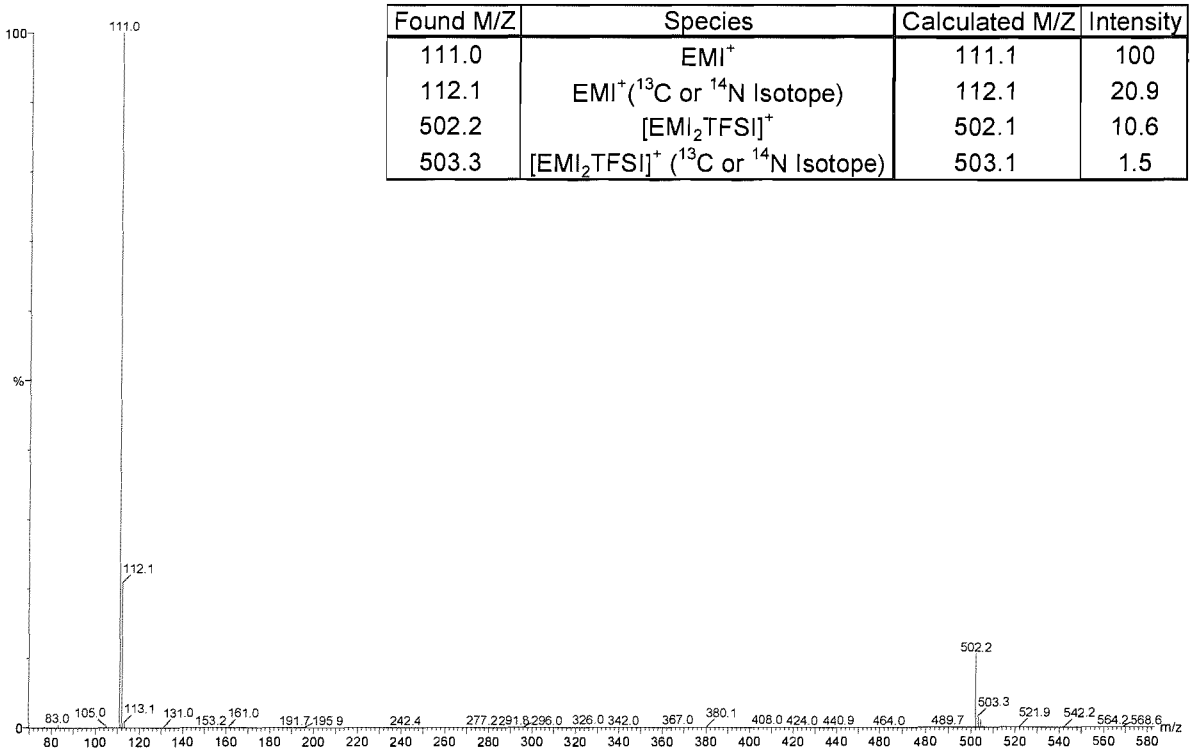

Fig. 2.5 Electrospray Ionisation Mass Spectra of the EMITFSI (cations)

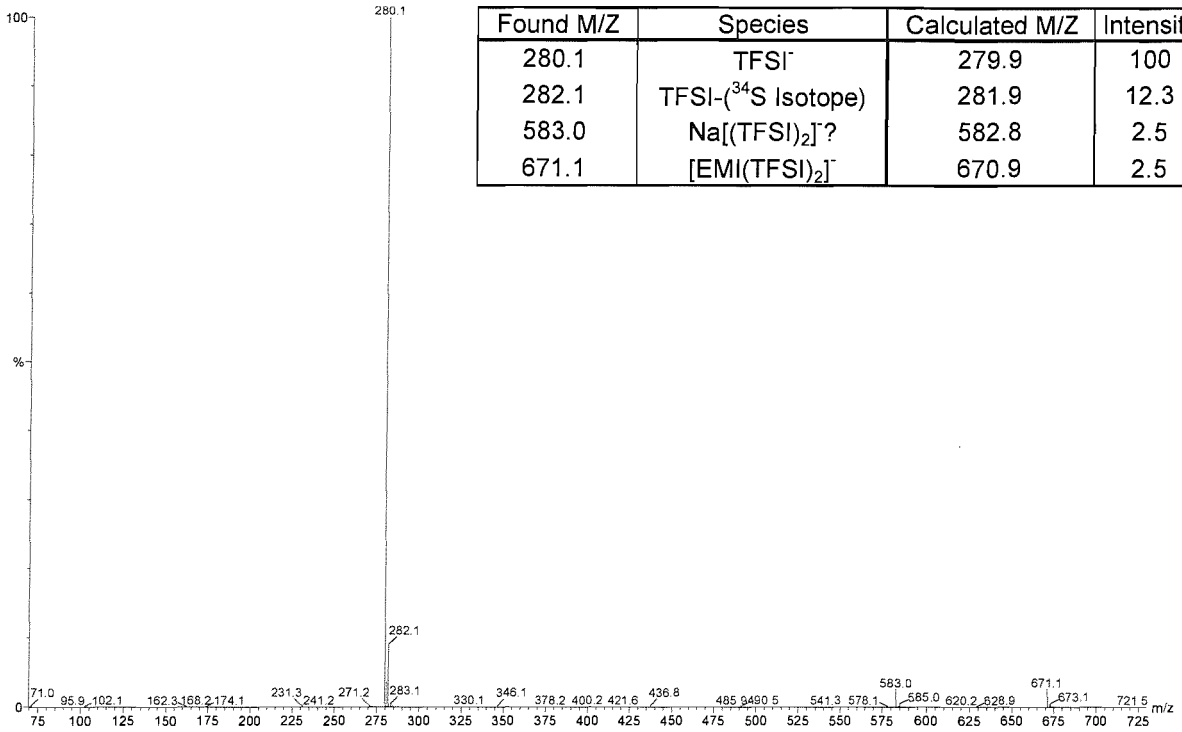

Found M/Z	Species	Calculated M/Z	Intensity
280.1	$TFSI^-$	279.9	100
282.1	TFSI-(^{34}S Isotope)	281.9	12.3
583.0	$Na[(TFSI)_2]^-$?	582.8	2.5
671.1	$[EMI(TFSI)_2]^-$	670.9	2.5

Fig. 2.6 Electrospray Ionisation Mass Spectra of the EMITFSI (anions)

The Electrospray Ionisation Mass Spectra (ESI-MS) of the EMITFSI is shown in Fig. 2.5 and Fig. 2.6. Large peaks were attributed to EMI^+ at 111.0 and TFSI- at 280.1. Minor side peaks at 112.1 and 282.1 are assumed to be isotopic effects. Remaining peaks are assigned in insets. The only impurity was $[Na(TFSI)_2]^-$ at 583.0, which may be contaminated from glassware because a high temperature was used to dehydrate the sample. Concentration of water in the ionic liquid determined by Karl Fischer measurement was less than 2.0 ppm.

2.3.2.2. Dehydration of EMITFSI

In the vacuum line, a few processes may limit the mass transportation of the moisture. The fraction of the solute (=moisture) is much smaller than the solvent; therefore the vapour pressure follows the Henry's Law when the gas/solution in the flask was equilibrated. The total vapour pressure was almost all from moisture because that of

ionic liquid was negligible [4]. The Henry's constant for water/EMITFSI has not been found but reported for water/1-butyl-3-methylimidazolium hexafluorophosphates [5]. The coefficients were extrapolated and $K_H = 6.6 \times 10^5$ [Pa] for 393 K was obtained. The vapour pressures, P_{water}[Pa] are related to moisture concentrations in the ionic liquid x [wtppm] in eq. 2.1.

$$P_{water} = 13\,x \qquad \text{eq. 2.1}$$

When the concentration of moisture is above 0.8 wtppm, the vapour pressure of the water, 11 Pa, is larger than the pressure of the vacuum system, 10 Pa; therefore the main factor of the mass transport is the difference of the pressures, following eq. 2.2.

$$Q = C\,\Delta P \qquad \text{eq. 2.2}$$

Where Q = the mass flow, C = the conductance and ΔP = the difference of pressures

Two types of flow, viscous and molecular states are known in vacuum systems. Tubes with a diameter of 8 mm were used for the dehydration and the flow was found to be in viscous state since Knudsen number was 0.8, according to eq. 2.3

$$K_n = \frac{\lambda}{L} = \frac{k_B T}{\sqrt{2}\pi\sigma^2 PL} \quad \left(\text{for air } K_n = \frac{0.68}{PL}\right) \qquad \text{eq. 2.3}$$

Where λ is the mean free path, T is the temperature, k_B is Boltzmann constant, P is total pressure, σ is the diameter of the molecule and L is diameter of the tube.

In the viscous flow, the conductance follows Poiseuille's law, eq. 2.4.

$$C = (\pi L^4 P)/(8\,\eta\, d) \qquad \text{eq. 2.4}$$

Where C is the conductance, L is the diameter of the tube, P is the total pressure, η is the viscosity of the gas (=1.8×10^{-5} [Pa s]) and d is the length of the tube.

For example, when the concentration of water in the ionic liquid was 1 ppm, P_{water} is 13 Pa and ΔP is 3 Pa. The flow rate of moisture via the tube is proportional to the concentration and calculated as 1×10^{-4} g/s from eq. 2.2 and eq. 2.4, which is very fast when we consider the amount of 1 ppm of water in 50 g of the ionic liquid. That

suggests the limitation is not in the tube as long as a pressure difference exists, but the diffusion of the moisture in the ionic liquid.

When the concentration is reduced to less than 0.7 ppm, the system lost the pressure difference because the vacuum pump can not reduce the pressure more. The main dynamics of the moisture flux changes to diffusion, which follows Fick's Law and much slower than a flow by pressure. The diffusion coefficient of air is a function of pressure [6] and the coefficient at different pressure follow eq. 2.5.

$$D_{P_1} = D_{P_0}\left(\frac{P_0}{P_1}\right)^{\frac{1}{3}} \qquad \text{eq. 2.5}$$

Where D_0= 0.20 $cm^2\ s^{-1}$ is the diffusion coefficient of air at 298 K in 10^5 Pa, P_0 =10^5 Pa and P_1 =10 Pa

Therefore, the diffusion coefficient in the tube is 4.3 $cm^2\ s^{-1}$ and the flux in the tube, 1.2 x 10^{-9} g s^{-1} is calculated from Fick's first law, shown in eq. 2.6. The equation was solved by a numerical analysis using Δt = 60 s and the results show the concentration of water can be decreased to undetectable level (<0.1 wtppm) in 25 hours (Fig. 2.7).

$$J = -D\ dc/dx \qquad \text{eq. 2.6}$$

Where J is the flux, D is the diffusion coefficient, dc is the difference of the concentration and dx is the distance

The calculation and results show ionic liquids can be dehydrated using this method, heat and vacuum. This is simple and supposed to be more efficient for industrial applications than distilling and adopting molecular sieves, which is used for ordinary volatile organic solvent.

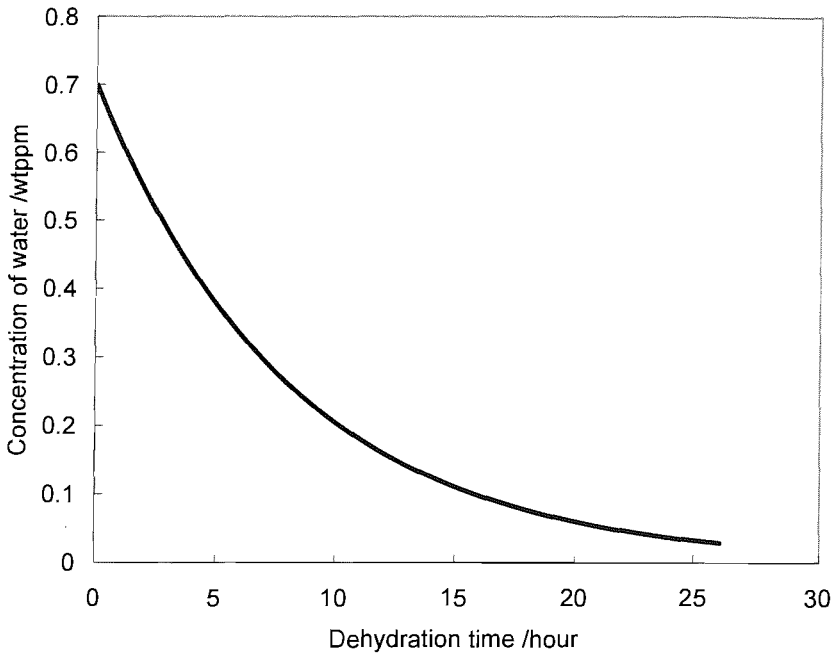

Fig. 2.7 Results of the numerical analysis of eq. 2.6

2.3.2.3. Voltammograms of EMITFSI

The cyclic voltammogram in synthesised EMITFSI on a platinum microdisc shows a wide stability with decomposition current less than 0.1 mA cm^{-2} between 1.1 V and 5.2 V *vs* Li. The cathodic potential limit is due to the decomposition of EMI cations because TFSI anions are known to be stable at less than 0 V [7]. No apparent electrochemical active impurity was detected in the range. A small anodic current was observed above 4.5 V, which may be due to an oxidation of the platinum; the standard electrode potential is 1.19 V *vs.* SHE, which is 4.23 *vs* Li. An opposite current corresponding to the reaction was not observed during the back potential sweep, suggesting oxidised platinum were passivated with the components of the ionic liquid. Other transition metals, such as copper were not appropriate to examine the stability of the electrolyte because they dissolved without forming passivation films at high potentials.

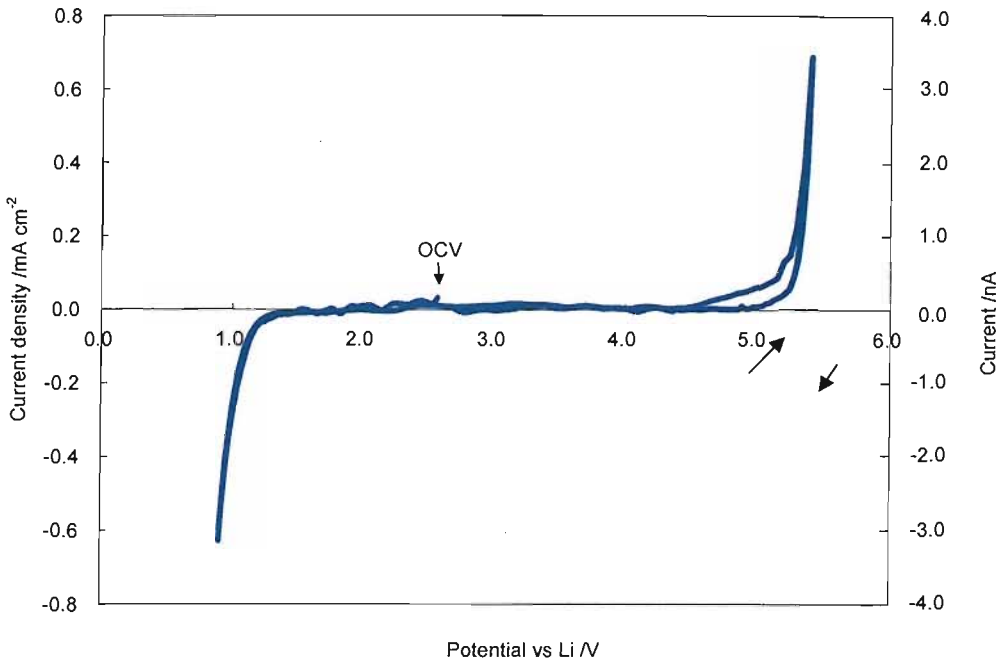

Fig. 2.8 Cyclic voltammogram of Pt microelectrode (diameter = 25 μm) in neat EMITFSI. The reference electrode was $Li_{1.2}Mn_2O_4$ in 10 mM LiTFSI / EMITFSI and the counter electrode was a Pt mesh. The scan rate was 5 mV s^{-1}.

The anodic potential limit, 5.2 V, suggests the chance of an application with higher potential electrode materials, *cf.* ordinary organic electrolytes which decompose around 5 V. The cathodic limit, 1.1 V, is far from the deposition potential of lithium. Therefore, the following investigations are mainly concerning the cathodic decomposition of EMITFSI.

The effects of different electrode materials on the cathodic limit are shown in Fig. 2.9 and the variation is more than 0.1 V between gold and platinum. Decomposition of EMI cations are known to start at the proton at the 2nd position in the imidazolium ring.[8] The results suggest the platinum may adsorb the proton more easily than the other metals and cause a catalytic decomposition of EMI cations.

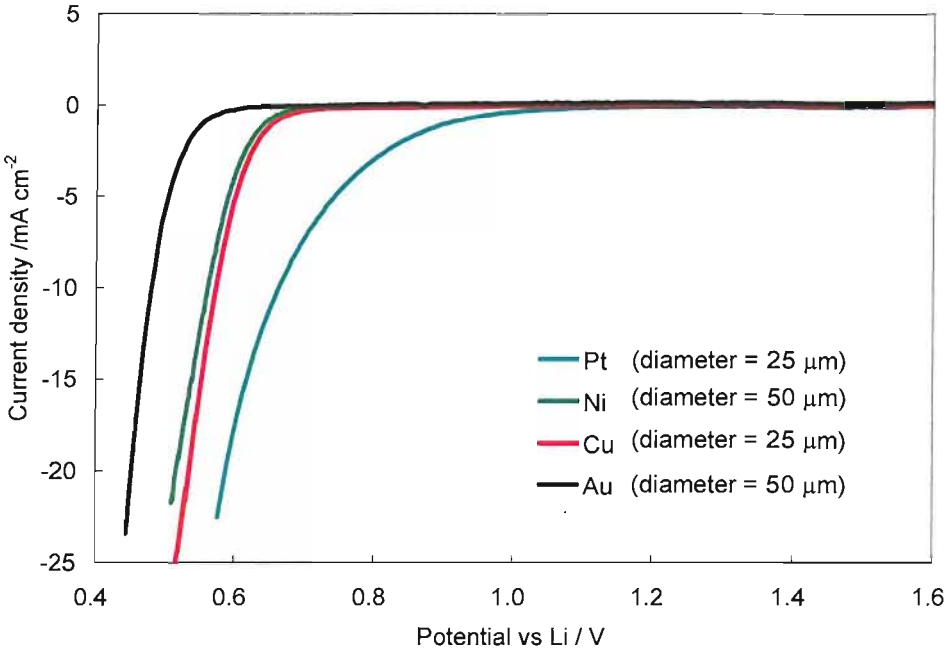

Fig. 2.9 Cathodic stabilities of EMITFSI on various metals. The reference electrode was $Li_{1.2}Mn_2O_4$ in 10 mM LiTFSI / EMITFSI and the counter electrode was a Pt mesh. The scan rate was 5 mV s^{-1}.

2.3.2.4. Oxidation of Br^-

Bromide is a common impurity from the synthesis residue. With LiBr addition, anodic currents were observed around 3.7 V *vs.* Li, 0.5 V lower than for aqueous LiBr. The difference of the potentials suggests a lower solvation energy of bromide anions in the ionic liquid than that of water. The first wave shown around 3.6 V in Fig. 2.10, indicates oxidation of Br^- to Br_3^-, and the second around 3.9 V is attributed to the production of dissolved bromine.

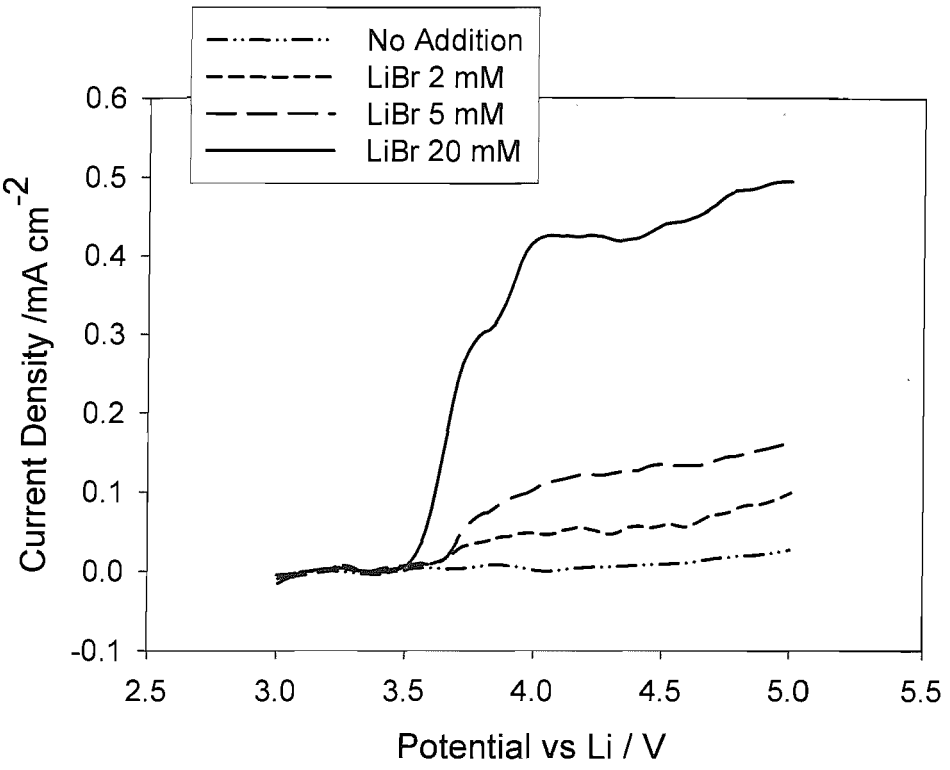

Fig. 2.10 Linear sweep voltammograms showing oxidation of Br^- in EMITFSI on Pt micro electrode (diameter = 25 μm). The scan rate was 5 mV s^{-1}.

Fig. 2.10 shows that anodic limiting current at 4.5 V *vs* Li depended on concentration of Br^- linearly and the gradient was $\Delta I/c = 2.2 \times 10^{-3}$ nA/wtppm = 1.17×10^{-4} A/(Br^- mol cm^{-3}). Therefore, diffusion coefficient D_{Br^-} in EMITFSI is evaluated as 2.3×10^{-7} cm^2 s^{-1}, following the eq. 2.8.

$$\Delta I = 4nFDca \qquad \text{eq. 2.7}$$

$$\text{Hence} \quad D_{Br^-} = \Delta I / (4nFca) \qquad \text{eq. 2.8}$$

Where ΔI is the limiting current, D_{Br^-} is the diffusion coefficient, c is the concentration of species and a is the radius of a microelectrode. No previous reports have been found concerning this system, although there are some reports in comparable systems. M.C. Buzzeo *et al.*[9] showed D_{O2} in EMITFSI = 2.7×10^{-6} cm^2 s^{-1} and Y. Katayama *et al.* [10] showed D_{Ag^+} in 1-ethyl-3-methyl- limidazolium tetrafluoroborate = 6.0×10^{-6} cm^2 s^{-1}. Then the diffusion coefficient evaluated in this experiment is significantly lower than

the values for above other species. This suggests that Br^- may exist principally as salt of a larger unit, *e.g.* EMI^+Br^- or $[EMI_2Br]^+$.

2.3.2.5. Estimation of Br concentration in synthesised EMITFSI

The synthesised EMITFSI is supposed to include remaining Br^-, which is from precursor material EMIBr. The concentration of Br^- in the raw EMITFSI was evaluated using the method of standard addition, as illustrated in Fig. 2.11. Extrapolation on to the horizontal axis shows that the Br^- concentration in the raw EMITFSI was less than 40 wtppm.

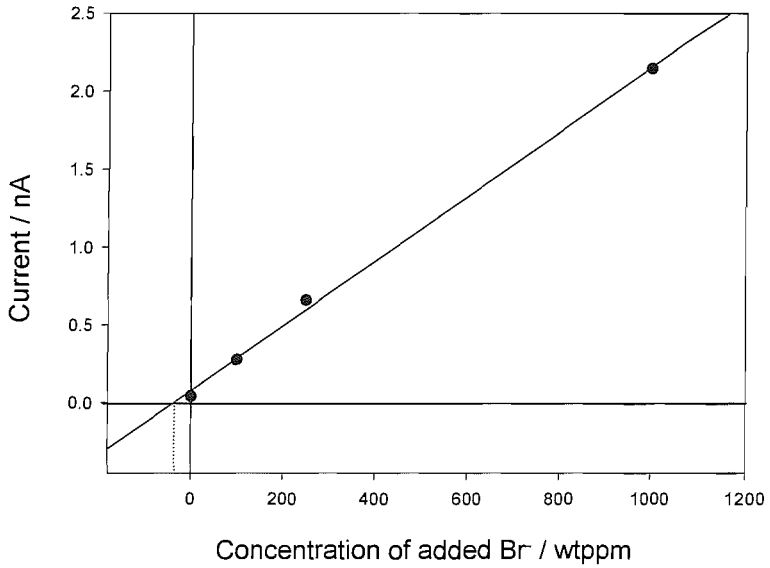

Fig. 2.11 Oxidation current at 4.5 V vs lithium of various concentrations of LiBr in EMITFSI

2.3.2.6. Influence of contaminants after the synthesis

Fig. 2.12 shows a comparison of two LSVs for a Pt microelectrode in a cell prepared in the glove box and sealed with a ground glass neck before removal. The first CV was taken immediately on removal and the second was taken after a day outside of the glove box. The result shows a small plateau with a half-wave potential of 1.9 V *vs* Li which can be attributed to an impurity. Assuming the impurity was not formed by an inherent

instability of the electrolyte, the signal must be due to ingress of either oxygen, water, or both. With an assumption that the reaction of the impurity was similar to oxygen in EMITFSI, the concentration is estimated to be 0.1 mmol dm^{-3} using eq. 2.7 and a diffusion coefficient of 7.6 x 10^{-6} cm^2 s^{-1} [9]. To identify the contaminants, water and oxygen were added into a new cell and their influence was measured as described below.

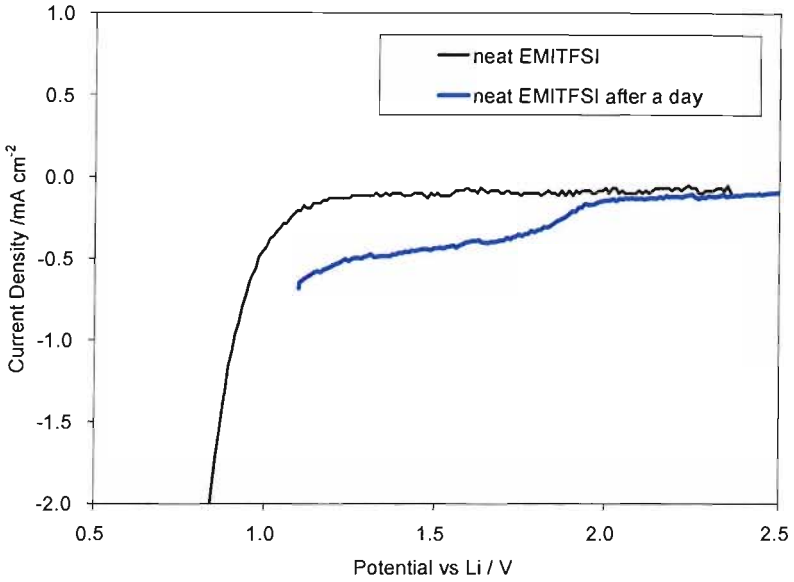

Fig. 2.12 Linear sweep voltammograms of the Pt microelectrode (diameter = 25 μm) in EMITFSI, immediately after cell assembly, and 24 h after storage outside the glove box. The common counter / reference electrode was $Li_{1.2}Mn_2O_4$ in 10 mM LiTFSI / EMITFSI. The scan rate was 5 mV s^{-1}.

2.3.2.7. Influence of oxygen addition.

Saturation of the solution with a stream of oxygen from a bubbler for 10 minutes gave a very large response below 2 V, as shown in Fig. 2.13. Although the response is complex, a rise in current can be seen at almost the same half wave potential as that of the contaminated sample of Fig. 2.12, indicating that the contaminant was indeed oxygen. Also, a limiting current is suggested by a shoulder at 4 mA cm^{-2} before the background due to reduction of a major component dominates.

Electroreduction of oxygen in EMITFSI has already been reported to occur by a one-electron transfer reaction with a half wave potential of -1 V *vs* Ag

$$O_2 + e^- \rightarrow O_2^-$$

The diffusion coefficient was reported to be 7.3 x 10^{-6} cm^2 s^{-1} [9] and the saturation concentration was 3.9 mmol dm^{-3} from pure oxygen at 20 °C. In the present study, the value of the current was used to find a value of D_{O2} = 1.0 x 10^{-5} cm^2 s^{-1} using eq. 2.7 and assuming the saturation concentration value.

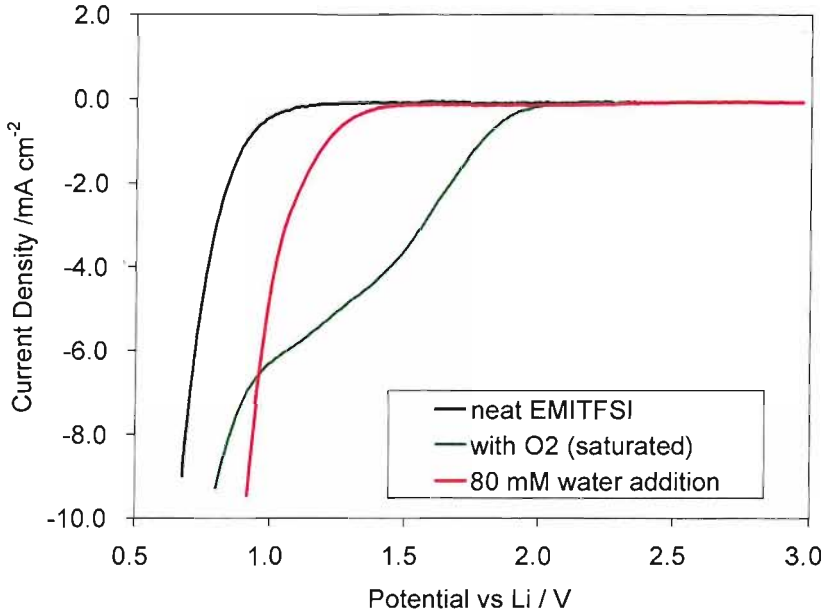

Fig. 2.13 Linear sweep voltammograms of the Pt microelectrode (diameter = 25 μm) in synthesised EMITFSI with water or oxygen. The common counter / reference electrode was $Li_{1.2}Mn_2O_4$ in 10 mM LiTFSI / EMITFSI. The scan rate was 5 mV s^{-1}.The scan rate was 5 mV s^{-1}.

Table 2.2 Diffusion coefficients in EMITFSI

	$O_{2\ obtained}$	$O_{2\ reported}$	$Br^-_{obtained}$	$O_{2\ reported}^-$
$D_{\text{ in EMITFSI}}$	1.0 x 10^{-5}	7.3 x 10^{-6}	2.3 x 10^{-7}	2.7 x 10^{-6}

Linear sweep voltammograms in EMITFSI with several concentrations of added water are also shown in Fig. 2.14. These do not show the expected plateaus due to diffusion limited water reduction, but instead a positive shift in the threshold potential for cathodic decomposition of the major component, EMITFSI. The shift may suggest that

water acted as a catalyst in the total reaction. With 800 mM of moisture, the current profile is noisier than those of smaller concentrations; this may be due to the convection at the surface of the electrode from generated hydrogen bubbles.

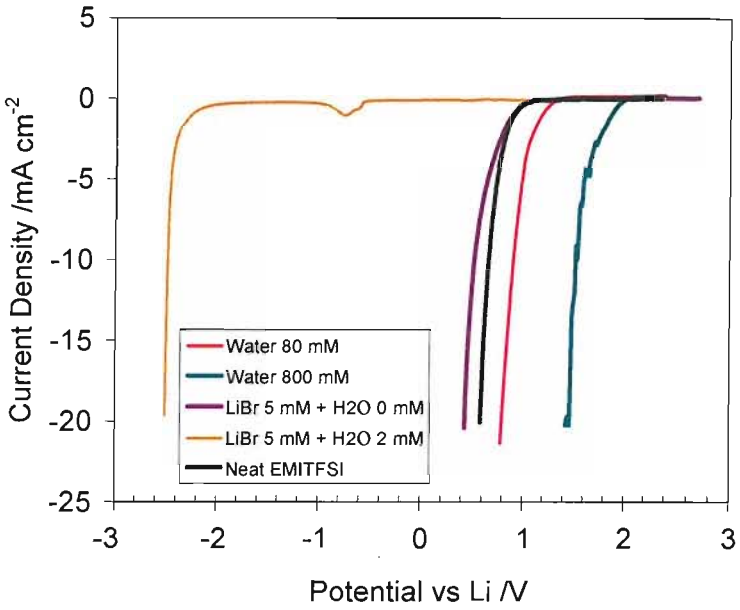

Fig. 2.14 Linear Sweep Voltammograms of Pt microdisc (diameter = 25 μm) in EMITFSI containing water and LiBr. The counter and reference electrode was $Li_{1.2}Mn_2O_4$ carbon composite immersed in 10 mM LiTFSI/EMITFSI The scan rate was 5 mV s^{-1}.

The expected shape of the current voltage curve for a simple electron transfer reaction under kinetic control is given by the Butler-Volmer equation.

$$i = i_0\left[\exp\left(\frac{\alpha_A nF}{RT}\eta\right) - \exp\left(-\frac{\alpha_C nF}{RT}\eta\right)\right] \qquad \text{eq. 2.9}$$

Where i_0 is the exchange current density, η is the overpoential, n is the number of electrons, α_A is the anodic transfer coefficient, α_C is the cathodic transfer coefficient

Fig. 2.15 shows Tafel plots for the cathodic decomposition of EMITFSI on the platinum microdisc. Without a water addition, the cathodic potential limit of 0.9 V *vs* Li was observed for a current of 1 mA cm^{-2}. At more negative potentials, we can express the cathodic limit of neat EMITFSI as below.

$$Ec = 0.93 - 0.28 \text{ x } \log i \qquad \text{eq. 2.10}$$

Where *Ec* is the potential vs Li /V, *i* is the current density /mA cm^{-2}

The plots for the ionic liquids with moisture are almost parallel to neat one and the shift is found to be proportional to the square root of the concentrations, described as below.

$$Ec = 0.93 - 0.28 \times \log i + 0.97 (c_{water})^{1/2} \qquad \text{eq. 2.11}$$

Where c_{water} is the concentration of water in EMITFSI /mol dm^{-3}

The fitting results calculated from the equation were close to the Tafel plots, as shown in Fig. 2.15. Therefore, the equation can be used to evaluate a concentration of water in the ionic liquid by measuring a cathodic linear sweep voltammetry.

When one electron transfer reaction determines the total reaction rate, a Tafel plot should show a slope of 120 mV/log *i*, whereas the results for EMITFSI on the platinum present 280 mV/log *i*. The large values for the gradient can be often seen on a partly passivated electrode by inhibitors [11] or a poisoning material [12]. The surface layer can act as a charge transfer barrier and increase overpotentials. Because of those complications, it is difficult to find whether the rate of this reaction is limited by one electron transfer reaction (EMI radical generation?) or two electron transfer reaction (water decomposition).

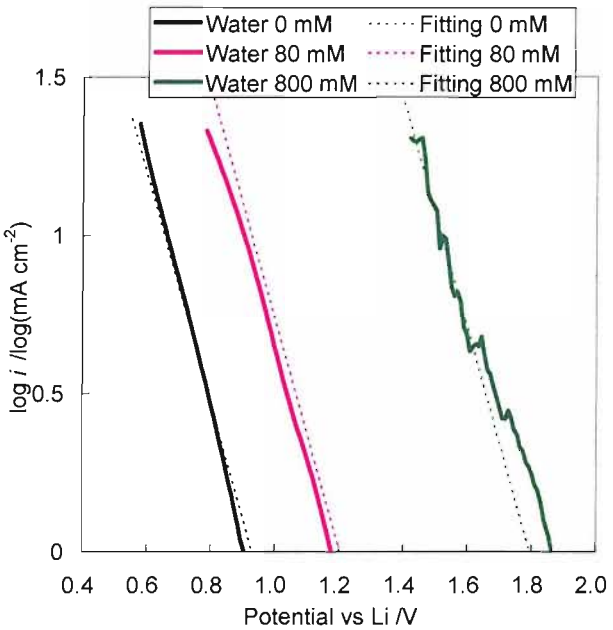

Fig. 2.15 Tafel polarisation plots for cathodic decomposition of EMITFSI containing varied concentrations of water on the Pt microdisc.

2.3.2.9. Influence of water addition (Au electrode)

To study the effects of water on the cathodic decomposition behaviour in detail, gold microelectrode array was used and the voltammograms are shown in Fig. 2.16. The expected diffusion limiting current for water was calculated with D_{water} = 1 x 10^{-5} cm^2 s^{-1}, using the published value for oxygen, D_{O2} = 7.3 x 10^{-6} cm^2 s^{-1}. [9] The voltammograms present a similar trend to the case with the platinum microdisc; the expected limiting current did not appear but the threshold potential for total decomposition of EMITFSI became positive depending on the concentration of moisture.

The decomposition of water was suppressed down to 0.6 V vs Li. An explanation for the phenomenon may be the adsorption of carbene on the gold electrode leading to slow kinetics of hydrogen evolution. The low water activity and possibly a shift in the equilibrium potential due to a highly basic solution formed from the presence of impurities in the ionic liquid.

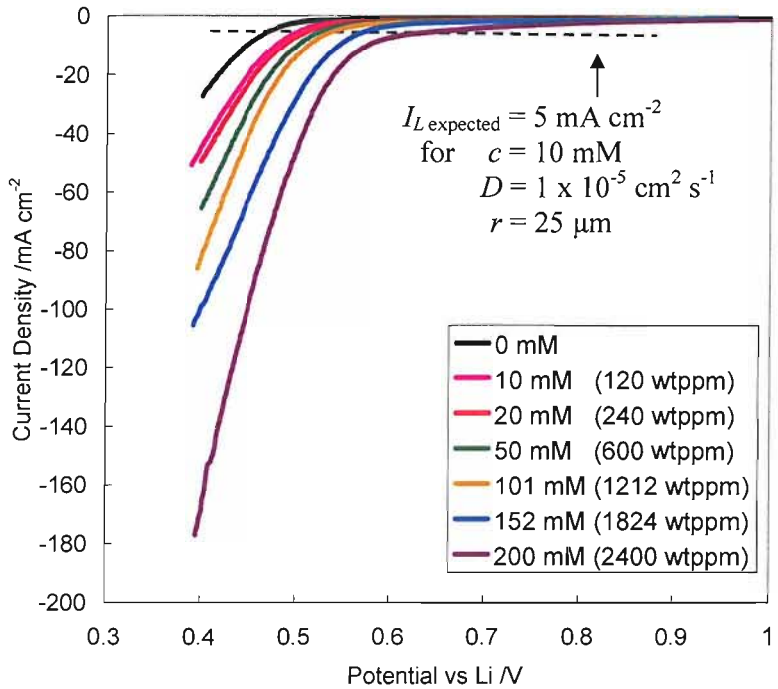

Fig. 2.16 Linear Sweep Voltammograms of Au microdisc (diameter = ca 30 µm) in EMITFSI containing various concentrations of water. The reference electrode was $Li_{1.2}Mn_2O_4$ carbon composite immersed in separated 10 mM LiTFSI/EMITFSI. The counter electrode is a Pt mesh.

Tafel plots for the reaction are shown in Fig. 2.17 and the gradients are very much alike (93 mV $(\log i)^{-1}$) around a current density of 10 mA cm^{-1}. The slope is less than 120 mV and this indicates the reaction involves more than one electron transfer. However, the slope is still larger than 60 mV; this is may be due to a surface film formed from decomposed compounds on the gold microelectrodes, same as in the case of the platinum electrode. The slope from Fig. 2.17 was smaller than the value for the Pt (280 mV $(\log i)^{-1}$). The variation of the gradients could imply that a different step limits the total rate of decomposition; however, more likely, a two electron transfer reaction is the rate controlling factor because EMI cations need two electrons to form stable dimers or decomposed compounds.

Plots for the electrolytes with high concentrations of water, such as 200 mmol dm^{-3}, show a plateau like current response. This may be from a water decomposition reaction at the diffusion limited current or can be from reduction of oxygen dissolved in water added. Consequently at lower potential, hydroxide anions produced from water may affect the reduction of EMI cations.

It is also observed for each plot that at the highest current density of each concentration, the curves begin to level off again, e.g. due to the electrolyte resistance.

To analyse the effect of water concentration on the slopes, the same procedure was used for fitting the results to an equation. The dependence of decomposition potentials and current on concentration of water was plotted as shown in Fig. 2.18. Without moisture, the decomposition potential of EMITFSI on gold is expressed as eq. 2.12.

$$Ec = 0.54 - 0.093 \times \log i \qquad \text{eq. 2.12}$$

Where Ec is the potential and i is the cathodic current density

The potential shifts of the threshold potential appear as proportional to the square root of water concentration, shown as.

$$Ec = 0.54 - 0.093 \times \log i + 0.27\,(c_{water})^{1/2} \qquad \text{eq. 2.13}$$

The fitting slopes and experimental results around 0.5 V show agreement except for the slop for 100 mM, as shown in Fig. 2.17; therefore the equation can be used to determine the concentration of water in the ionic liquid by an easy method.

eq. 2.13 shows the logarithmic decomposition currents are proportional to the square root of the moisture concentration. A clear explanation for the relationship was not found. However, the following relationship may explain why the effect of the concentration is a square root.

$$[H^+][OH^-] = k_w \cdot a_{H_2O}$$

$$[H^+] = [OH^-] = \sqrt{k_w \cdot a_{H_2O}} = k_w^{1/2} \cdot \gamma_{H_2O}^{1/2} \cdot c_{H_2O}^{1/2} \qquad \text{eq. 2.14}$$

Where k_w is the ionic product, a_{H2O} is the activity of water, γ_{H2O} is the activity coefficient of water and c_{H2O} is the concentration of water

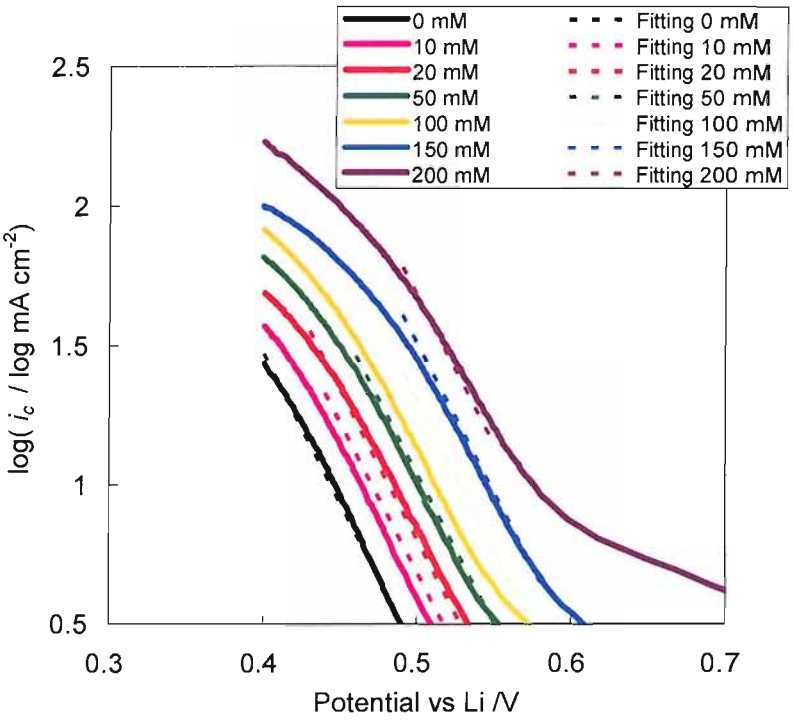

Fig. 2.17 Tafel plots of cathodic decomposition of EMITFSI with moisture on Au microdisc (diameter = ca 50 μm). The reference electrode was $Li_{1.2}Mn_2O_4$ carbon composite immersed in separated 10 mM LiTFSI/EMITFSI. The counter electrode was a Pt mesh.

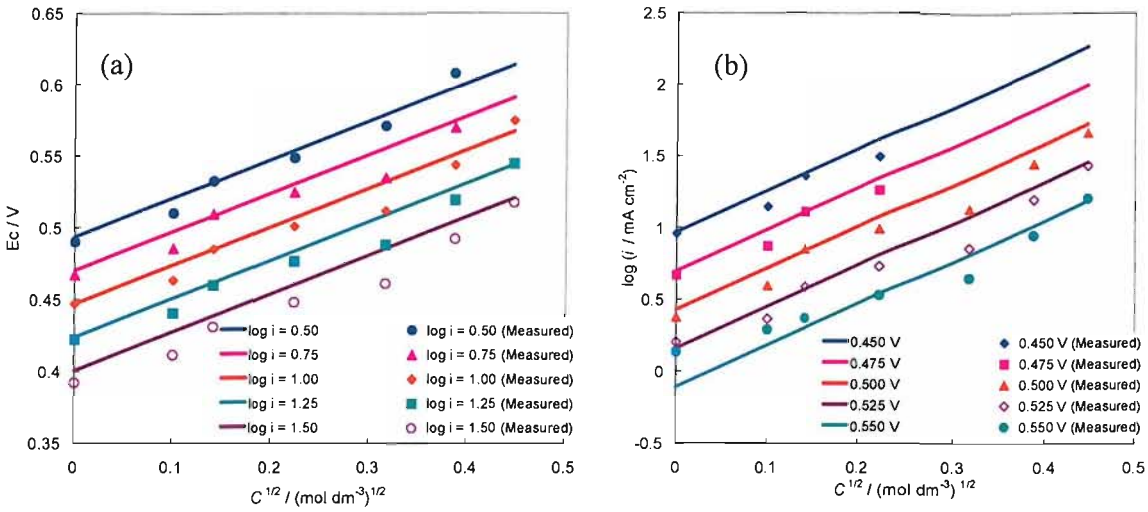

Fig. 2.18 Plots showing dependences of *Ec* (a) and log *i* (b) on concentrations.

The above fitting show good agreement only around 0.5 V and 10 mA cm^{-2} and the theoretical basis is imperfect; therefore, an alternative approach to investigate the reaction is required. The decomposition current data for wider ranges than Fig. 2.17 were presented against the concentration of moisture, as shown in Fig. 2.19.

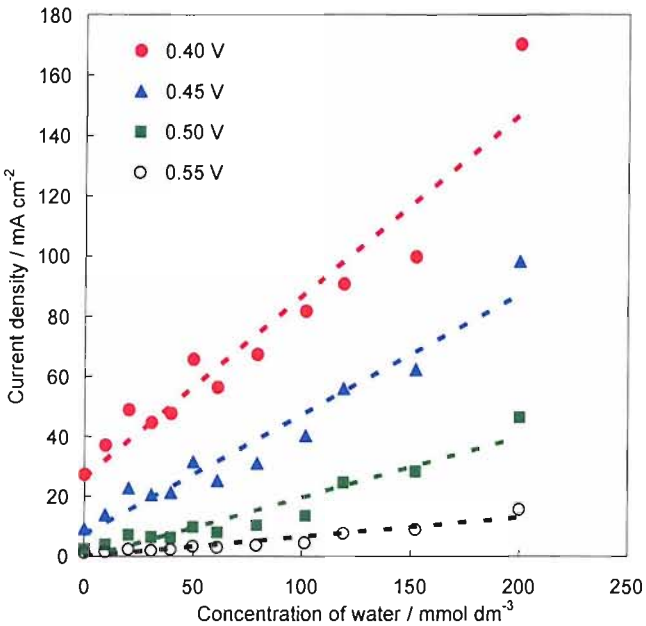

Fig. 2.19 Cathodic decomposition currents for EMITFSI on Au microdisc electrode array, depending on the concentration of water.

Since a change in the standard reduction potential (EMITFSI) with water concentration is unlikely, we seek an explanation in terms of an increase in the pre-exponential factor of the Butler-Volmer equation, j_o, that is proportional to the water concentration. This may be obtained by proposing an EC' mechanism where the effective rate constant for EMI reduction is proportional to the concentration of the catalyst. [13]

$$k' = C_{H2O}\, k, \text{ such that } j' = C_{H2O}\, j_o \qquad \text{eq. 2.15}$$

In Fig. 2.19, decomposition currents for EMITFSI were observed without water but when we inspect the increase of decomposition current by moisture, the values are a almost linear function of the water concentration at each potential. That is consistant with the relationship shown in eq. 2.15. The gradients variation suggests the rate constant, k varies depending on the potentials.

The following scheme as shown in Fig. 2.20 was proposed for the decomposition mechanism of EMI cations under the influence of water. The process starts with the decomposition of water, shown as (1) and produces hydrogen and hydroxide anions, which attack the protons in EMI cations (2). Thus, EMI decomposes to dimers or the ring opens and forms another compound. The hydroxide anions return to water; then the water is not consumed totally.

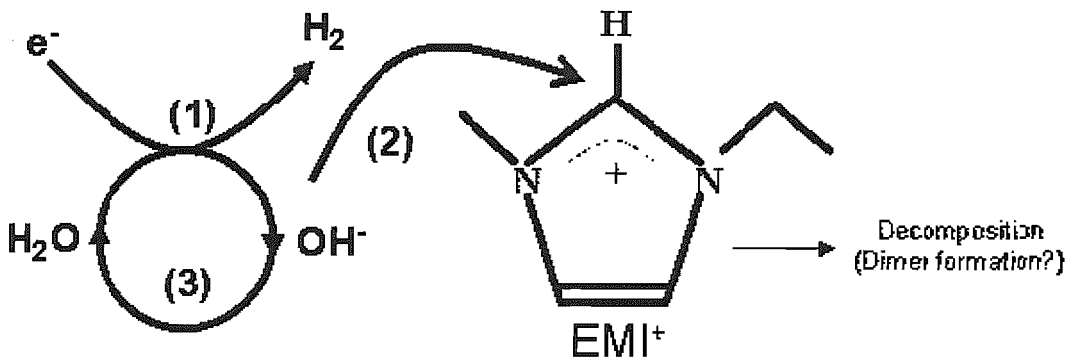

Fig. 2.20 Proposed decomposition scheme of EMI cations under the influence of water catalytic mechanism

2.3.2.10. Influence of LiBr addition

In very dehydrated condition, a small residual LiBr (5 mM) slightly affects the decomposition behaviour at the cathodic potential limit as shown in Fig. 2.14. Although the threshold potential is still higher than 0 V, lithium has been reported to deposit above 0 V on Pt by underpotential deposition (UPD) [14] (However, the reaction was highly possible to be an alloy formation); therefore deposited lithium might react with EMI cations, accordingly hindering the decomposition rate. When a small amount of water additionally contaminated into the EMITFSI, the effect became significant and the cathodic limit shifted down to -2.5 V *vs.* Li, suggesting the formation of a passivating layer of LiOH according to the reactions:

$$H_2O + e^- \rightarrow OH^- + \tfrac{1}{2} H_2 \quad \text{and} \quad Li^+ + OH^- \rightleftharpoons LiOH\downarrow$$

A small current peak was observed around -0.5 V *vs* Li in Fig. 2.14 but the peak was sometimes shifted ±0.5 V or not present. This behaviour may be explained by disruption, then self-restoration of the passivating film, which was very sensitive to the state of the electrode surface. Although the apparent cathodic limit was extended to below 0 V vs Li, no anodic current was observed when the potential sweep was reversed after the cathodic current. Therefore, the shift of cathodic potential limit is only ascribed to an electrode fouling and the film does not allow the permeation of lithium ions.

2.3.2. LiTFSI/EMITFSI

To use the ionic liquid for lithium batteries, lithium ions must be introduced into the electrolyte. The stability of the mixture on various metals and the effect of contamination of water were studied.

2.3.2.1. Cathodic stability on various metal

With addition of LiTFSI, the cathodic limit of the electrolyte on each metal extended to more negative potentials than that without lithium salt. This suggests formation of a solid electrolyte interface (SEI) on the surface of microelectrodes. For example, in the

case of a nickel microdisc, the threshold potential for decomposition of EMITFSI without LiTFSI was over 0.6 V vs Li. On the contrary, severe decomposition was not observed down to 0 V with the lithium salt. Moreover, reversible lithium deposition was confirmed by stripping when the sweep was reversed at an appropriate potential. The coulombic efficiency of the stripping charge against deposition charge was 60 %, which is a normal value for deposited lithium on nickel because usually the forefront of dendritic lithium loses the electric contact from the substrate during anodic dissolution [15].

After the second cycle, both cathodic and anodic current decrease significantly, suggesting a passivation film formed on the deposited lithium and limited the rate of the reaction.

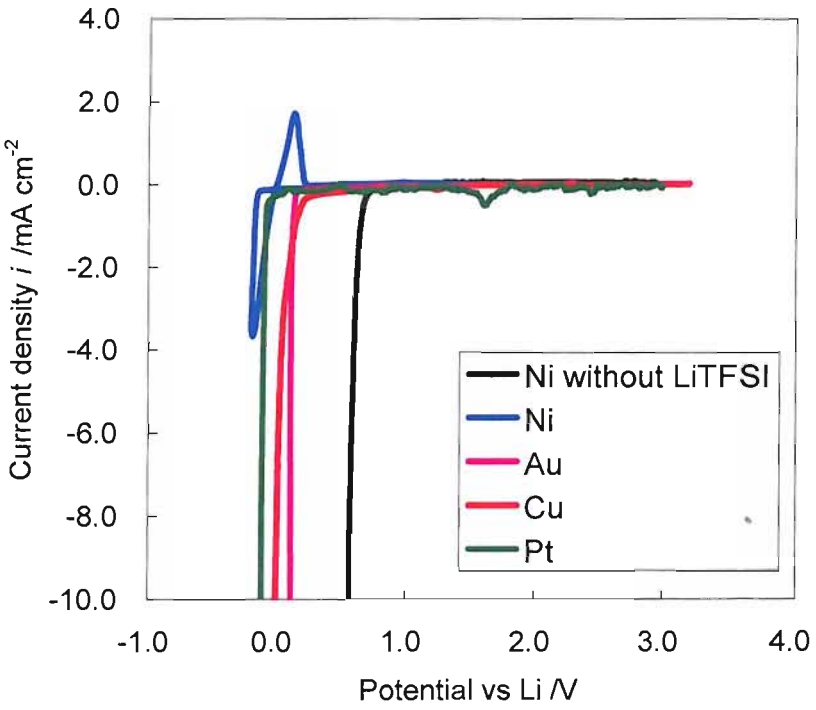

Fig. 2.21 Voltammograms showing cathodic currents on various metals in 0.47 mol dm^{-3} LiTFSI/EMITFSI. The scan rate was 5 mV s^{-1}.

Although all metals show the extension of the potential window, reversible deposition of lithium was observed only with the nickel electrode. Nickel has a unique property, which strictly does not form an alloy with lithium, therefore is used in the studies on lithium deposition and stripping. The other metals tested here, copper [16], platinum [17] and gold [18] have been known to produce alloys with lithium. Lithium insertion into metals causes expansion of the electrode, causing tension of the solid electrolyte interface and resulting in cracks in the fragile SEI.

2.3.2.2. Solid electrolyte interface on lithium in LiTFSI / EMITFSI

The open circuit potential of the lithium metal electrode was against -2.90 V vs $Li_{1.2}Mn_2O_4$ reference electrode and kept the same value for more than 2 days. This confirms the stability of the LiTFSI / EMITFSI with lithium metal because the measured potential was within 10 mV of the potential measured in conventional electrolyte, $LiPF_6$ / EC : DMC.

The impedance spectrum of lithium in the three electrode cell in LiTFSI/EMITFSI (Fig. 2.22) shows a slightly depressed semi-circle, of which diameter is 170 ohm cm^2. The intercept at the highest frequency is attributed to electrolyte resistance and other electrical resistive components, such as the electrode itself. In the middle frequencies, the semi-circle represents capacitance in parallel with a resistance, which only responds at relatively slow frequencies.

The capacitance value was calculated by the equation below

$$C = \frac{1}{2\pi Rf} \qquad \text{eq. 2.16}$$

Where C is the capacitance, R is the parallel resistance and f is the frequency

Assuming that the relative static permittivity, ε_r, of the capacitance component is 100, the thickness of the layer is calculated as 4.5 nm, which is small for the SEI on the lithium surface [19].The diameter of the semi-circle is attributable to the resistance corresponding to lithium ion transfer in the SEI; however, the formed layer is thin,

therefore presumably not as robust as the SEI formed with an organic solvent, such as PC and EC.

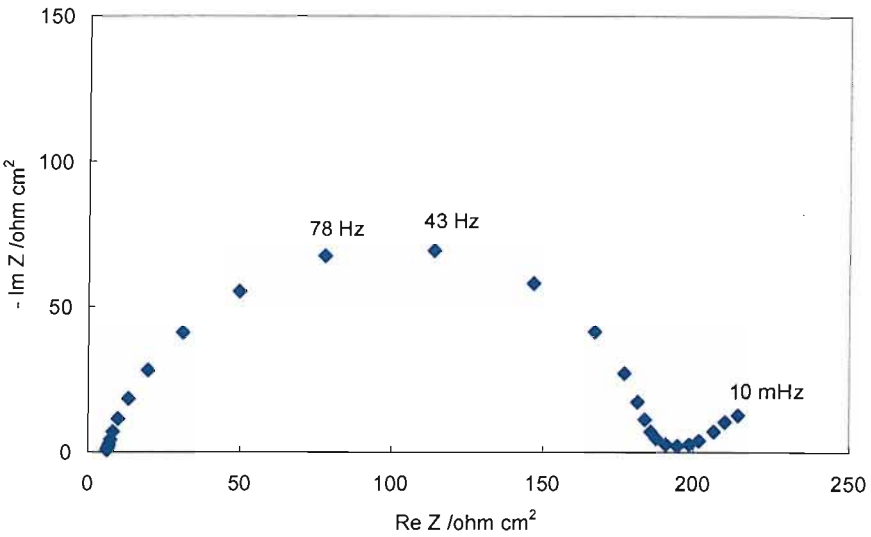

Fig. 2.22 Impedance spectrum of lithium electrode immersed in 0.47 mol dm^{-3} LiTFSI / EMITFSI at the OCV.

Fig. 2.23 shows cyclic voltammograms of a lithium disc electrode at varied scan rates for several cycles. Although the open circuit potential is out of the "potential window" of neat EMITFSI, violent decomposition current was not observed. Voltammograms did not depend on the scan rates but seems to be controlled by one resistive factor. The gradient from -0.2 V to 0.2 V is 5.5 mA cm^{-2} / V, which is ascribed to the resistance of 181 ohm cm^2. The resistance is constant both below and above 0 V vs Li, suggesting that the state of the SEI is affected by neither lithium deposition nor stripping.

The information from the impedance spectrum and the cyclic voltammograms suggests formation of a stable SEI on the surface of the lithium metal. The SEI may prevent decomposition of the electrolyte by blocking electron transfer but still allows lithium ion permeation through the layer

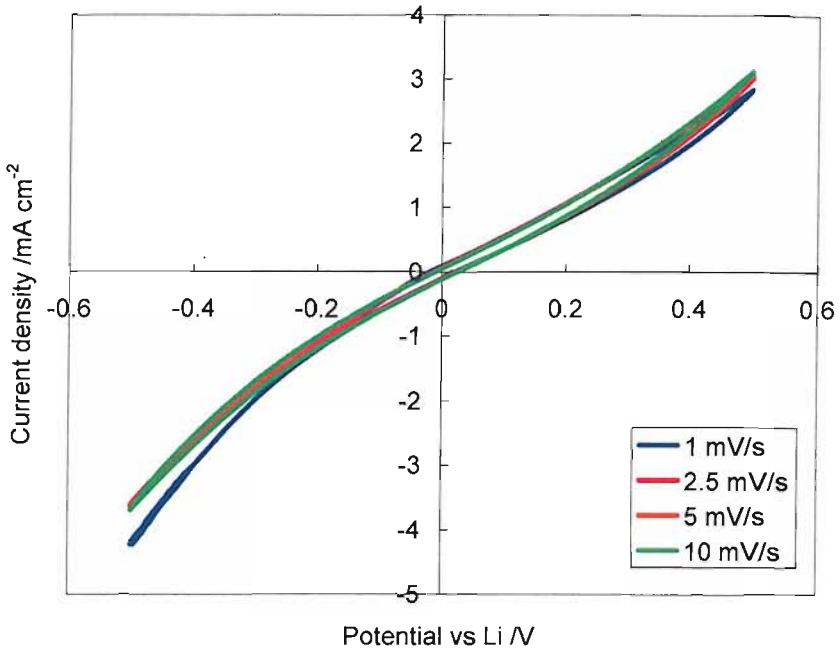

Fig. 2.23 Cyclic voltammograms of a lithium disc electrode in 0.47 mol dm^{-3} LiTFSI/EMITFSI.

2.3.2.3. Effects of water addition to LiTFSI / EMITFSI

As shown in Fig. 2.24, voltammograms show large cathodic currents at less than 0.2 V vs Li. In the case without water, after the potential sweep was reversed to positive, the cathodic current increased. The shapes of the voltammograms may be explained by the nucleation of the reaction. To trigger the decomposition of the ionic liquid, a high overpotential is required due to the formed passivation film on the electrode. By contrast, little anodic current was observed, suggesting that lithium ions were not inserted into gold because of electrolyte decomposition, which may be due to destruction of a passivating layer.

The effect of water addition into LiTFSI/EMITFSI seems to be opposite to that for neat EMITFSI. Cathodic currents decreased with an increase of water concentration, suggesting formation of LiOH on the gold electrodes. At 21 mmol dm^{-3}, the cathodic

decomposition current was not observed down to 0.1V vs Li; therefore, a further potential sweep was implemented down to -0.3 V vs Li, as shown in Fig. 2.25.

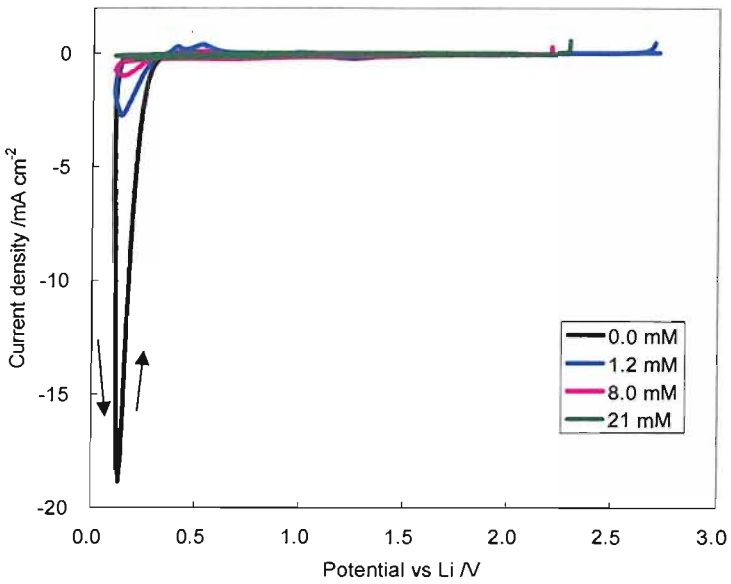

Fig. 2.24 Cyclic voltammograms measured on gold microelectrodes in 0.47 M LiTFSI/EMITFSI containing various concentrations of water. The common reference and counter electrode was $Li_{1.2}Mn_2O_4$ carbon composite electrode in 10 mM LiTFSI/EMITFSI. (At low concentrations of water)

Under 0.2 V vs Li, cathodic current was still observed with the electrolyte containing 21 mM of water, but this time, the current was limited and showed a plateau-like shape. This is attributable to diffusion limiting current or passivation or these mixtures. After the potential sweep is reversed, an anodic current peak was seen. The threshold for the cathodic current was above 0 V vs Li; therefore the current does not correspond to deposition of lithium but is attributed to formation of a lithium-gold alloy. The anodic current is for elimination of lithium ions from the alloy but the peak is ca 0.9 V distant from the cathodic peak. This suggests a large IR drop due to the LiOH passivating layer. For the electrolyte containing more water, thicker layers may form and cause larger IR drop as shown in Fig. 2.25. It was found that lithium is reversibly inserted into gold in

LiTFSI/EMITFSI when the concentration of water is in the appropriate range. However, those reversible current responses were only seen for the first cycle on polished electrode; therefore it is difficult to use this reaction in practical rechargeable battery.

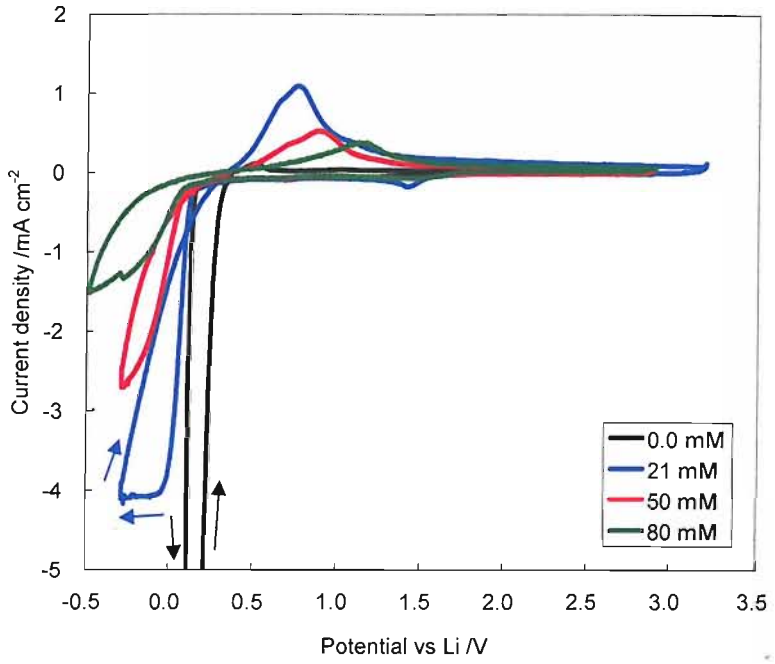

Fig. 2.25 Cyclic voltammograms measured on gold microelectrodes in 0.47 M LiTFSI/EMITFSI containing various concentrations of water. The common reference and counter electrode was $Li_{1.2}Mn_2O_4$ carbon composite electrode in 10 mM LiTFSI/EMITFSI. The scan rate was 5 mV s^{-1} (At high concentrations of water)

2.3.2.4. Tin as negative electrode in EMITFSI

a) Tin deposition on the substrates

The coulombic efficiency for electro deposition of tin on platinum or copper microdisc was estimated as 92 % from stripping voltammetry. The thickness of the tin layer was estimated as 1.8 μm, using Faraday's law.

b) Lithium insertion into tin

Fig. 2.26 shows evidence for lithium insertion and extraction on a tin electrode. This is the first report of this reaction in EMITFSI, and the second report as ionic liquids since the previous work on lithium insertion into a tin in a mixture of 1-ethyl-3-methylimidazolium chloride and aluminium chloride[20], which has disadvantages on its high reactivity with moisture. The multiple peaks correspond to the existence of more than one phase of Li_xSn within this potential range. Stoichiometric coefficient x in Li_xSn was calculated according to

$$x = \frac{nQ_D}{Q_{str}} \qquad \text{eq. 2.17}$$

and the "discharge capacity[coulomb/g]" by

$$C_D = \frac{Q_D}{Q_{str} M /(nF)} \qquad \text{eq. 2.18}$$

Where C_D : the discharge capacity, Q_D : the electrical charge of discharge, Q_{str} : the electrical charge of stripping voltammetry, M : the molecular weight, n: number of electron for deposition of tin, F: Faraday constant

These quantities are shown in Table 2.3 and Fig. 2.28 shows the variations in charge and discharge capacity with cycling conditions. It was found that lithium was inserted nearly up to Li_2Sn. Except for the first charge showing irreversible capacity, both insertion and extraction charges for a tin layer on Pt increased up to cycle 5 (corresponding to an increased penetration depth) after which the charges decreased suddenly, possibly due to exfoliation of tin from the substrate. Similar cycle behaviour was noted for tin on copper.

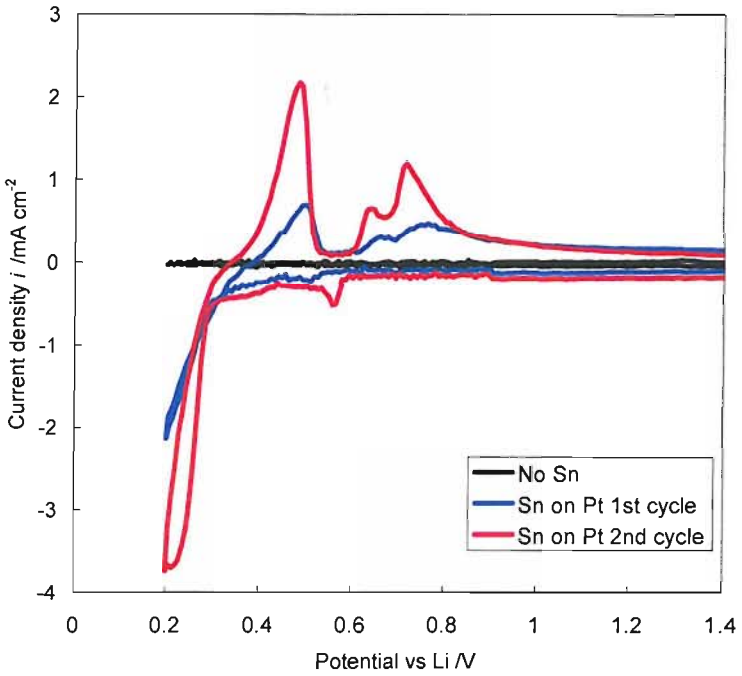

Fig. 2.26 Cyclic Voltammograms of the Tin electrode deposited on Pt microdisc (diameter = 25 μm) in 1mol dm^{-3} LiTFSI/EMITFSI. The counter and reference electrode was $Li_{1.2}Mn_2O_4$. The scan rate was 1 mV s^{-1}

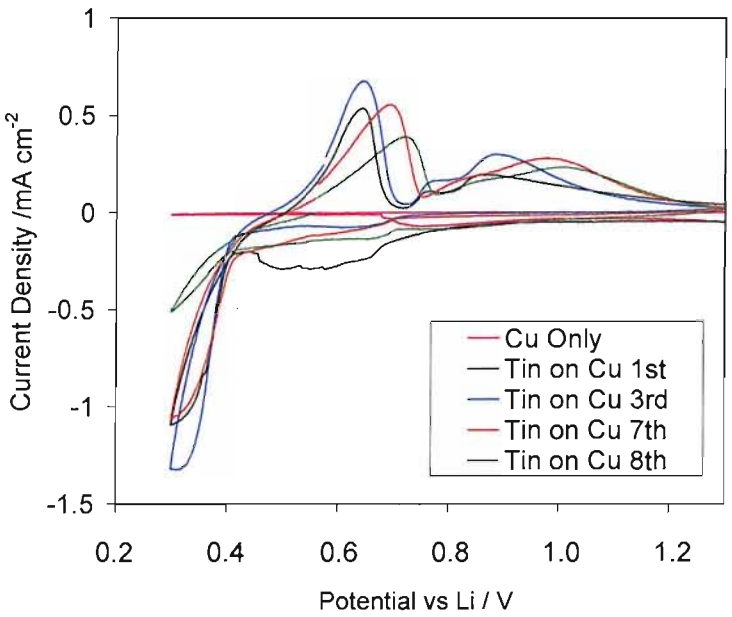

Fig. 2.27 Cyclic Voltammograms of the Tin electrode deposited on Cu disc (diameter = 190 μm) in 1mol dm^{-3} LiTFSI/EMITFSI. The reference electrode was $Li_{1.2}Mn_2O_4$ carbon composite and the counter electrode was LiFePO4 carbon composite (Three electrode cell). The scan rate was 0.2 mV s^{-1}.

Table 2.3 Theoretical capacity of Li_xSn

Capacity	LiSn	$Li_{1.5}Sn$	Li_2Sn
mAh g^{-1}	213	312	406

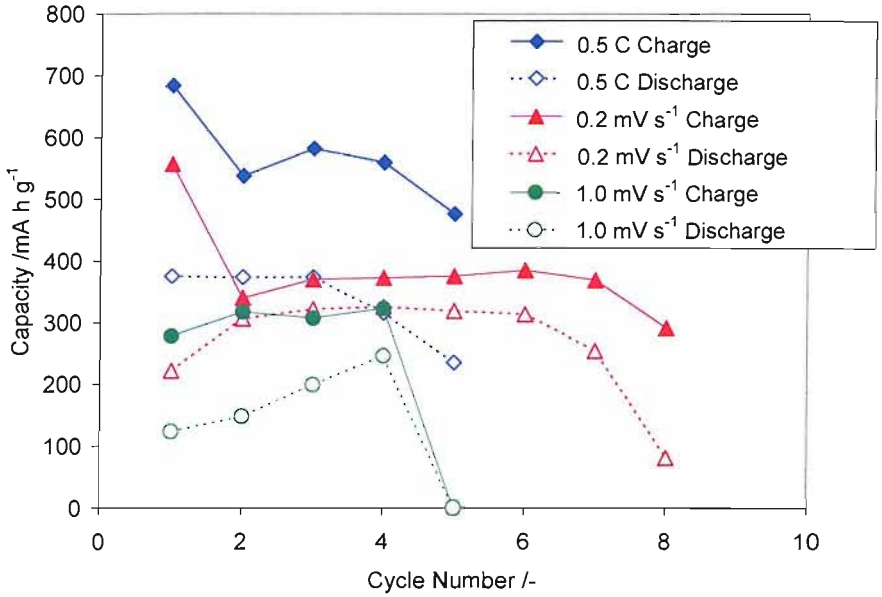

Fig. 2.28 Capacity dependence on cycle number for the Tin electrode deposited on Cu or Pt disc in 1mol dm^{-3} LiTFSI/EMITFSI.

With constant current charge and discharge at C/2[1]* a decline in charge capacity with cycle number was observed as shown in Fig. 2.28 The theoretical capacity for Li_2Sn, 406 mA h g^{-1} was adopted to calculate the C rate.

2.3.2.5. Graphite as negative electrode in LiTFSI/EMITFSI

Cyclic voltammetry was used to investigate lithium insertion into graphite from EMITFSI containing 1M LiTFSI. The first cycle, Fig. 2.29, shows a sudden increase in cathodic current to 0.7 mA cm^{-2} at about 0.9 V *vs* Li, close to the potential where

[1]* The "C" rate is a unit of current, which can charge/discharge the expected capacity of the cell for an hour.

irreversible capacity is often observed in propylene carbonate based electrolytes due to solvent co-intercalation and reduction. The current falls rapidly at around 0.6 V *vs* Li and thereafter approximates to an ohmic response corresponding to a reaction potential of 0.9 V and a resistance of about 3 $k\Omega\ cm^2$, with a number of superimposed current pulses smaller than the initial event. A possible explanation for this behaviour is a localised electrolyte reduction concurrent with lithium insertion, *e.g.* at the exposed edge planes of the graphite. The decrease in current after the initial event is probably due to passivation by insoluble reaction products forming an SEI with a resistance of 3 $k\Omega cm^2$. Further peaks are attributed to other localised events similar in nature. The anodic sweep shows continued cathodic current, presumably due to insertion, and a remarkable coincidence of the potential at the point of zero current that is observed on the initial cathodic sweep. Evidence of lithium extraction is shown in the following anodic current, which is smooth and shows a peak around 1.4 V at a current higher than the resistance-limited value. The total charge extracted is, however, much less than the cathodic charge even if we exclude the initial anodic peak.

On the second cycle the current crosses the axis at a more positive potential than before, and smoothly rises to a peak at 0.6 V before a sudden rise in current. The current decay is more gradual than before, and after scan reversal the current continues to decrease as before. However, after current reversal at 1 V the extraction peak is much reduced and the third cycle shows only a small peak at around 0.5 V. The three cycles therefore indicate a passivation event, very erratic at first, but gradually forming an SEI of rather high resistance which limited the insertion current to less than 0.2 $mA\ cm^{-2}$.

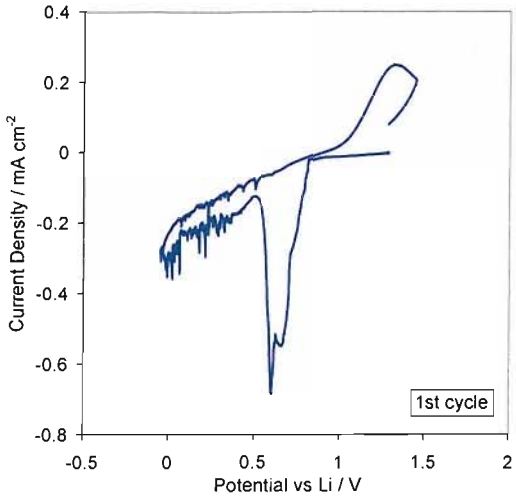

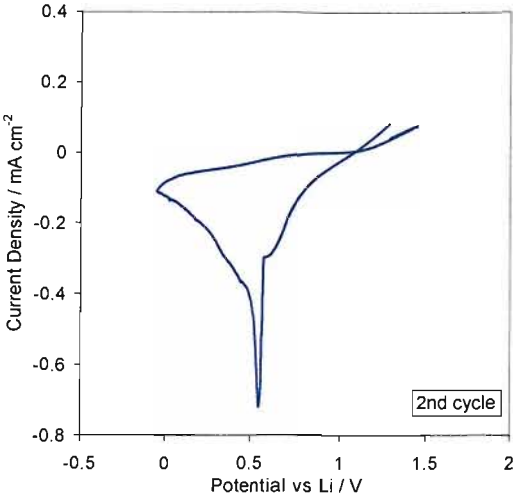

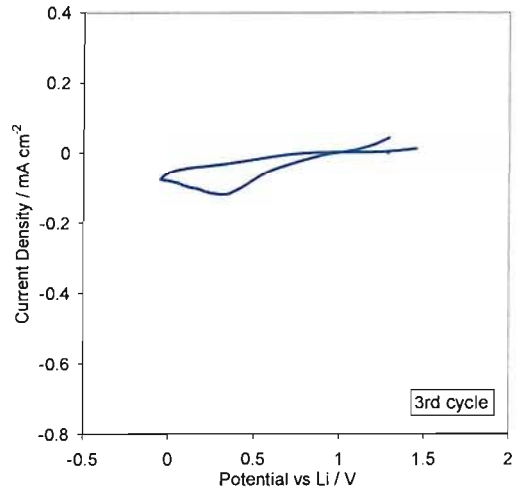

Fig. 2.29 Cyclic Voltammograms of the graphite disc electrode (diameter = 1.0 mm) in 1 mol dm^{-3} LiTFSI/EMITFSI. The reference electrode was $Li_{1.2}Mn_2O_4$ carbon composite and the counter electrode was $LiFePO_4$ carbon composite (Three electrode cell). The scan rate was 0.1 mV s^{-1}.

2.4. Conclusion of the chapter

EMITFSI was synthesised and the impurities were checked by voltammetry, as well as analytical equipment. Less than 40 ppm Br^- was found to remain in synthesised EMITFSI. The diffusion coefficient of Br^- in EMITFSI was evaluated as $D_{Br^-} = 2.3 \times 10^{-7}$ cm^2 s^{-1}. The effect of O_2 was also studied and it was found to be the main contaminant of EMITFSI after synthesis.

Effects of water were studied using a platinum microdisc electrode and a gold microdisc electrodes array. In presence of water, an expected plateau was not observed but the cathodic potential limit of the ionic liquid was shifted to the positive side. When the decomposition current was 10 mA cm^{-2}, Tafel plots for EMITFSI containing varied concentrations were parallel and the shift was proportional to the square root of the concentrations of water. Therefore, the shift of potential is useful to estimate the moisture concentration in the ionic liquid. It was also found that an increase of the cathodic current is linear to the moisture concentration. This suggests the cathodic decomposition of EMI cations proceeds under a water catalytic EC' mechanism.

The cathodic stability limit potential of EMITFSI on platinum was shifted to the negative side with addition of LiBr. The shifts with addition of LiTFSI were more significant on the surface of platinum, tin and copper. These phenomena were attributable to the formation of a solid electrolyte interface (SEI) on the metal electrode from lithium salt in the electrolyte. Moreover, on the surface of a nickel microdisc, reversible lithium reaction was observed in LiTFSI/EMITFSI. To the contrary, with copper or gold or platinum, the electrolyte decomposes before lithium deposition/stripping occurs. This may be attributed to the formation of alloys; accordingly, the volume expansion damages the SEIs.

On lithium metal electrode in LiTFSI/EMITFSI, the formation of a SEI (180 ohm cm^2) was confirmed from a stable open circuit potential, the semi-circle of an impedance spectrum and the behaviour of cyclic voltammograms. It was found that neither deposition nor stripping of lithium affects the state of the SEI.

When water is contaminated into LiTFSI/EMITFSI, LiOH is deposited on the electrode and the cathodic limit was extended. At an appropriate concentration, the deposited LiOH film allows permeation of lithium ions, thus reversible lithium deposition on gold microdiscs.

A preliminary study of tin and graphite electrodes as lithium insertion negative electrodes was made and the results suggest formation of a lithium ion permeable SEI on tin, allowing a reversible insertion up to a composition Li_2Sn, with a discharge capacity of ca 400 mA h g^{-1}. On the other hand, lithium insertion and extraction in graphite were accompanied by complicating side reactions which caused large and variable ohmic drops.

References

1. P. Bonhote, A. P. Dias, N. Papageorgiou, K. Kalyanasundaram and M. Gratzel, *Inorg. Chem.*, **35**, 1168 (1996)

2. M.A. Augelli, V.B. Nascimento, J.J. Pedrotti, G.R. Gutz, L. Angnes, *Analyst* **122,** 843 (1997)

3. S.J. Konopska, B. McDuffie, *Anal. Chem.*, **42,** 1741 (1970)

4. J. P. Armstrong, C. Hurst, R. G. Jones, P. Licence, K. R. J. Lovelock, C. J. Satterley and I. J. Villar-Garcia, *Phys. Chem. Chem. Phys.*, **9**, 982 (2007).

5. J. L. Anthony, E. J. Maginn and J. F. Brennecke, *J. Phys. Chem. B*, **105**, 10942 (2001).

6. G.P. Mathur and G. Thodos *American Inst. Chemical Eng. J.* **11** 164 (1965)

7. S. Sylla, J. Y. Sanchez and M. Armand, *Electrochim. Acta*, **37**, 1699 (1992).

8. L. Xiao and K. E. Johnson, *J. Electrochem. Soc.*, **150**, E307 (2003).

9. M.C. Buzzeo, O.V. Klymenko, J.D. Wadhawan, C. Hardacre, K.R. Seddon and R.G. Compton, *J. Phys. Chem. A*, **107**, 8872 (2003)

10. Y. Katayama, S. Dan, T. Miura and T. Kishi, *J. Electrochem. Soc.*, **148**, C102 (2001)

11. M. Metikos-Hukovic, R. Babic and Z. Grubac, *J. Applied Electrochem.*, **32**, 35 (2002).

12. K.K. Bhatia, C.-Y. Wang, *Electrochim. Acta*, 49 2333 (2004)

13. A.J. Bard and L.R. Faulkner, *Electrochem. Methods*, P455, P468 (1980)

14. J. Xua, J. Yang, Y. NuLia, J. Wanga and Z. Zhang, *J. Power Sources*, **160**, 621 (2006)

15. T. Takei, *J. Applied Electrochem.*, **9**, 587 (1979).

16. O.A. Lambri, J.I. Perez-Landazabal, A. Penaloza, O. Herrero, V. Recarte, M. Ortiz, C.H. Worner, *Mater. Res. Bul.*. **35**, 1023 (2000) 1023

17. M.B. Avdalyan, Y.M. Povarov, *Soviet Electrochem.*, **23** (1987) 602.

18. D. Aurbach, M. Daroux, P. Faguy, E. Yeager, *J. Electroanal. Chem.*, **297**, 225 (1991)

19. E. Peled, D. Golodnitsky, G. Ardel, V. Eshkenazy, *Electrochim. Acta*, 40, 2197 (1995)

20. Y.S. Fung and D. R. Zhu, *J. Electrochem.. Soc.*, **149**, A319 (2002).

Chapter 3. Ion transport in the ionic liquid

3.1. Introduction

Ionic liquids have relatively high conductivity, such as 10 mS cm^{-1} for EMITFSI, which is not far inferior to 10.7 mS cm^{-1} for 1 mol dm^{-3} $LiPF_6$ /EC:DMC [1] and even better than 5.8 mS cm^{-1} for 1 mol dm^{-3} $LiPF_6$ / PC [2]. Therefore, it is often said that ionic liquids are good candidates for new electrolytes [3]. However when we think about the application of electrolytes for lithium ion batteries, the mobility of lithium ions in electrolytes can be a problem. If lithium ion transfer is slow, it may cause lithium ion depletion (electrolyte starvation effect[4]) when lithium ions are inserted into the active material and accumulation when the ions are extracted. Accordingly full capacities of active materials would not be obtained under those circumstances [5,6].

When we use organic electrolytes such as propylene carbonate, the transference numbers for lithium ions do not change significantly as long as the same lithium salt is used [7]; therefore lithium ion mobility can be easily estimated from their conductivity. On the other hand, in the case of a mixture of ionic liquids and lithium salt, the mobilities of lithium ions do not simply relate to the total conductivity of electrolytes because a supporting electrolyte, the ionic liquid itself, has a great contribution to the total conductivity.

Although a number of studies have been reported on the conductivities of ionic liquids and their mixtures with lithium salt, few investigations have been made on the lithium ion mobility (diffusion) in electrolytes containing ionic liquids. These investigations were by NMR [8,9], therefore, need a modification to the expensive equipment. Moreover, the compatibility of these diffusion coefficients to the values obtained by an electrochemical method is uncertain.

In this chapter, investigations on lithium ion transfer in the ionic liquid, EMITFSI, were implemented and the effect of salt concentration on the conductivities and the diffusion coefficients is discussed.

3.2. Experimental

3.2.1. Synthesis of EMITFSI and LiTFSI/EMITFSI

1-Ethyl-3-methylimidazolium bis-(trifluoromethylsulfonyl)-imide (EMITFSI) and LiTFSI/EMITFSI were prepared as mentioned in Chapter 2.

The concentration of lithium salt in the ionic liquid was controlled by a weight ratio because of the convenience of handling but was mentioned in the manner of mol dm^{-3} in this thesis, to help theoretical studies. To transform the units, the mass densities of samples at various concentration of lithium salt were measured by weighing 100 μl of electrolyte samples at 298 K.

3.2.2. Electrochemical measurement

All electrochemical measurements were implemented in a Faraday cage to eliminate a disturbance from electrical noises. Cells used for electrochemical measurements were assembled in a glove box filled with argon (H_2O, O_2 < 0.1 ppm) and sealed in stainless steel containers and viton® o-rings.

3.2.2.1. Conductivity measurement

A PTFE (poly-tetrafluoroethylene) cylindrical (inner diameter = 5 mm, thickness = 1.2 mm) holder was placed on the top of a stainless steel current collector and an electrolyte sample was poured into the holder. The sample was covered by the other current collector and assembled into a two electrode cell, as shown in Fig. 3.1. The conductivity of the electrolyte was measured by AC-impedance method, using frequencies from 200 kHz to 2 kHz with VMP2/Z (Princeton Applied Research). The impedance spectrum obtained was extrapolated onto the horizontal axis and the real part of the impedance was evaluated. The cell constant of the PTFE holder is also calibrated using KCl 0.1 mol dm^{-3}

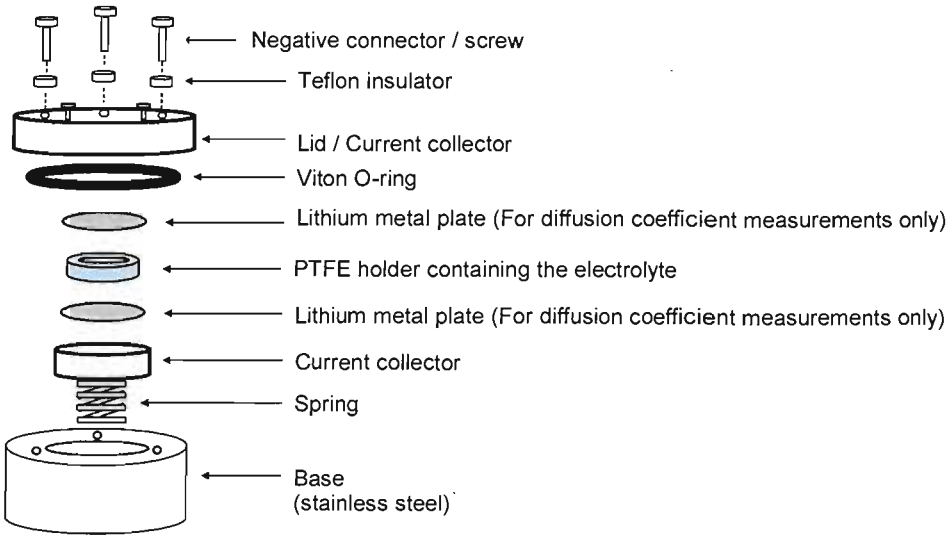

Fig. 3.1 Cell for impedance measurements and diffusion coefficient measurements

3.2.2.2. Diffusion coefficient measurement 1: Microelectrode Technique

A nickel microelectrode (φ = 50 μm) was used as the working electrode and a lithium foil was used as the common reference and counter electrode. To obtain a very dehydrated condition of the electrolytes, the measurement cell was kept in the glove box for one hour after the assembly, to let lithium remove a small trace of moisture in the electrolyte.

Linear sweep voltammetry was implemented in 0.47 mol dm^{-3} LiTFSI/EMITFSI. After each measurement, an electrolyte sample was replaced and the microdisc electrode was polished. The measurements were performed at several scan rates and the diffusion limiting current was observed to determine the diffusion coefficients of lithium ions in the ionic liquid.

3.2.2.3. Diffusion coefficient measurement 2: Restricted Diffusion Method

Electrolyte samples were contained in PTFE (poly-tetrafluoroethylene) holders (inner diameter = 5 mm, thickness = 1.2 mm) and placed between lithium metal electrodes. A

0.5 mA cm^{-2} of constant current was applied between electrodes for 15 minutes to give a polarisation and a potential relaxation was monitored up to 24 hours. The diffusion coefficient was estimated from the gradient of the linear portion of the plot of ln E vs. time [10,11].

3.3. Results and discussion

3.3.1. Mass density of a mixture of LiTFSI and EMITFSI

The mass densities of variously concentrated samples were measured and the concentration unit was transferred from wt% to mol dm^{-3}, which is more convenient for the following investigations, as shown in Fig. 3.2. The density of electrolytes greatly depends on the concentration of lithium salt and gives a 7 % increase from neat EMITFSI to 1.5 mol dm^{-3} LiTFSI / EMITFSI. The increase in the value may suggest the existence of stronger ionic interaction between cations and anions at higher concentrations of lithium salt.

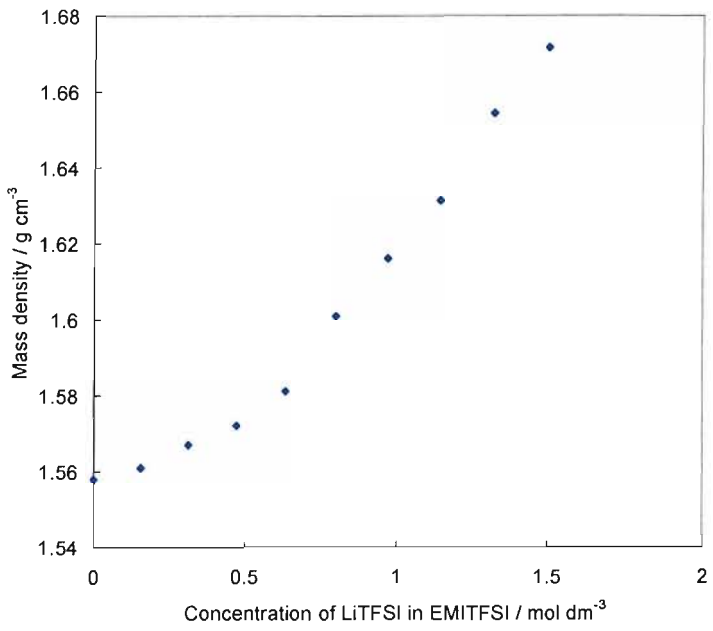

Fig. 3.2 Mass densities of mixtures of LiTFSI and EMITFSI at 298 K

3.3.2. Conductivity

Fig. 3.3 shows a typical result of impedance spectra obtained from LiTFSI/EMITFSI. With using stainless steel blocking electrodes, the electron transfer according to a redox reaction at the interface between the current collectors and electrolyte samples is prevented. The shapes of spectra present almost ideal behaviour of a circuit which has a series component of a resistor and capacitor. Therefore, the intercept onto the horizontal axis gives a resistance of electrolytes. The resistance decrease with an increase in temperature, indicating that the total conductivity of electrolytes was enhanced.

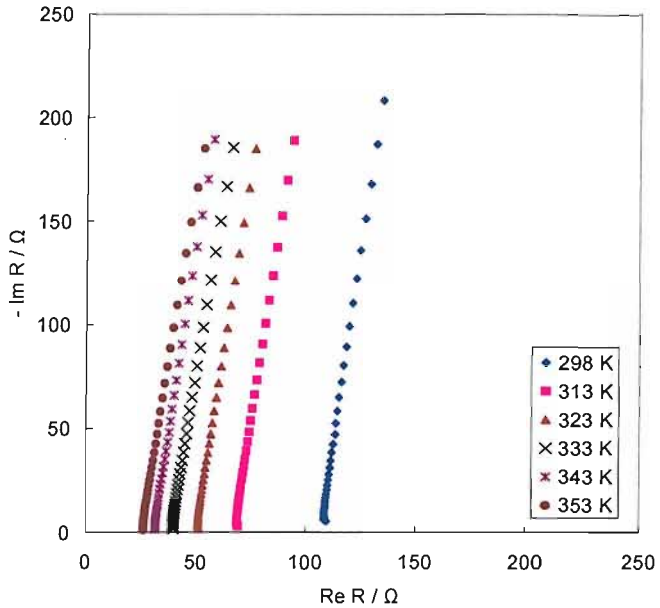

Fig. 3.3 Impedance spectra of 0.47 mol dm^{-3} LiTFSI/EMITFSI, measured with blocking electrodes (stainless steel current collectors)

The dependence of conductivity on temperature and lithium salt concentration is summarised in Fig. 3.4. With an increase in LiTFSI concentration, the conductivities of the electrolytes decrease, presumably because of the viscosity increase due to lithium ions associating with the ionic liquid. A mean activation energy for existing ions in the electrolyte, such as EMI^+, $TFSI^-$ and Li^+ can be calculated from temperature dependence of the conductivity and will be discussed later.

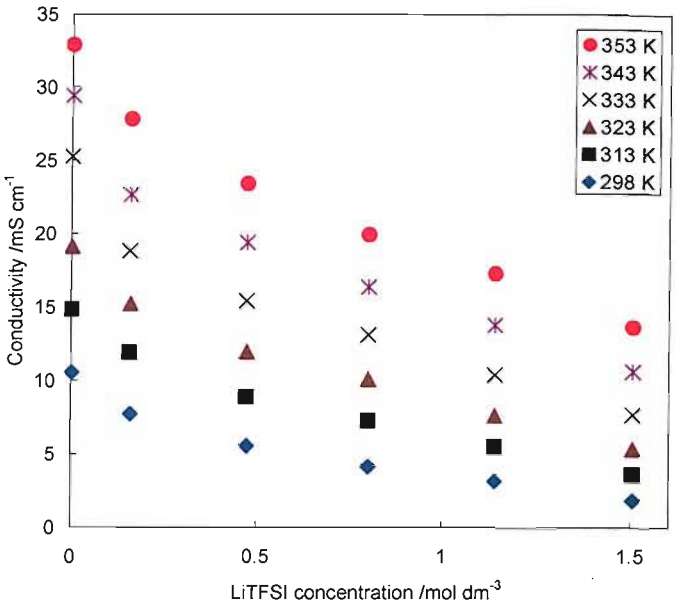

Fig. 3.4 Conductivities of LiTFSI / EMITFSI electrolytes at the various concentrations of LiTFSI and temperature.

For comparison, the trend of conductivities on lithium salt concentration is shown in Fig. 3.5. Here, there is a peak of conductivities around the concentration of 1 mol dm^{-3} because organic solvents need charge carriers (ions) to present conductivities but the excessive concentration of salt makes them more viscous. In contrast, the ionic liquid has a simple trend on conductivities without a peak. Therefore, it is considered to be more difficult for ionic liquids than for organic solvents to optimise the lithium salt concentration in electrolytes for lithium batteries. This will be discussed more in Chapter 4.

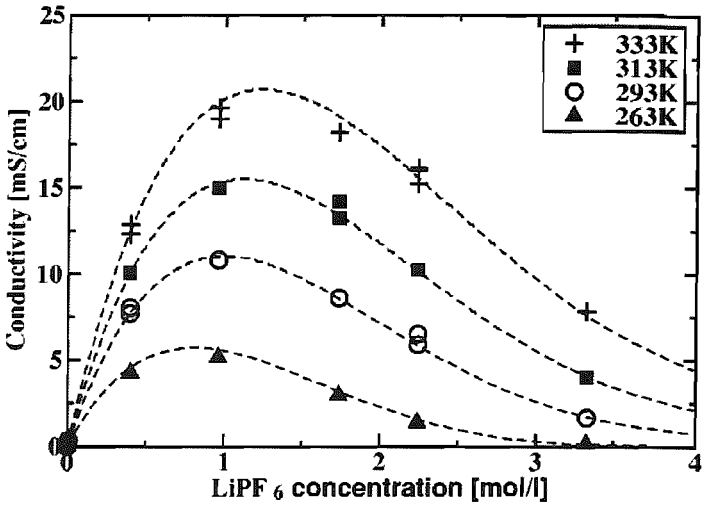

Fig. 3.5 Dependence of the conductivities of lithium ions on concentration of $LiPF_6$ in PC/EC/DMC [7]

3.3.3. Diffusion coefficient by the potential relaxation method

In Chapter 2, we suggested that reversible lithium deposition and stripping is possible on lithium metal without violent decomposition of EMITFSI due to the formation of a solid electrolyte interface.

The procedure applied here to obtain the diffusion coefficient of lithium ions in the ionic liquid was "Restricted Diffusion Method" which has been reported by the Barkley Group [10,11]. The main concept is to measure the potential relaxation using two non-blocking electrodes after a constant current pulse is given between them. The voltage of cells follows eq. 3.1 below, as concentration profiles relax.

$$-\frac{\ln \chi}{t} = \frac{\pi^2 D}{L^2} \qquad \text{eq. 3.1}$$

Where χ is the voltage of the cell, t is time, D is the diffusion coefficient and L is the distance between electrodes

As shown in Fig. 3.6, the initial voltage of the cells after the assembly is 0 V since this is a symmetrical cell and a constant current pulse gave a polarised state; at the vicinity of the anode, lithium ion concentration is high and around the cathode, the other way around. Immediately after the interruption of the pulse, the potential profile showed an

IR drop, followed by the double layer discharge. Subsequently, the profile presented an approximately exponential decay of voltage, which corresponded to the relaxation of distributed ions.

One advantage of this method is that it should not involve the resistance of the SEI film at the surface of lithium electrode because this is potential profile measurement without a current flow.

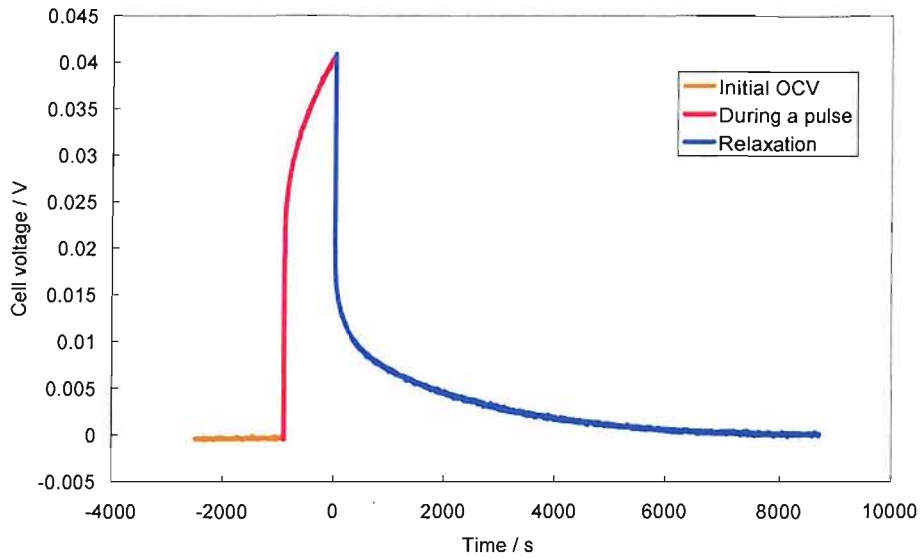

Fig. 3.6 Potential profile during the potential relaxation method; 0.47 mol dm^{-3} LiTFSI / EMITFSI between lithium metal electrodes at 353 K

To investigate the rate of relaxation quantitatively, the potential decay was transformed into the logarithmic scale as shown in Fig. 3.7. Slopes with larger gradient reflect that the electrochemical system needed less time to relax the concentration distribution. If we chose a too early stage of the relaxation profiles to estimate the inclination, the value is affected by a potential decay depending on a square of time (semi-infinite boundary condition), and if too late, we cannot get an accurate value for the inclination because we must treat a data with less than 1 mV change in a few hours. Therefore, the gradient is measured at the last stage of relaxation. In this way we should be able to eliminate

any other processes, such as discharge of some pseudocapacitance under a mixed potential situation at a non uniform SEI. The chosen gradient gives a value for the time constant of the slowest process, which we assume to be relaxation of concentration gradients in the electrolyte region by diffusion alone. Fig. 3.7 shows a typical example of the slopes from a LiTFSI / EMITFSI sample and the gradient increase at higher temperature.

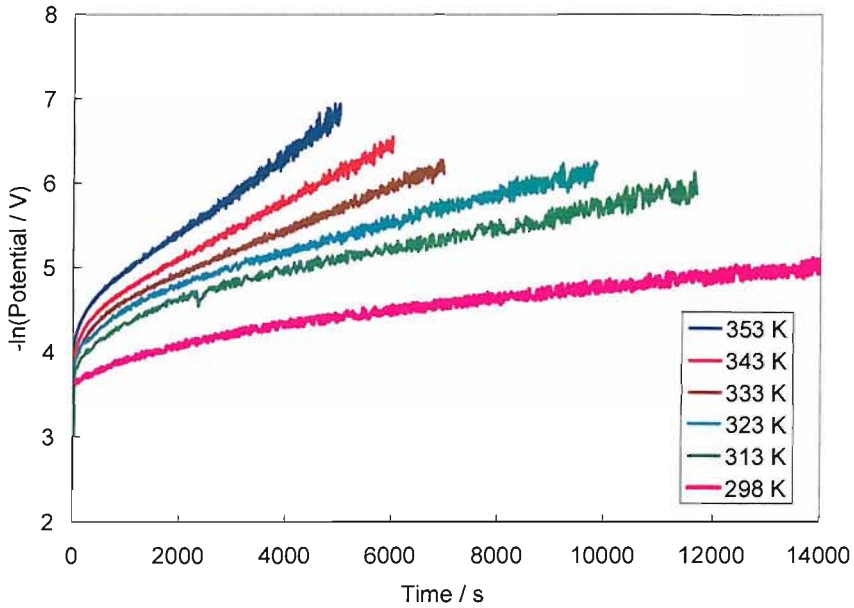

Fig. 3.7 Examples of the gradient calculation; 0.47 mol dm^{-3} LiTFSI / EMITFSI

As the gradient is a function of the diffusion coefficient as expressed in eq. 3.1, the results are exhibiting the expansion of the diffusion coefficient by temperature.Those values for diffusion coefficients of lithium ions were summarised in Fig. 3.8. Two trends can be observed from the figure; temperature dependence and lithium salt concentration dependence. At any concentrations, diffusion coefficients were larger at higher temperatures and this will be quantitatively analysed later as the activation energy. The diffusion coefficients decreased to the half as the concentration of lithium increased from 0.17 mol dm^{-3} to 1.5 mol dm^{-3} and the trend is similar to that of conductivities.

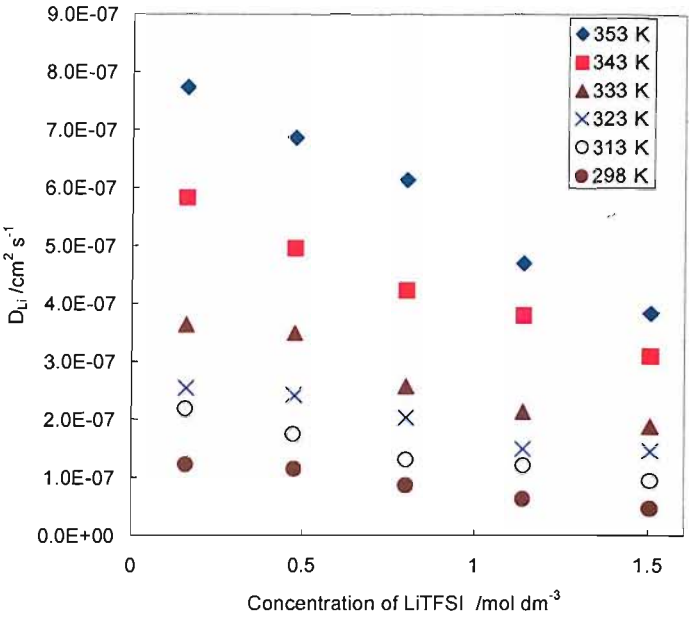

Fig. 3.8 Diffusion coefficients of lithium ion constitutions in EMITFSI containing various concentrations of LiTFSI, obtained by a potential relaxation method

The value obtained here for 0.47 mol dm^{-3} in the mixture of LiTFSI and EMITFSI at 298 K is 1.2 x 10^{-7} cm^2 s^{-1}, which is *ca.* 100 times smaller than the diffusion coefficients in $LiPF_6$ / EC:DMC, 1.4 x 10^{-5} cm^2 [12]. However, the trend of the diffusion, a simple decrease with the salt concentration, is similar to that of the electrolyte with organic solvents.

3.3.4. Diffusion coefficient by the microelectrode technique

It is known that the values of diffusion coefficients are sometimes affected by a method used to determine them. Therefore, it is desirable to regard more than two experimental values from different techniques to consider the validity of results.

As studied in Chapter 2, at a very dehydrated condition and on a nickel microdisc electrode, it was suggested that a protective layer (a solid electrolyte interface) is formed at the interface between the electrode and the ionic liquid in the existence of LiTFSI salt. The layer prevented violent decomposition of the electrolyte and allowed

lithium deposition and stripping; therefore kinetics of lithium reaction including lithium ion diffusion may be studied in the mixture of LiTFSI and EMITFSI.

Linear sweep voltammograms on the nickel microdisc in 0.47 mol dm^{-3} LiTFSI / EMITFSI at several scan rates are shown in Fig. 3.9. Generally speaking, 10 mV s^{-1} is a relatively slow scan rate for a microelectrode study, but still an obvious current peak was obtained, suggesting that the scan rate is too fast to obtain steady state voltammograms. With decreasing the scan rate, voltammograms show nearly ideal behaviour corresponding to metal plating limited by hemispherical diffusion in the solution phase. The peak diminished and steady state voltammogram was obtained at 1 mV s^{-1}.

The total reaction rate might be affected by the resistive protective film between the electrolyte and the electrode; however the effect should be small because the shape of voltammograms were not controlled by one simple resistive factor, which should show straight line shape voltammograms as seen in Fig 2.23.

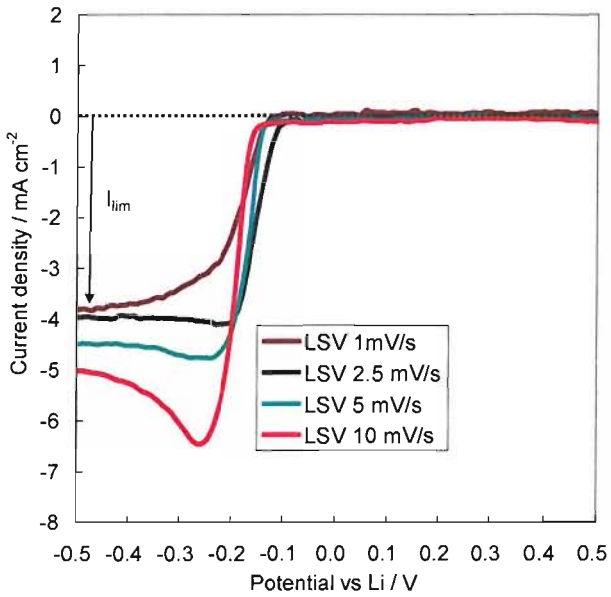

Fig. 3.9 Linear sweep voltammograms on a nickel microdisc (diameter = 45 μm) in 0.47 mol dm^{-3} LiTFSI / EMITFSI

The diffusion coefficient of lithium ions in the electrolyte was calculated using the eq. 2.7 ($I = 4nFDac$) and the obtained value was 1.4 x 10^{-7} cm^2 s^{-1}, which is close to the value 1.2 x 10^{-7} cm^2 s^{-1} reported for a similar ionic liquid system, 0.5 mol dm^{-3} $LiBF_4$ in $EMIBF_4$ [9]. These values are 1 - 2 order smaller than the diffusion coefficients in ordinary organic electrolytes or an aqueous system. Therefore, it is reasonable that voltammograms needed to be relatively slow to obtain a steady state.

In Chapter 2, it was shown that the electrolyte does not decompose violently during lithium deposition and stripping; however a small part of the electrolyte may decompose to form the protective layer especially at a high overpotential. With this microelectrode technique for determining the diffusion limiting current, it is difficult to eliminate this additional decomposition current perfectly and the diffusion coefficient of lithium might be calculated larger, which can be one of the reasons why the value obtained here is slightly larger than that from the restricted diffusion method as shown in Table 3.1. On the other hand we note that the results of the restricted diffusion and microelectrode method agree within the error limits. This gives some confidence regarding the assumption that the time constant observed during relaxation related to diffusion in the electrolyte and not to some other process.

Table 3.1 Diffusion coefficients of Lithium ions in 0.47 mol dm^{-3} LiTFSI / EMITFSI and comparable systems (Estimations of the standard error are 10% for both restricted diffusion and microelectrode methods.)

D in cm^2 s^{-1}	0.47 mol dm^{-3} LiTFSI / EMITFSI	0.47 mol dm^{-3} LiTFSI / EMITFSI	0.5 mol dm^{-3} $LiBF_4$ /$EMIBF_4$	1.0 mol dm^{-3} $LiPF_6$ in EC:DMC
Restricted diffusion	1.2 x 10^{-7}			
Microelectrode		1.4 x 10^{-7}		
NMR			1.5 x 10^{-7} [9]	
Rotating electrode				1.4 x 10^{-5} [12]

3.3.5. Activation energy

Fig. 3.10 shows the temperature dependence of the total ionic conductivities of EMITFSI containing various concentrations of LiTFSI. The dependency fits closely to

the straight line of Arrhenius plot, suggesting no emergent change in the state of each ion in the electrolyte in this temperature region. Therefore, from each gradient, we can estimate the sum of the activation energies of conduction performed by each ionic species existing in the electrolyte.

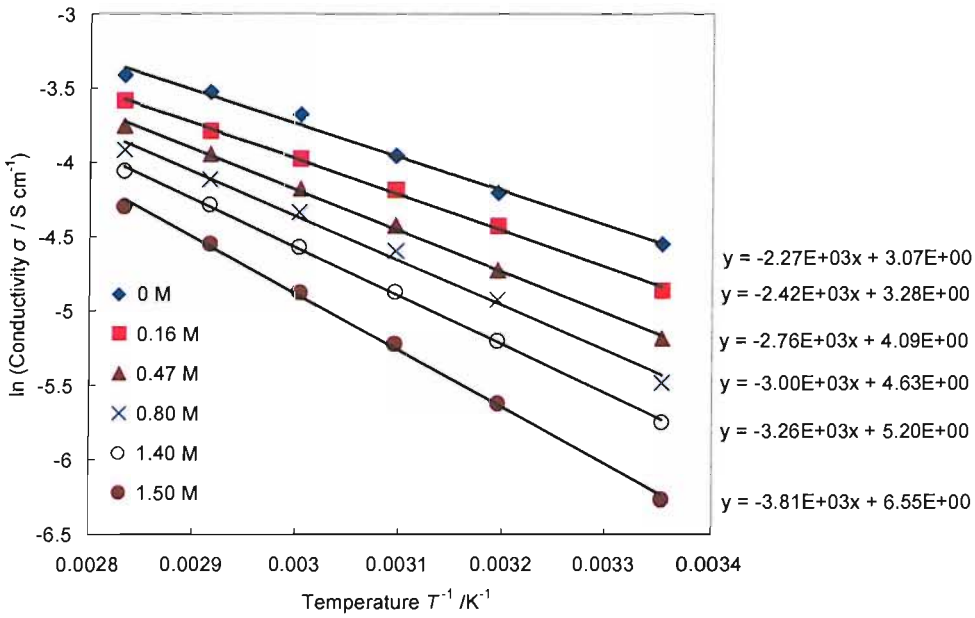

Fig. 3.10 Temperature dependence of total conductivities of LiTFSI / EMITFSI

The temperature dependence of the diffusion coefficients of lithium ions in the ionic liquid is shown in Fig. 3.11. Unlike with the case of the total conductivity, these plots have more scatters from the straight line of Arrhenius plot. This impreciseness is attributable to the long measurement duration for the diffusion coefficients; the 1 day long measurement may give convection problem. A low Signal / Noise rate also could have affected the result.

Those Arrhenius plots at various concentrations of lithium salt show uniform gradients, indicating that the activation energy for the solvation of lithium ions are not much influenced by the concentration.

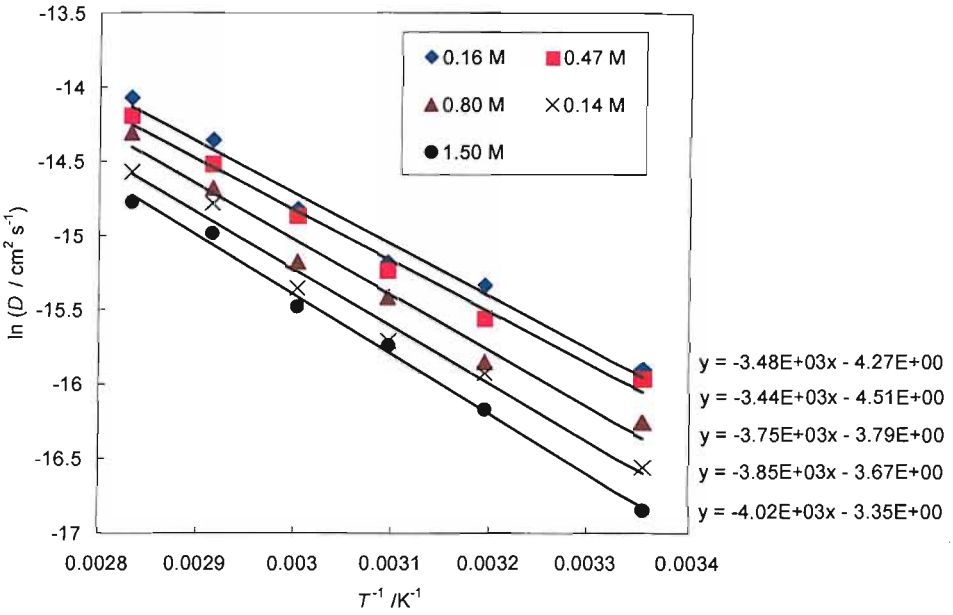

Fig. 3.11 Temperature dependence of diffusion coefficients of lithium ions in LiTFSI / EMITFSI

Activation energies of the lithium diffusion and total ion conduction at the various concentrations of lithium salt are shown in Fig. 3.12. Two obvious trends have been found from the figure. The first is that the activation energies for the lithium diffusion were larger than those of the total ion conduction, especially at lower concentrations. The second is that both activation energies increase with the concentration of lithium ions. Each results suggest the interaction between lithium ions and TFSI anions is more intensive that between EMI cations and TFSI anions.

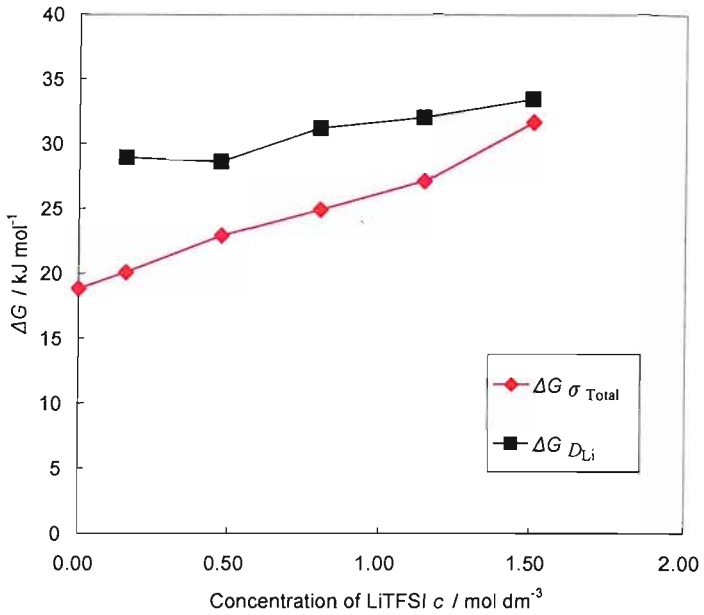

Fig. 3.12 Activation energies of the total ion conduction and the lithium diffusion in the mixture of LiTFSI and EMITFSI

3.3.6. Transference number

The transference number is described as below.

$$t_{Li^+} = \frac{\sigma_{Li^+}}{\sigma_{Li^+} + \sigma_{EMI^+} + \sigma_{TFSI^-}} \qquad \text{eq. 3.2}$$

Where t_{Li+} is the transference number of lithium ions, σ_{Li+} is conductivity of lithium ions, σ_{EMI+} is conductivity of EMI cations, σ_{TFSI-} is the conductivity of TFSI anions

The conductivity due to lithium ions was evaluated from the diffusion coefficient of lithium ions according to Nernst-Einstein Equation

$$\sigma = \frac{z^2 F^2 cD}{RT} \qquad \text{eq. 3.3}$$

Where z is the valence of the ion, F is the Faraday constant, c is concentration of the ion, D is the diffusion coefficient of the ion, R is the gas constant and T is the temperature

Hence, the transference number was derived as below.

$$t_{Li^+} = \frac{F^2 c_{Li^+} D_{Li^+}}{RT\sigma_{total}} \qquad \text{eq. 3.4}$$

Fig. 3.13 shows the transference numbers of the electrolyte at various concentrations calculated by the above method. As it was expected, the number becomes large with an increase in the concentration of lithium ions. This is completely different from the trend of lithium salt in organic solvents, which shows less dependence on the concentration.

Although limited numbers of studies have been made for the transference numbers of ionic liquids containing lithium ions, one example [9] shows a small number, t = 0.015 for lithium ions in 0.5 mol dm^{-3} $LiBF_4$ / $EMIBF_4$. On the other hand, the value obtained for 0.47 mol dm^{-3} LiTFSI / EMITFSI in our investigation was more than twice, t = 0.035.

The difference may be from the variation of viscosity and ion dissociation [13,14]. TFSI anions have a larger size than that of BF_4 anions; therefore samples including TFSI anions are more viscous and less conductive than those of BF_4 anions when the concentration of lithium ions is same. To the contrary, due to the high level of the charge delocalisation of the imide anions, TFSI anions are known to dissociate very well even in low dielectric solvents and the degree of dissociation is better than BF_4 anions. Collectively, the high dissociation of TFSI samples countervails the smaller conductivity and makes the similar diffusion coefficients of lithium ions as BF_4 samples have. Finally, the smaller conductivities and similar diffusion coefficient cause the high transference number of TFSI samples.

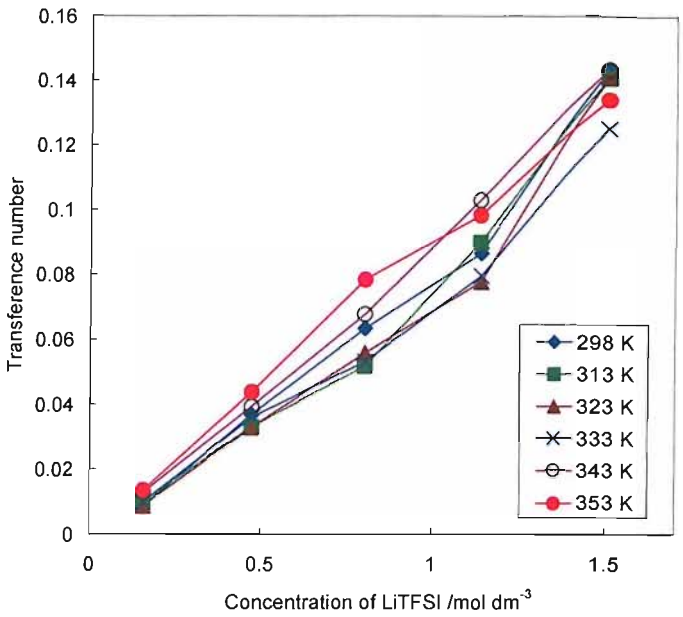

Fig. 3.13 Transference numbers of lithium ions in the mixture of LiTFSI and EMITFSI at various concentrations

The effect of temperature on the transference number is less than that of lithium salt concentration. However, a closer inspection into Fig. 3.14 presents an increasing trend of the transference numbers with temperature, except for the case for 1.5 mol dm^{-3}. This is because the total conductivities have less dependence on temperature (= the activation energy) than the diffusion coefficients at lower concentrations.

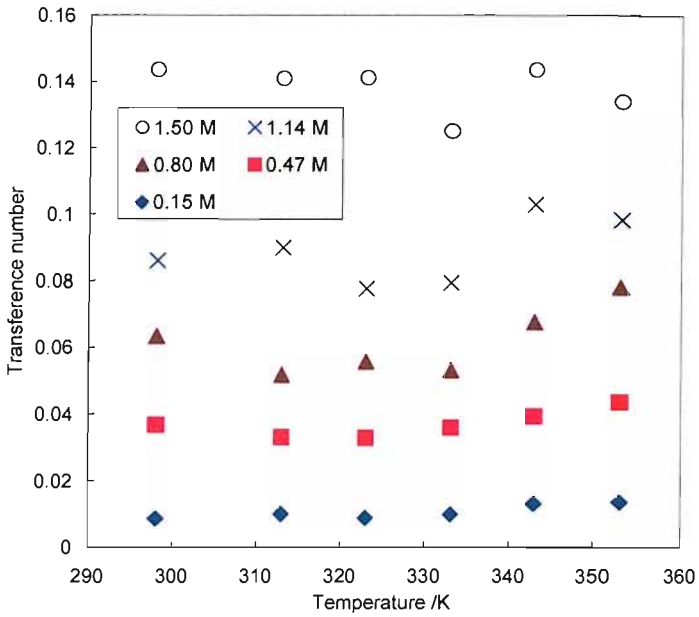

Fig. 3.14 Temperature dependence of transference numbers in the mixture of LiTFSI and EMITFSI

3.4. Conclusion of the chapter

To consider the potential of EMITFSI as an electrolyte for lithium batteries, various concentrations of LiTFSI were added into the ionic liquid and ion transport properties, such as conductivities, diffusion coefficients and transference numbers in the ionic liquid electrolyte were studied.

Neat EMITFSI has a conductivity of 10.5 mS s^{-1} at 298 K and is as conductive as 1 mol dm^{-3} $LiPF_6$ / EC:DMC, which is one of the most conductive electrolytes for practical lithium ion batteries. Conductivities decrease with an increase in lithium salt concentration but are still relatively high for non-aqueous electrolytes; 5.6 mS s^{-1} for 0.47 mol dm^{-3} LiTFSI / EMITFSI at 298 K.

Diffusion coefficients of lithium ions in the ionic liquid were measured by the restricted diffusion method and microelectrode technique. Increasing the concentration of lithium salt causes a decrease in the diffusion coefficients. This is similar to the dependence of the conductivities on the concentrations. Both results imply strong association of lithium ions with anions. The diffusion coefficient obtained for 0.47 mol dm^{-3} LiTFSI / EMITFSI was .1.2 x 10^{-7} cm^2 s^{-1} by restricted diffusion method and 1.4 x 10^{-7} cm^2 s^{-1} by microelectrode technique. Even though conductivities are several times smaller than those of $LiBF_4$ / $EMIBF_4$, the diffusion coefficients of lithium ions in both ionic liquid systems did not have a significant difference. It was found that the coefficients in the ionic liquids are ca. 100 times smaller than the value for 1 mol dm^{-3} $LiPF_6$ / EC:DMC, 1.2 x 10^{-5} cm^2 s^{-1}

Activation energies for the total ion conduction are smaller than those for the lithium diffusion. Also, both activation energies exhibit a linear increase with the concentration of lithium salt. Each result suggests a stronger interaction of lithium ions with $TFSI^-$ than that of EMI^+.

From the total ion conductivities and diffusion coefficients, the transference number of lithium ions in the ionic liquid was calculated. The numbers are proportional to the concentration of the lithium salt and show small dependence on temperature. As compared to the transference number of $LiBF_4$ / $EMIBF_4$, the numbers of LiTFSI /

EMITFSI are higher at the same concentrations of lithium salt and the same temperatures. The difference may be explained with two factors; the difference size and dissociation level of anions.

References

1. M. Schmidt, U. Heider, A. Kuehner, R. Oesten, M. Jungnitz, N. Ignat'ev and P. Sartori, *J. Power Sources*, **97**, 557 (2001).

2. M. Ue and S. Mori, *J. Electrochem. Soc.*, **142**, 2577 (1995).

3. M. Galinski, A. Lewandowski and I. Stepniak, *Electrochim. Acta*, 51, 5567 (2006).

4. W. G. Pell, B. E. Conway and N. Marincic, *J. Electroanal. Chem.*, **491**, 9 (2000).

5. D. Y. W. Yu, K. Donoue, T. Inoue, M. Fujimoto and S. Fujitani, *J. Electrochem. Soc.*, **153**, A835 (2006).

6. M. Gaberscek, M. Kuzma and J. Jamnik, *Phys. Chem. Chem. Phys.*, **9**, 1815 (2007).

7. L. O. Valoen and J. N. Reimers, *J. Electrochem. Soc.*, **152**, A882 (2005).

8. A. Noda, K. Hayamizu and M. Watanabe, *J. Phys. Chem. B*, **105**, 4603 (2001)

9. K. Hayamizu, Y. Aihara, H. Nakagawa, T. Nukuda and W. S. Price, *J. Phys. Chem. B*, **108**, 19527 (2004).

10. Y. P. Ma, M. Doyle, T. F. Fuller, M. M. Doeff, L. C. Dejonghe and J. Newman, *J. Electrochem. Soc.*, **142**, 1859 (1995).

11. H. Hafezi and J. Newman, *J. Electrochem. Soc.*, **147**, 3036 (2000).

12. S. I. Lee, U. H. Jung, Y. S. Kim, M. H. Kim, D. J. Ahn and H. S. Chun, *Korean J. Chem. Eng.*, **19**, 638 (2002).

13. A. Webber, *J. Electrochem. Soc.*, **138**, 2586 (1991).

14. M. Ue, *J. Electrochem. Soc.*, **141**, 3336 (1994).

Chapter 4. Ion transport in porous electrodes

4.1. Introduction

In Chapter 3, we investigated lithium ion transfer parameters, such as conductivity, and diffusion in bulk LiTFSI / EMITFSI. The diffusion coefficient is 100 times smaller than that of 1 mol dm^{-3} $LiPF_6$ / EC:DMC, and therefore should significantly affect the behaviour of batteries. A few studies have been made for batteries using ionic liquids; however those are usually charged / discharged at very slow rates, such as C/8.

It is well known that larger conductivities and diffusion coefficients cause better battery performance; however, few quantitative studies have been made for the relation between these parameters and the rate capabilities of lithium batteries.

In this chapter, the diffusion of lithium ions in $LiFePO_4$ composite electrodes will be investigated and how the lithium mobility affects the charge/discharge behaviour of the cell using the ionic liquid electrolyte will be discussed.

4.2. Experimental

4.2.1. Synthesis of EMITFSI and LiTFSI/EMITFSI

1-Ethyl-3-methylimidazolium bis-(trifluoromethylsulfonyl)-imide (EMITFSI) and LiTFSI/EMITFSI were prepared as mentioned in Chapter 2.

4.2.2. Electrochemical measurement

a) Measurements of lithium ion diffusion coefficient in a glass filter paper

The diffusion coefficient of lithium ions in glass filter soaked with a mixture of LiTFSI and EMITFSI was measured by the restricted diffusion method as mentioned in Chapter 3.

b) Preparation of electrodes

As positive electrodes, carbon coated $LiFePO_4$ (Aldrich, Battery Grade) was made into ink with acetylene black and PVdF-HFP (Aldrich, Battery Grade) at the weight ratio of 70:20:10 in cyclopentanone. The ink was coated on an aluminium foil (15 μm) by K-bar method. As negative electrodes, the same method was applied for $Li_4Ti_5O_{12}$ (Süd Chemie, EXM 1037). Positive electrodes were coated at 6 to 50 μm thickness; negative electrodes were 100 μm thick. For reference electrodes, a copper wire was coated with a mixture of $LiMn_2O_4$ and $Li_2Mn_2O_4$ (synthesised as in Chapter 2) ink or wrapped with lithium foil.

b)Assembly of lithium ion cells

The cells were assembled as shown in Fig. 4.1. Two sheets of glass filter paper were used as the separator and soaked with mixtures of LiTFSI and EMITFSI or 1 mol dm^{-3} $LiPF_6$ / EC:DMC. The reference electrode was pierced through the o-ring and inserted between those separator sheets. After the assembly, the cells were heat treated at 60 °C for 12 hours to allow the penetration of the electrolyte into the composite electrodes.

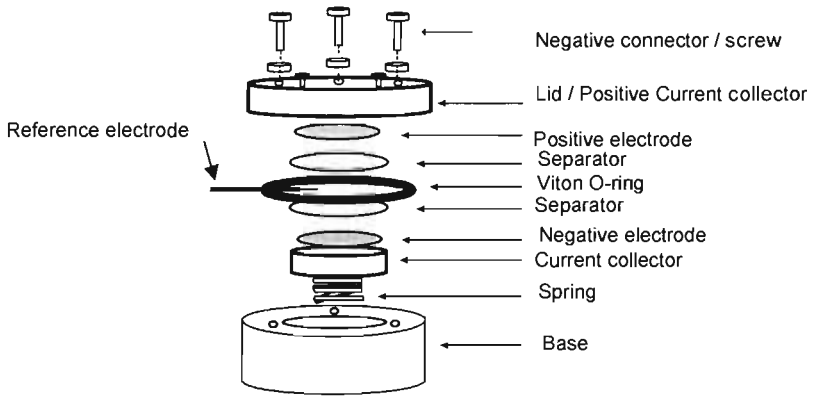

Fig. 4.1 Illustration showing a cell used for the measurements of rate capability of $LiFePO_4$ composite electrodes containing the ionic liquid.

c) Charge and discharge of the cells

Cells were charged to 4.5 V vs Lithium and discharged to 2.0 V vs Lithium. Before increasing the charge or discharge current, cells were cycled 8 times at 0.25 C to obtain stable discharge capacities. To study the effects of charge rates, the currents were varied from 0.25 C to 90 C while the discharge rate was kept at 0.25 C and discharge capacities were used to compare the rate capabilities. Charge currents were held at 0.25 C when the discharge rates were varied from 0.25 C to 90 C.

d) GITT technique

Galvanostatic Intermittent Titration Technique (GITT) was performed on the same configuration of cells, including reference electrode. After a constant current pulse (1 C) was applied, the cell was kept at open circuit and potential relaxation profiles were monitored for 20 minutes. The pulses and relaxation were repeated until the cell potential reached 4.5 V vs. Li. The polarity of pulses was changed and GITT for cell discharge was also performed down to 2.0 V.

4.3. Results and discussion

4.3.1. Diffusion coefficient of lithium ions in the separator

In this chapter, we will investigate the effect of lithium diffusion in composite electrodes of lithium batteries. However, lithium ion diffusion might be also hindered in glass filter separators and the effect would make the results difficult to separate from the effect which we will study. Therefore, the diffusion in the separator immersed in the ionic liquid electrolyte was measured by restricted diffusion method using lithium metal electrodes as the non-blocking electrode.

The diffusion coefficients in separators containing a mixture of LiTFSI / EMITFSI were measured as shown in Fig. 4.2. The values appear less accurate than those for bulk LiTFSI / EMITFSI; this may result from the poor accuracy of the electrode distance. A 0.1 mm error in the measurement of thickness can cause a 20 % of difference in the

final value of diffusion coefficients. The diffusion coefficients in the separators are within 30 % from those in the same formula for bulk electrolytes. This is attributable to the error mentioned above It was shown that the influence of the glass filter is insignificant and the electrolytes contained in separators can be treated as the bulk.

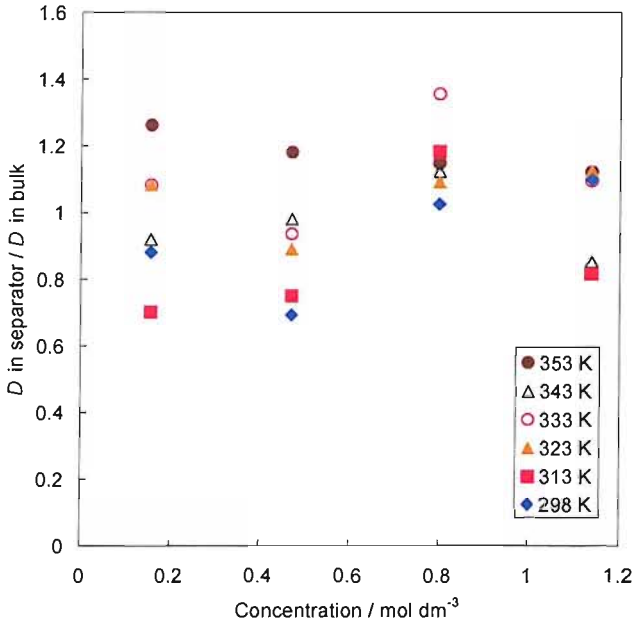

Fig. 4.2 Diffution coefficients of lithium ions in glass filter separators containing a mixture of LiTFSI and EMITFSI, measured by the restricted diffusion method

4.3.2. Electrode porosity and uniformity

The purpose of the chapter is to study the diffusion of lithium ions in the ionic liquid electrolyte penetrating into the voids of composite electrodes. Therefore, it is important to know the morphology of particles used as active materials and the porosity of electrodes. Also, we need to obtain relatively uniform composite electrodes in terms of thickness and structure.

Fig. 4.3 shows the $LiFePO_4$ particles morphology. These particles are more flake or bar shaped than spheres or cubes and the longest side of the particles is from 2 μm to 10 μm.

Fig. 4.3 SEM images of $LiFePO_4$ particles used for positive electrode

Fig. 4.4 shows that the trend is almost linear and that confirms the structure such as the porosity and tortuosity of the electrodes from the same $LiFePO_4$ ink is uniform. The porosity of electrode was calculated as 0.65, using the true density of $LiFePO_4$ = 3.5 g cm^{-3}, acetylene black (assuming the value is same as that of graphite) = 2.2 g cm^{-3} and PVdF-HFP = 1.8 g cm^{-3}.

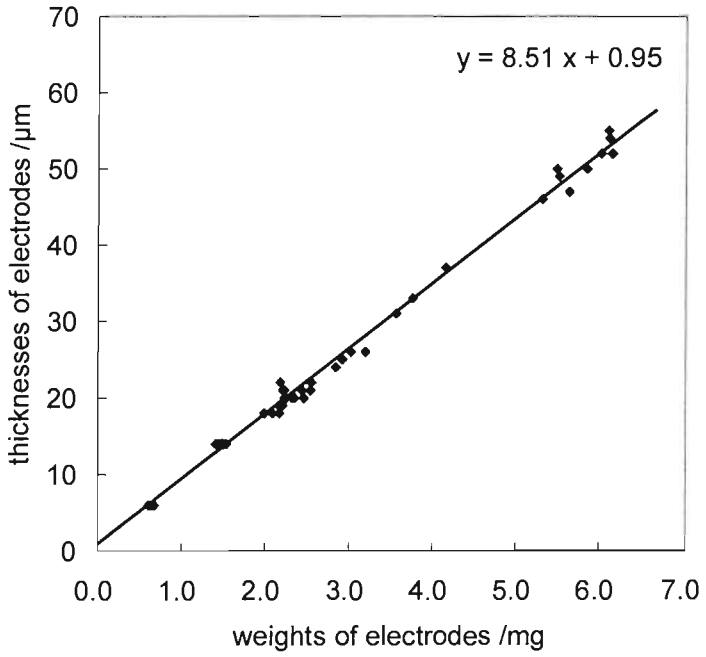

Fig. 4.4 Relation between electrode thickness and weight

Although particles which have the 10 μm sides were found from SEM images, the trend does not present steps but a relatively smooth linear line, even down to 6 μm thickness. As shown in Fig. 4.3, the particles are not cubic or spherical and have shorter sides. Therefore, the particles can lie when the solvent is volatised from the ink and pile as shown in Fig. 4.5. This is an explanation of why the size effect was not observed on the relation between thickness and weight. Nevertheless, to obtain a uniformity of the electrode, its thickness must be more than the shortest sides of the particles, estimated at around 5 μm.

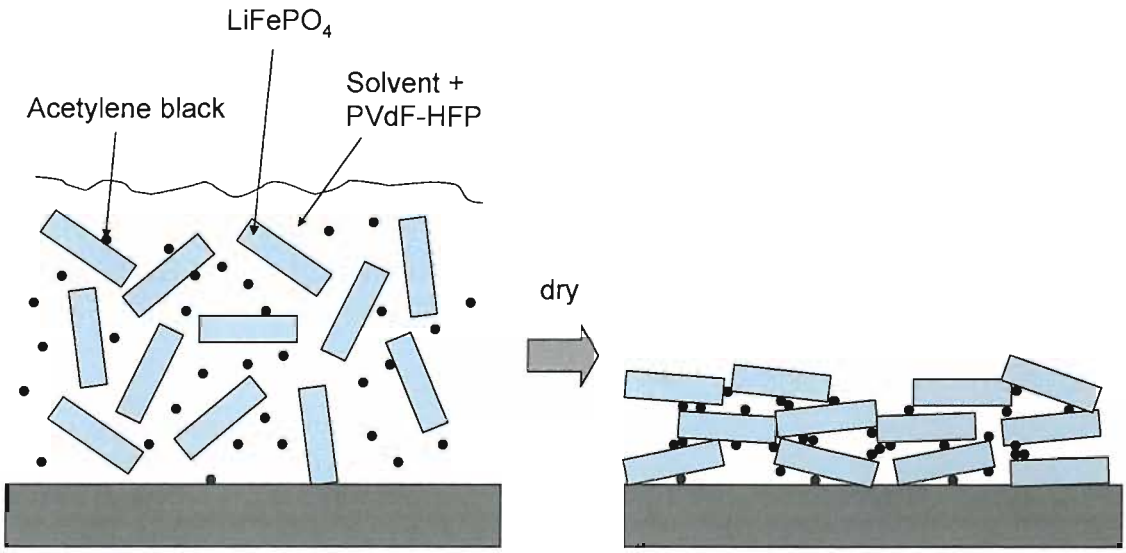

Fig. 4.5 Schematic illustration showing formation of a film from an ink

4.3.3. 2 electrode cell (Lithium counter electrode)

Initially, our investigations were based on 2 electrode cells because it was difficult to seal thoroughly a reference electrode in the measurement cell containing the ionic liquid electrolyte, which requires very dehydrated conditions.

Lithium is usually used as the common counter / reference electrode for investigations on lithium rechargeable batteries because it is believed that the redox potential is stable and the reaction is fast enough to observe the phenomena at the positive electrode. In chapter 2, the stability of the solid electrolyte interface formed between lithium and LiTFSI / EMITFSI was shown; therefore, our first attempt of studies on the rate

capabilities of lithium batteries containing the ionic liquid electrolyte was made using lithium counter electrodes.

Typical discharge potential profiles of the cell are shown in Fig. 4.6. The capacities decreased with an increase in the discharging rate. In the case of the 6 μm thickness electrode (Fig. 4.6), the cell retained a capacity of 100 mAh g^{-1} at 10 C and 70 mAh g^{-1} at 30 C. These values at such fast C-rate are high compared with those reported [1]. From the particle sizes, it is estimated that the $LiFePO_4$ particles formed only one or a few layers in the thickness direction of the 6 μm thickness electrode. Therefore, the Li ionic current flow was not greatly hindered in the porous electrode structure. On the other hand, in the case of the 49 μm thickness electrode (Fig. 4.7), the capacities decreased significantly with the increase in current from 0.5 C to 1 C. During the "discharge", lithium ions are inserted into $LiFePO_4$ and the result shows that lithium ions are not sufficiently supplied into the deep part of the electrode. The last part of each discharging profile (from 2.5 V to 2.0 V), the curves are almost straight lines and the gradients are constant in Fig. 4.6.

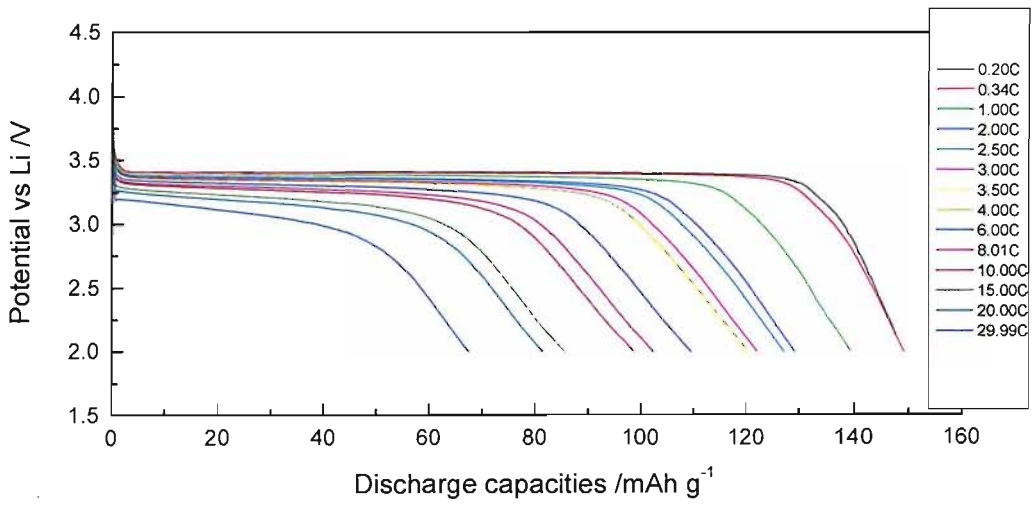

Fig. 4.6 Potential profiles of a 6 μm $LiFePO_4$ electrode in 0.47 mol dm^{-3} LiTFSI / EMITFSI at various discharge rates. The common counter / reference electrode is lithium metal.

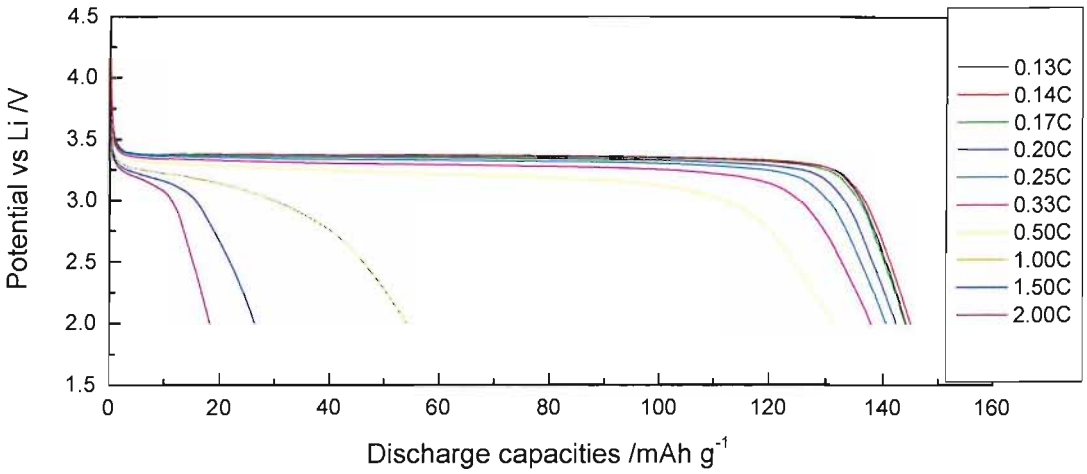

Fig. 4.7 Potential profiles of a 49 μm $LiFePO_4$ composite electrode in 0.47 mol dm^{-3} LiTFSI / EMITFSI at various discharge rates. The common counter / reference electrode is lithium metal.

The effects of the electrode thickness including above results are shown in Fig. 4.8. In the case of 20 and 49 μm electrodes, we can clearly see that plots are on the straight line at high discharge current; however, the extrapolation is not via the origin. Interpretation of the date in Fig. 4.8 shows that capacities were partially limited by a diffusion factor; however, the other factors such as the passivation or decomposition of the electrolyte at the counter electrode also might affect the result.

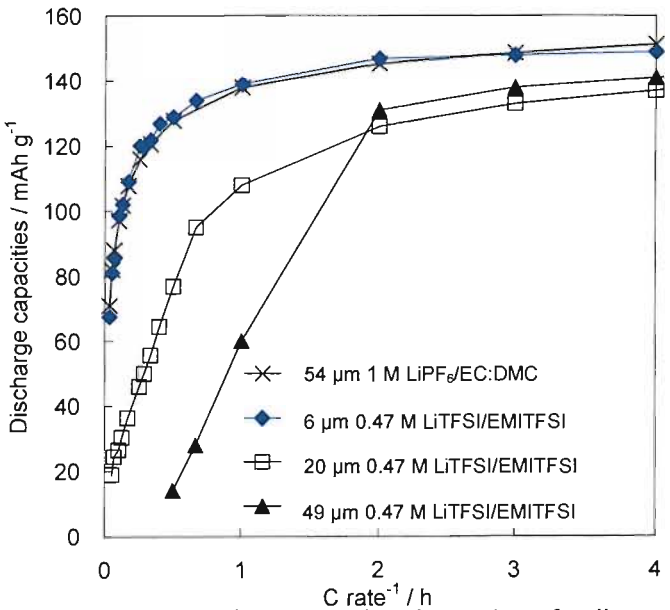

Fig. 4.8 Rate capabilities of $LiFePO_4$ composite electrodes of cells containing 0.47 mol dm^{-3}. The common counter / reference electrode was lithium metal.

4.3.4. 2 electrode cell ($Li_4Ti_5O_{12}$ counter electrode)

Instead of using lithium metal as the common counter / reference electrode, the use of $Li_4Ti_5O_{12}$ was also studied. The advantage to use $Li_4Ti_5O_{12}$ as the counter electrode is that the material is definitely stable with EMITFSI and the lithium insertion potential is much higher than lithium then we don't need to be concerned about the decomposition of the electrolyte.

Fig. 4.9 shows an example of potential profiles during constant current charge and discharge of the $LiFePO_4$ composite electrode. In the case of the lithium counter electrode, the profiles show stable plateaus at 3.5 V vs lithium and the start of charge and end of discharge are angular as shown in Fig. 4.10. In contrast, the start of charge and end of discharge show rounded curves when $Li_4Ti_5O_{12}$ was used as the common counter / reference electrode.

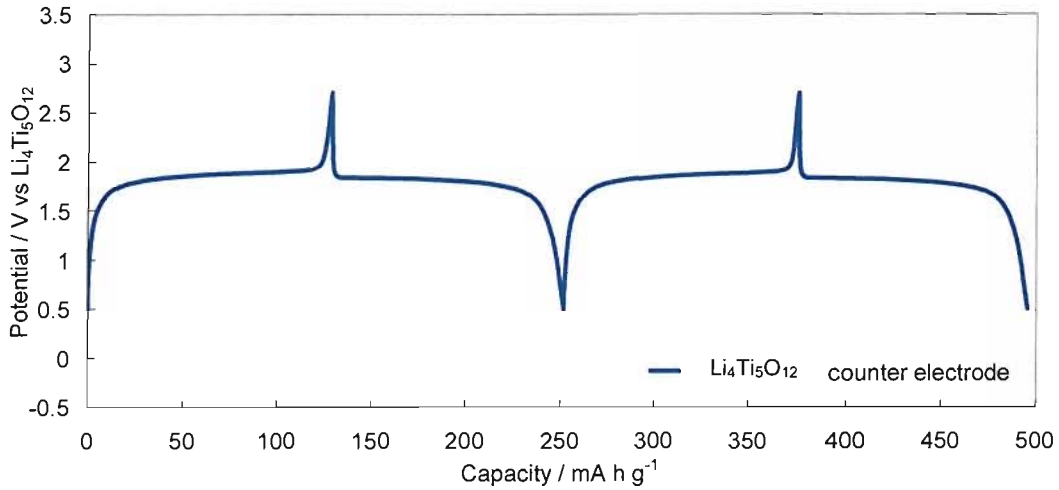

Fig. 4.9 Charge / discharge profile of 6 μm $LiFePO_4$ composite electrode of cells containing 0.47 mol dm^{-3} LiTFSI / EMITFSI. The common counter / reference electrode was $Li_4Ti_5O_{12}$. The current rate was 0.25 C for both charge and discharge.

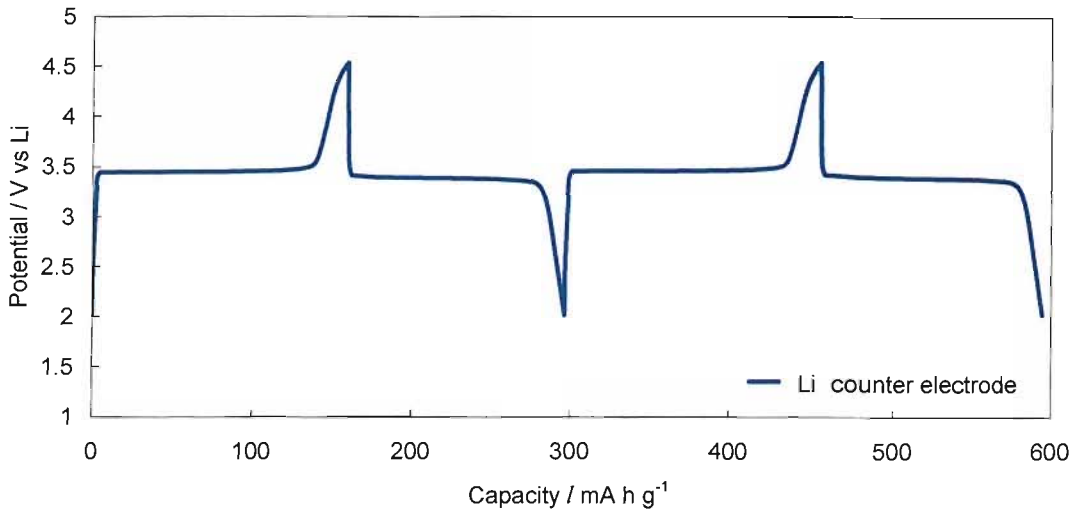

Fig. 4.10 Charge / discharge profile of a 6 μm $LiFePO_4$ composite electrode in 0.47 mol dm^{-3} LiTFSI / EMITFSI. The common counter / reference electrode was lithium. The current rate was 0.25 C for both charge and discharge.

The comparison of the results between $Li_4Ti_5O_{12}$ and lithium metal counter electrodes suggests a shift of the potential at the former. The following factors can cause the variation of the potential at the counter electrode.

- To give an enough capacity as the counter electrode, a thick composite electrode is needed.
- The reaction of lithium insertion/extraction is slow.
- Even though the material has a very flat plateau at 1.6V vs Li, the potential for $Li_4Ti_5O_{12}$ is about 3 V.

Because of the potential shift at the counter electrode, deciding the termination of discharge with the cell voltage is difficult. This decreases the discharge capacities of a thin electrode to ~120 mAh g^{-1} because the potential of the counter electrode is higher than the plateau of $Li_4Ti_5O_{12}$ when the cell has terminated the discharge.

The summary of rate capabilities of the $LiFePO_4$ composite electrodes with varied thicknesses is shown in Fig. 4.11. We can observe the same trend as in Fig. 4.8; capacities are retained at high rates with thin electrodes better than those with thick electrodes. As previously discussed, the capacities of thin electrodes at slow rates are

smaller than those of thick electrodes due to the problem of the counter electrodes. We can eliminate the risk of electrolyte decomposition or passivation at the counter electrode using $Li_4Ti_5O_{12}$, however, must consider the polarisation at the counter electrode. Therefore, extracting the pure phenomena of the working electrode and implementing the studies of lithium diffusion in the electrode may be difficult by 2 electrode systems.

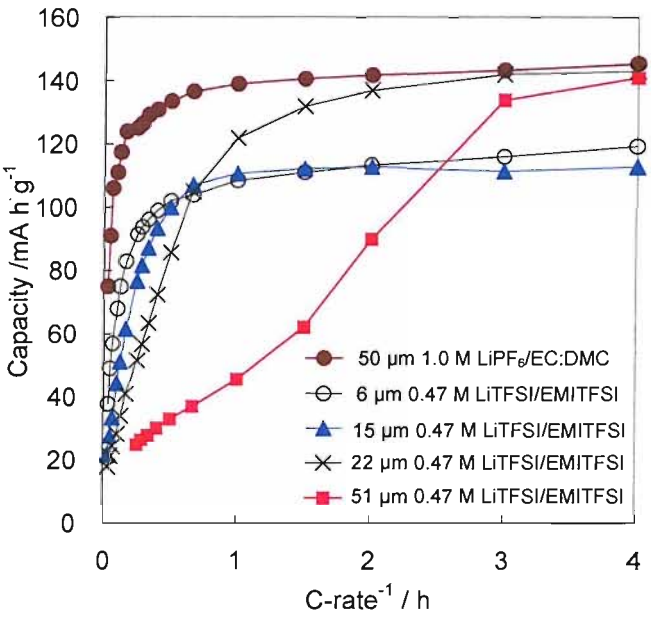

Fig. 4.11 Rate capabilities of $LiFePO_4$ composite electrodes of cells containing 0.47 mol dm^{-3}. The common counter / reference electrode was $Li_4Ti_5O_{12}$ composite electrode.

4.3.5. 3-electrode cell

The effects of electrode thickness were roughly observed using the 2 electrode cells with the lithium counter electrode or $Li_4Ti_5O_{12}$ counter electrode; however, the rate characteristics of the cells also implied that the results were affected by the polarisation at the counter electrode.

As discussed in Chapter 2, the ionic liquid electrolyte requires very dehydrated conditions so that cells used for long term cycling measurement must be sealed thoroughly. Two electrode test cell can be sealed relatively easily and the technique has been already established in our group [2]. In contrast, inserting the third electrode with

perfect seals and without an electrical contact either to the working electrode or to the counter electrode is difficult.

To solve the problem, a thin copper wire covered with polyvinyl chloride was pierced through a viton® ring. The combination of materials provided a perfect seal with a robust binding pressure. The end of the wire was stripped, coated by the active materials which supply stable reference potentials and sandwiched between separators; therefore the reference potential was not interfered by either the working electrode or counter electrode.

With the reference electrode, the potentials of both the working electrode and counter electrode were monitored, as shown in Fig. 4.12. Unlike the potential profile in Fig. 4.9 in which case only 118 mA h g^{-1} was exhibited as a discharge capacity, the plateau shows a stable potential and the start of charge and the end of discharge are acute. It is now clearly found that the effect of polarisation at the counter electrode is significant and indeed limits the rate capability of cells.

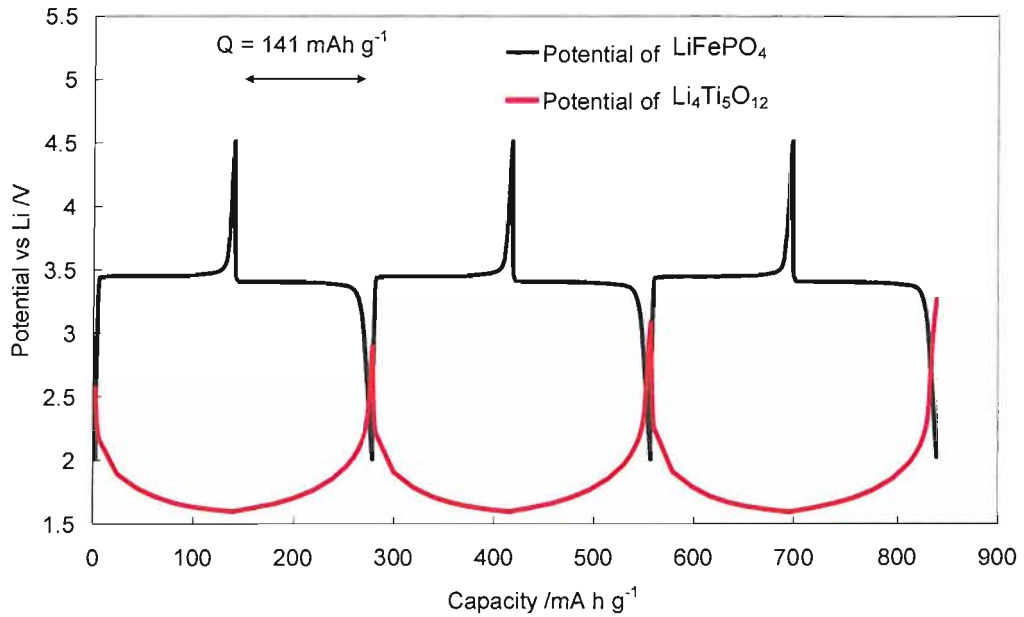

Fig. 4.12 Charge / discharge potential profiles of the 6 μm $LiFePO_4$ working electrode and the $Li_4Ti_5O_{12}$ counter electrode. The current rate was 0.25 C for both charge and discharge.

4.3.6. Counter electrodes

Fig. 4.13 shows discharge profiles of a $LiFePO_4$ positive electrode with 20 μm thickness at 8.0 C, (ca. 2 mA cm^{-2}, Li insertion into $LiFePO_4$ and extraction from the counter electrode) using a lithium metal counter electrode (a) or a $Li_4Ti_5O_{12}$ composite electrode (b). Lithium usually has a relatively stable potential and allows fast deposition and stripping, therefore, the electrode is widely used as a common counter and pseudo reference electrode. However, in the case shown in Fig. 4.13 (a) the potential of the lithium counter electrode elevated to 10 V and the discharge capacity was limited by the overrange of the potential at the counter electrode. If the 2 electrode system had been used for the cell, the discharge curve would be the blue curve shown in Fig. 4.13 (a). The ascent of potential of lithium suggests a transformation of a solid electrolyte interface (SEI) into a nonconductive passivation film or formation of a new nonconductive layer, such as voids formed from decomposed electrolytes between the SEI and lithium metal. This behaviour was observed neither at a lower current nor shorter duration nor in the case of the deposition of lithium. Therefore, the parallel potential profiles observed at the end of discharge (Fig. 4.6 and Fig. 4.7) using lithium counter electrodes and two electrode cells may be due to these effects. On the other hand, the $Li_4Ti_5O_{12}$ composite counter electrode did not limit the discharge capacity even at a high current density.

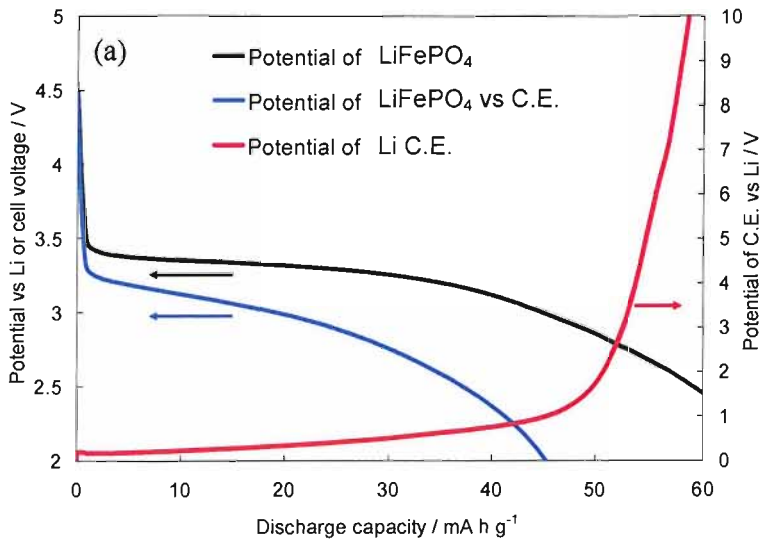

Fig.4.13 (a) Potential profiles of 20 μm LiFePO4 electrodes and the counter electrodes, lithium at 8.0 C

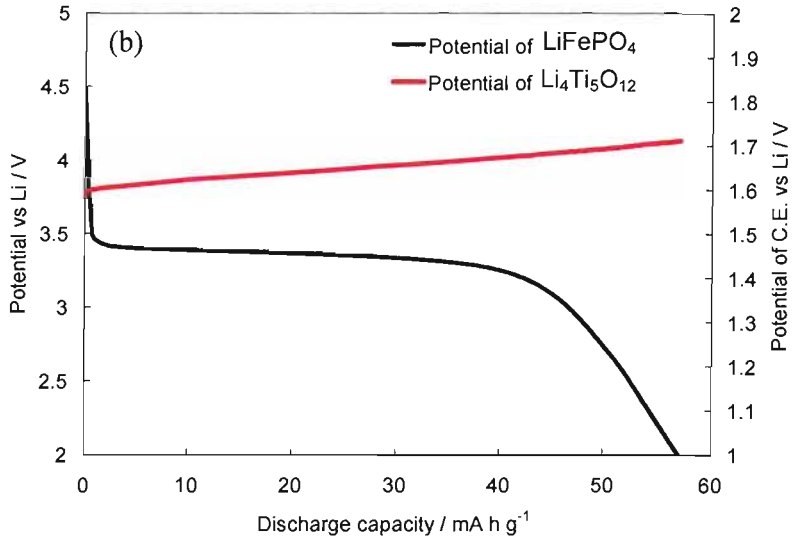

Fig. 4.13 (b) Potential profiles of 20 μm LiFePO4 electrodes and the counter electrodes, $Li_4Ti_5O_{12}$ at 8.0 C

Hence the following investigations were implemented using the $Li_4Ti_5O_{12}$ composite counter electrode with the 3-electrode cell configuration.

4.3.7. Effects of electrode thickness

Discharge potential profiles with 3 electrode cells (Lithium ion insertion into $LiFePO_4$) are shown in Fig. 4.14. Each graph shows the profile of an electrode at various discharge rate and we can observe degradation of discharge capacities with an increase in rates. For example, discharge capacities decreased to less than 40 % of the full capacity at 30 C in the case of a 6 μm electrode. However, a significant IR drop was not observed for any electrodes and this is not the main factor of this capacity reduction at these rates.

Discharge profiles at the same C-rates are shown in Fig. 4.15; thus we can clearly see the effects of electrode thickness. The discharge capacities obtained for thicker electrodes are smaller at the same discharge rate. At high rates of discharge, *e.g.* 10 C, a steeper end of discharge is observed for thicker electrodes.

At the lowest rate of discharge (0.25 C), the end of discharge (from 3 V to 1.5 V) is relatively steep in all cells with various thicknesses. With an increase in rates, The gradient decreases to the minimum value and is maintained at further faster rates; e.g. for 14 μm electrode, the end of discharge curves sequentially become more moderate up to 1.0 C and then turn into approximately parallel profiles from 1.0 C through 20 C. We have not reached a clear conclusion for these parallel potential profiles; however, the slope may be attributable to a degree of inhomogeneity against the electrode thickness. Accordingly, the steep end of discharge was observed for thicker electrodes at high rate, as shown in Fig. 4.15 (10 C). $LiFePO_4$ particles have a significant size; therefore, the morphology of a composite electrode is not perfectly uniform. As a result, the lithium ions can diffuse further at some region than others in the electrodes; therefore, discharge profiles are ending with slopes, instead of showing a sudden drop of potential.

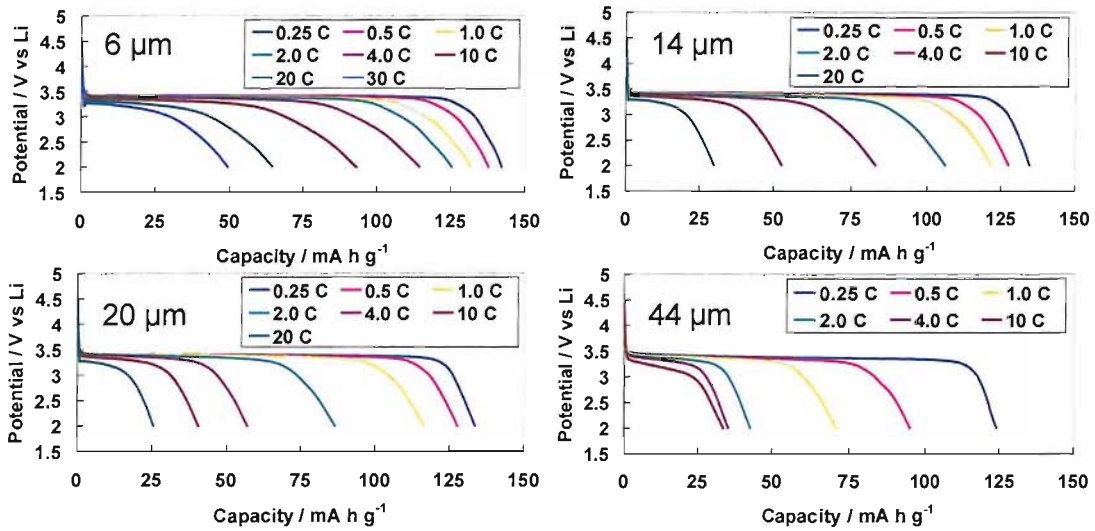

Fig. 4.14 Discharge potential profiles of $LiFePO_4$ electrodes at various discharge rates. The counter electrode was a $Li_4Ti_5O_{12}$ composite electrode and the reference electrode was a $LiMn_2O_4/Li_2Mn_2O_4$ composite electrode.

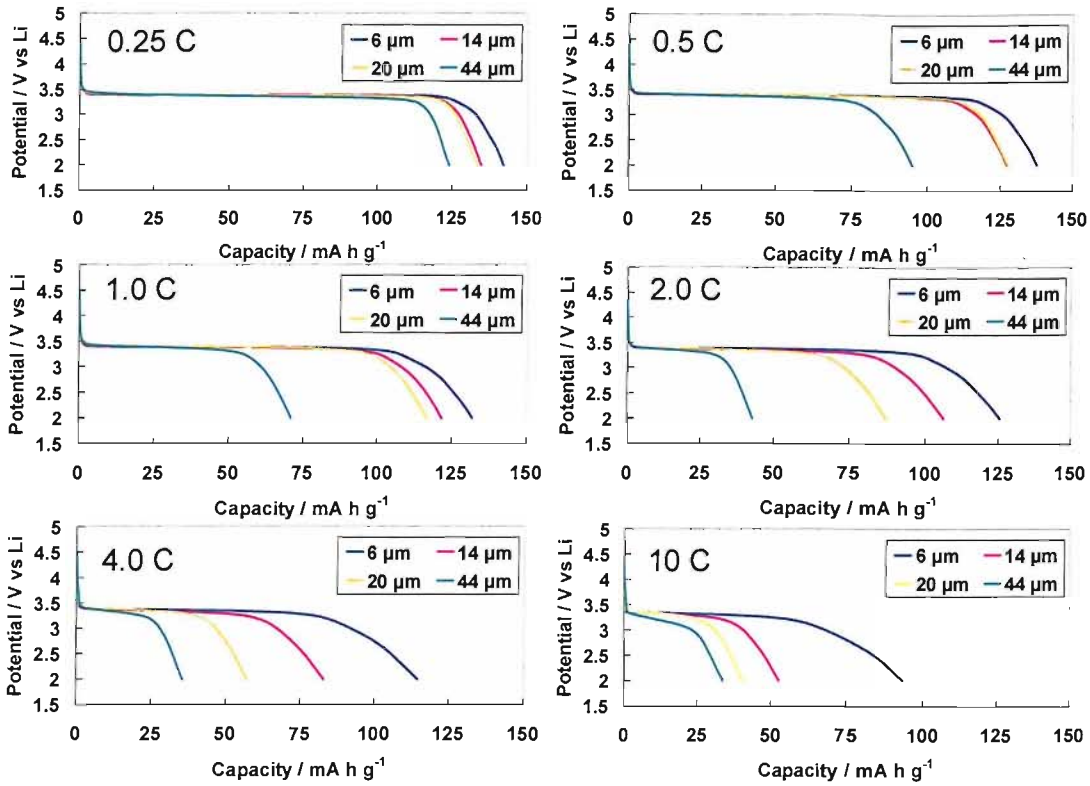

Fig. 4.15 Discharge potential profiles depending on electrode thicknesses. The counter electrode was a $Li_4Ti_5O_{12}$ composite electrode and the reference electrode was a $LiMn_2O_4/Li_2Mn_2O_4$ composite electrode.

Those discharge capacities at various rates are plotted as shown in Fig. 4.16. At slow discharge rates, capacities are limited by the finite capacity of the active material, $LiFePO_4$. On the other hand, at high rates, the trend of capacities shows an almost linear dependence on $(\text{C-rates})^{-1}$ up to 50 % of the full capacity. The linear part was extrapolated toward the maximum capacity line to obtain the time value at the intercept. This was defined as "transition time, τ_0" and used as an inverse measure of the rate characteristics of $LiFePO_4$ composite electrodes. These trends can be observed more clearly than that in Fig. 4.8 or Fig. 4.11, suggesting the influence of counter electrodes was eliminated by introducing the reference electrode.

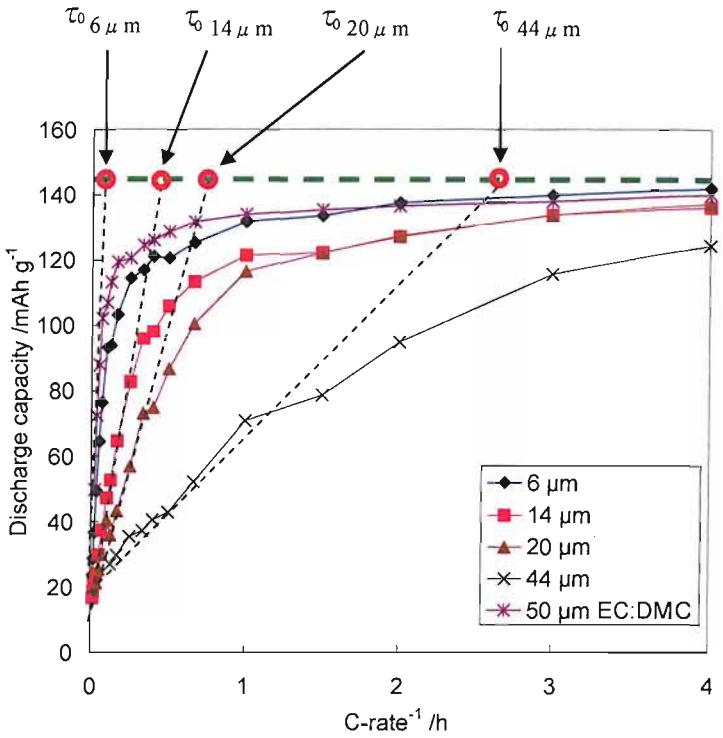

Fig. 4.16 Rate dependence of discharge capacities from $LiFePO_4$ electrodes with various thicknesses on discharge rates.

Fig. 4.17 also shows the dependence of discharge capacities on rates but per electrode area. In this way, it is clearly shown that larger capacities per area at high discharge rate were obtained from the electrode with $LiPF_6$ / EC:DMC than that with the ionic liquid electrolyte. In the case of cells containing the ionic liquid, the rate dependence of discharge capacities is unique at high rates and the inclination can be observed as almost linear from the origin. The trend suggests that capacities are controlled by one factor, which is attributable to the diffusion of lithium ions in the composite electrodes.

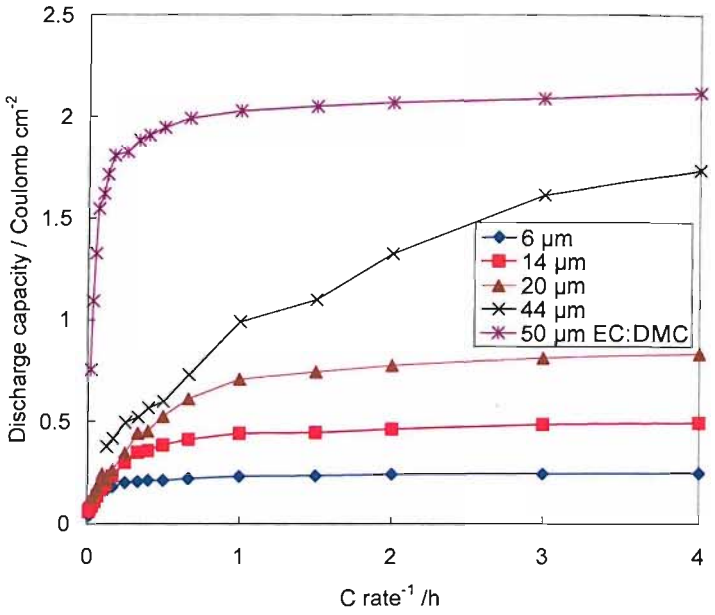

Fig. 4.17 Rate dependence of discharge capacities per area from $LiFePO_4$ electrodes with various thicknesses on discharge rate.

4.3.8. Effects of charge rates and discharge rates

The effects of charge rates and discharge rates on discharge capacities of a 20 μm $LiFePO_4$ electrode are shown in Fig. 4.18. Especially at high rates, the difference between charge rates and discharge rates in the degree of capacity reduction can be observed clearly; the charge rate affects less the discharge capacity than the discharge rate. The results suggest that the effects of lithium depletion in the porous structure seriously decrease the available capacity during the discharge but the accumulation of lithium ions during the fast charge less influences the capacity.

The intercept onto the vertical axis from the discharge capacities at various discharge rates is ca. 10 mAh g^{-1} and the value is approximately common for various thickness electrodes as shown in Fig. 4.16. As discussed in 4.3.2, the porosity of the composite electrodes is 0.65 and the weight fraction of $LiFePO_4$ in them is 70 wt%. The mass density of $LiFePO_4$ is 3.5 g cm^{-3} and its molecular weight is 157.8 g mol^{-3}. Therefore,

the amount of lithium ions, which is required to discharge the electrode completely, is calculated as 5.4 mol dm^{-3}. On the other hand, the concentration of LiTFSI in the ionic liquid is 0.47 mol dm^{-3} and thus the fraction of lithium ions in the electrolyte in the voids of the composite electrode is 0.31 mol dm^{-3}. Hence, 5.7 % of $FePO_4$ in the composite electrode can be discharged from the lithium ions in the voids; this is 8.6 mA h g^{-1} of 150 mA h g^{-1} which is practically obtained at slow rates. Therefore, the intercept is ascribed to the capacity, which is derived from lithium ions in the electrolyte in the electrode.

In contrast, the capacities while charge rates were varied are not limited by the starvation of lithium ions but the different factor, lithium ion accumulation; therefore, they present the higher intercept because lithium ions extracted from $LiFePO_4$ can exist in the electrolyte in the composite electrode; the electrolyte can concentrate more than three times, 1.5 mol dm^{-3}.

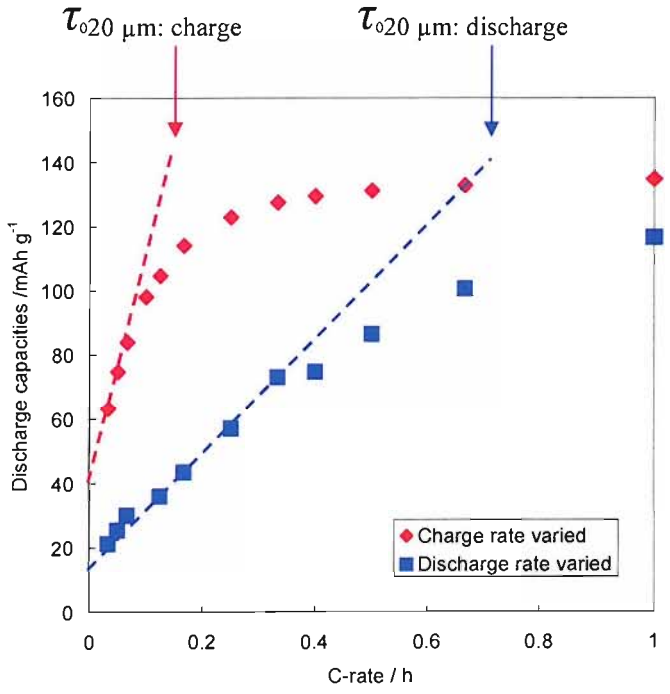

Fig. 4.18 Discharge capacities of a 20 μm $LiFePO_4$ electrodes with 0.47 mol dm^{-3} LiTFSI / EMITFSI, while charge or discharge rates are varied.

4.3.9. Effective diffusion coefficient

The transition times obtained from Fig. 4.16 are shown in Fig. 4.19. Likewise, the transition times while charge rates were varied (*e.g.* Fig. 4.18) were also evaluated and are shown here. Both values present an approximately linear inclination against the square of the electrode thickness. We defined this gradient as D_{eff}, which indicates the trend of the diffusion of the charge/discharge state, being expressed as an equation below.

$$D_{eff} = \frac{\ell^2}{\tau_0} \qquad \text{eq. 4.1}$$

D_{eff} : the effective diffusion coefficient, ℓ: the electrode thickness and τ: the transition time of the electrode.

The effective diffusion coefficient for varied charge rates is five times as that of varied discharge, signifying that the same capacity can be obtained at five times faster charge than discharge.

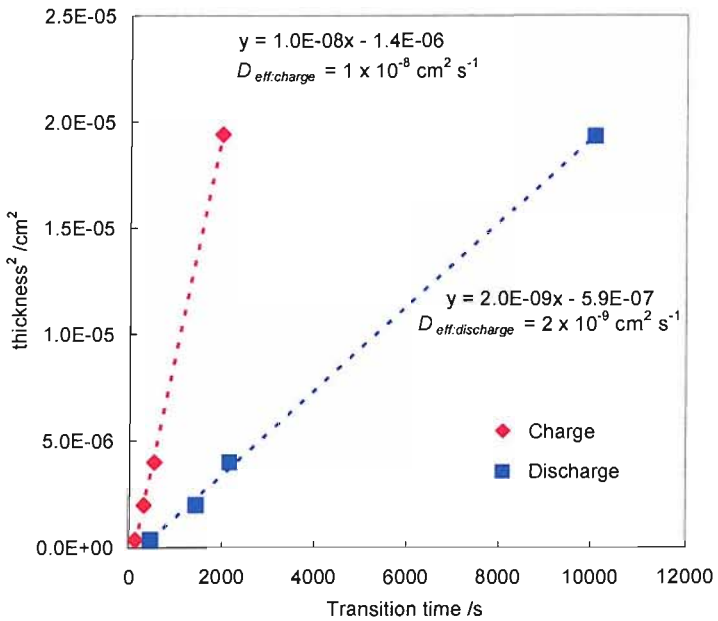

Fig. 4.19 Charge / discharge effective diffusion coefficient in 0.47 mol dm^{-3}

4.3.10. Effects of Li salt concentration

The effects of lithium salt concentration in electrolytes on the rate characteristics of electrodes were also studied. The dependence of discharge capacities on charge / discharge rate in 1.5 mol dm^{-3} LiTFSI / EMITFSI is shown in Fig. 4.20. Unlike the case of the 0.47 mol dm^{-3} electrolyte, the capacities were reduced at the high charge rates more greatly than the high discharge rates. It is also found that the extrapolation onto the vertical axis for high rates (trend line (a)) is approximately zero or less, suggesting that capacities are not limited by the same mechanism as in the case of the 0.47 mol dm^{-3} electrolyte in this high rate region. At high rates shown as trend line (a) in the 1.5 mol dm^{-3} electrolyte, the capacities may be limited by solid state lithium diffusion in the $LiFePO_4$ particles but not lithium ion diffusion electrode along the direction of the electrode thickness in the voids of the composite,

Neglecting this high rate region (a), the transition time and the intercept for each electrode were evaluated form the discharge capacities up to 50 % of the full capacity as shown in Fig. 4.20 (b). The intercept is not very accurate, but estimated as ca. 25 mA h g^{-1}, approximately corresponding the calculated value, 27 mA h g^{-1}, which is evaluated for 1.5 mol dm^{-3} using the same approach shown in 4.3.8. Therefore, in this region (b), the intercept is attributed to the amount of lithium ions in the voids of the composite electrode since the capacities are limited by the lithium ion diffusion along the direction of electrode thickness.

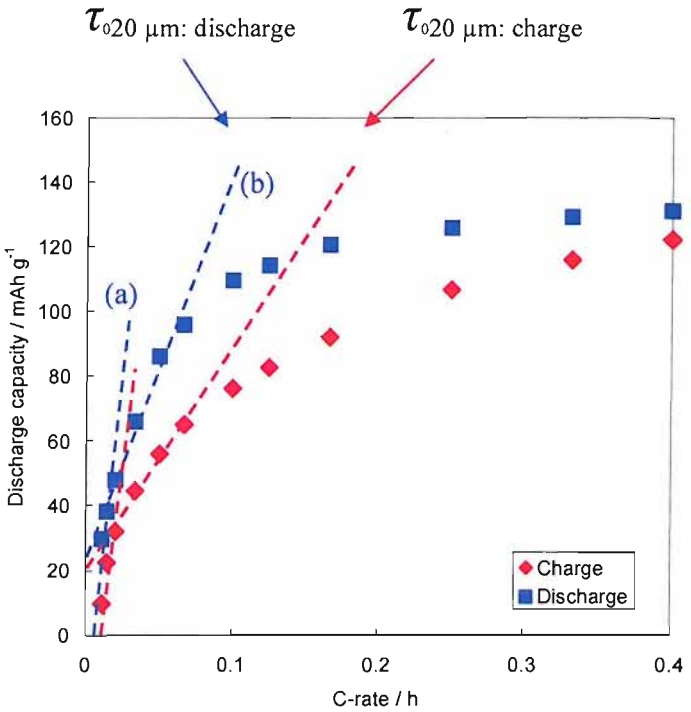

Fig. 4.20 Discharge capacities of a 20 μm $LiFePO_4$ electrodes with 1.5 mol dm^{-3} LiTFSI / EMITFSI, while charge or discharge rates are varied.

The transition times for charge / discharge rates with various concentrations of Li salt are summarised in Table 4.1. From these values, effective diffusion coefficients were calculated and are shown in Fig. 4.21. It is clearly shown that electrolytes with higher concentration allow faster discharge from $LiFePO_4$ composite electrodes than that with lower concentration, suggesting the existence of the electrolyte depletion effect during discharge. In contrast, an increase of lithium salt concentration in electrolytes reduces the rate capability of the composite electrodes, implying that lithium ions are excessively accumulated in the porous structure.

Table 4.1 Transition time for 20 μm $LiFePO_4$ composite electrodes with various concentrations of Li salt in the ionic liquid electrolyte.

Concentration of LiTFSI / mol dm^{-3}	0.47	1.14	1.51
Transition time for Charge / hour	0.11	0.18	0.19
Transition time for Discharge / hour	0.70	0.16	0.11

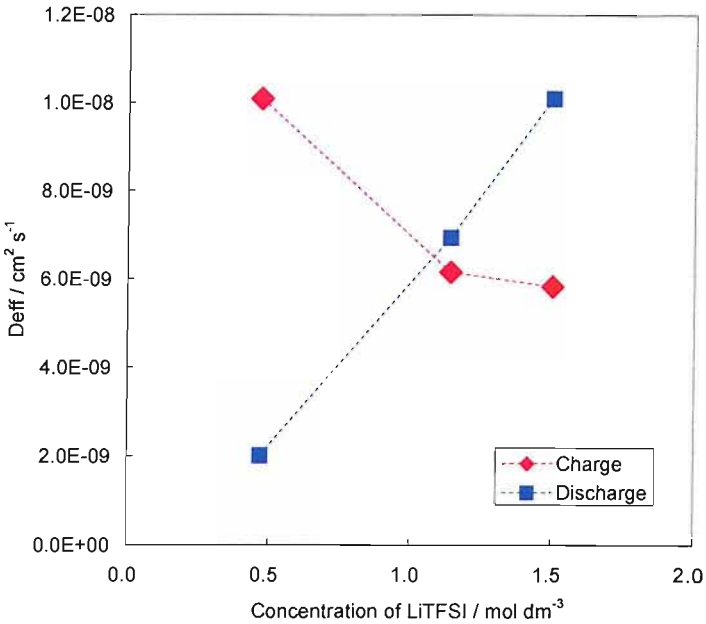

Fig. 4.21 Effects of Li salt concentration on the effective diffusion coefficients

4.3.11. Preliminary GITT measurements

To investigate the diffusion coefficients during charge and discharge, Galvanostatic Intermittent Titration Technique (GITT) was implemented on a three electrode cell. A typical example of GITT profiles is shown in Fig. 4.22.

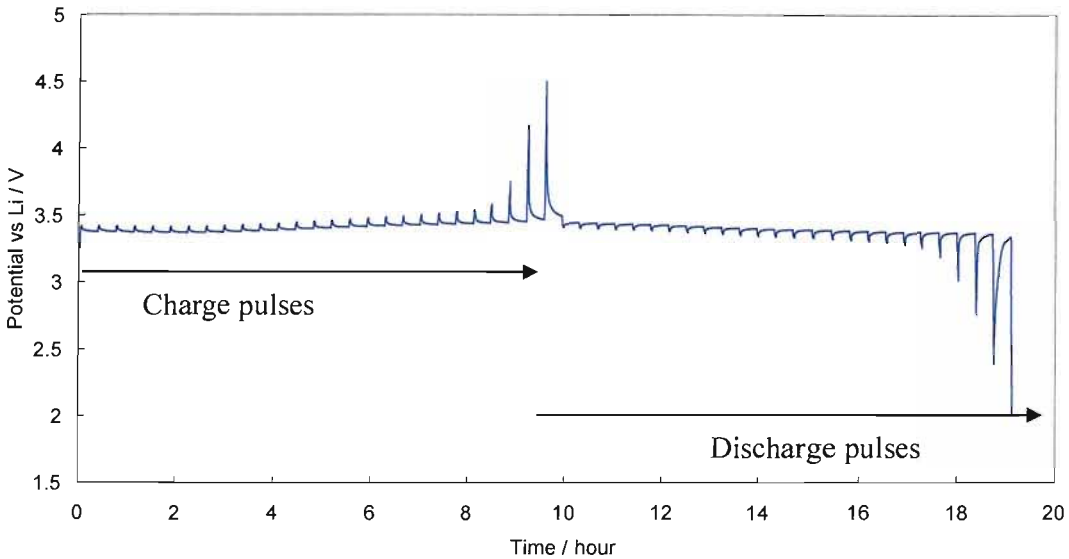

Fig. 4.22 GITT profile of a 20 um thick $LiFePO_4$ electrode in 0.47 mol dm^{-3} LiTFSI / EMITFSI. The counter electrode was a $Li_4Ti_5O_{12}$ composite and the reference electrode was a $LiMn_2O_4/Li_2Mn_2O_4$ composite. The pulse was at 1.0 C for 2 minutes and then the cell was relaxed for 20 minutes.

It is necessary to know the equilibrium potential E_0 of the electrode to calculate the diffusion coefficients from potential relaxation profiles *e.g.* in Fig. 4.23. The potential can be obtained by maintaining a circuit open for long duration. For example, the approximate time constant, τ, for this relaxation is 1.1 hour (calculated for 20 μm electrode, D = 1 x 10^{-9} cm^2 s^{-1}). Therefore, after *ca* 5.5 hours, the measured potential reaches 99.9% close to the relaxed potential from the polarised potential. However, this method requires days to measure many diffusion coefficients during the charge / discharge in a battery. Hence, the relaxed potentials were estimated by a fitting method.

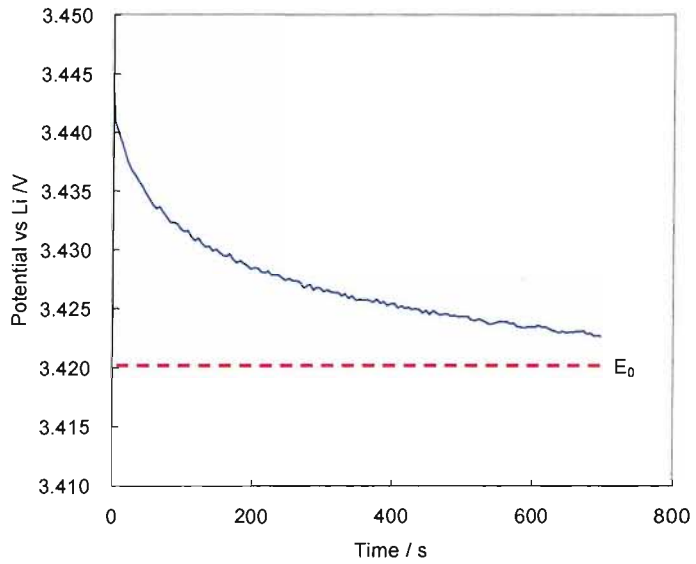

Fig. 4.23 Potential relaxation profile of a cell using 20 μm thick $LiFePO_4$ electrode and 1.1 mol dm^{-3} LiTFSI / EMITFSI

To find the equilibrium potential, the linearity of $-\ln(E - E_0) / t$ was tested. In the case that E_0 is evaluated too high, the slope is diverted to infinity as shown in Fig. 4.24 (b) and in the case that E_0 estimated too small the slope show a curve remaining finite (c); therefore, the validity of the E_0 can be judged from a shape of the slope.

Practically a macro of Microsoft Excel was programmed to evaluate the E_0 and the time constants. A starting value for E_0 was substituted and the difference between "Gradient 1" and "Gradient 2" was evaluated. Accordingly the value for E_0 was increased by 1 μV

and the increase was repeated until the difference became smaller than 0.02 % as shown in Fig. 4.24 (a).

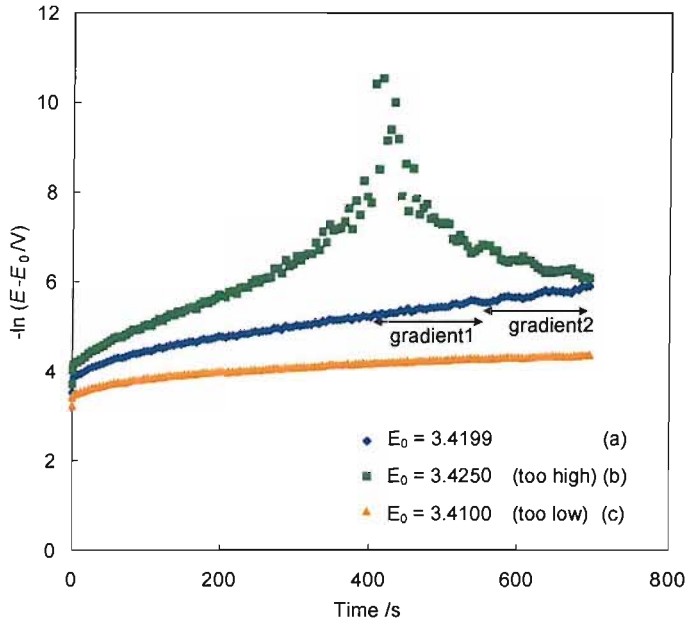

Fig. 4.24 linearity of logarithmic potential profiles. The curves were varied from the values substituted to E_0.

The equilibrium potentials and time constants obtained from the above method are shown in Fig. 4.25. The potentials show symmetric profiles, with similar potentials recorded during charge and discharge, confirming the validity of the data. Time constants for the relaxation were calculated according to eq, 4.2 and shown in Fig. 4.25. Diffusion coefficients will be presented later with a discussion of the appropriate diffusion distance ℓ to be used in the calculation.

$$\frac{\ln(\Delta\phi)}{t} = -\frac{D\pi^2}{\ell^2} + B' = \frac{\pi^2}{\tau} + B' \qquad \text{eq. 4.2}$$

Where ϕ is the cell voltage, t is the time, D is diffusion coefficient, ℓ is the diffusion distance and τ is the time constant

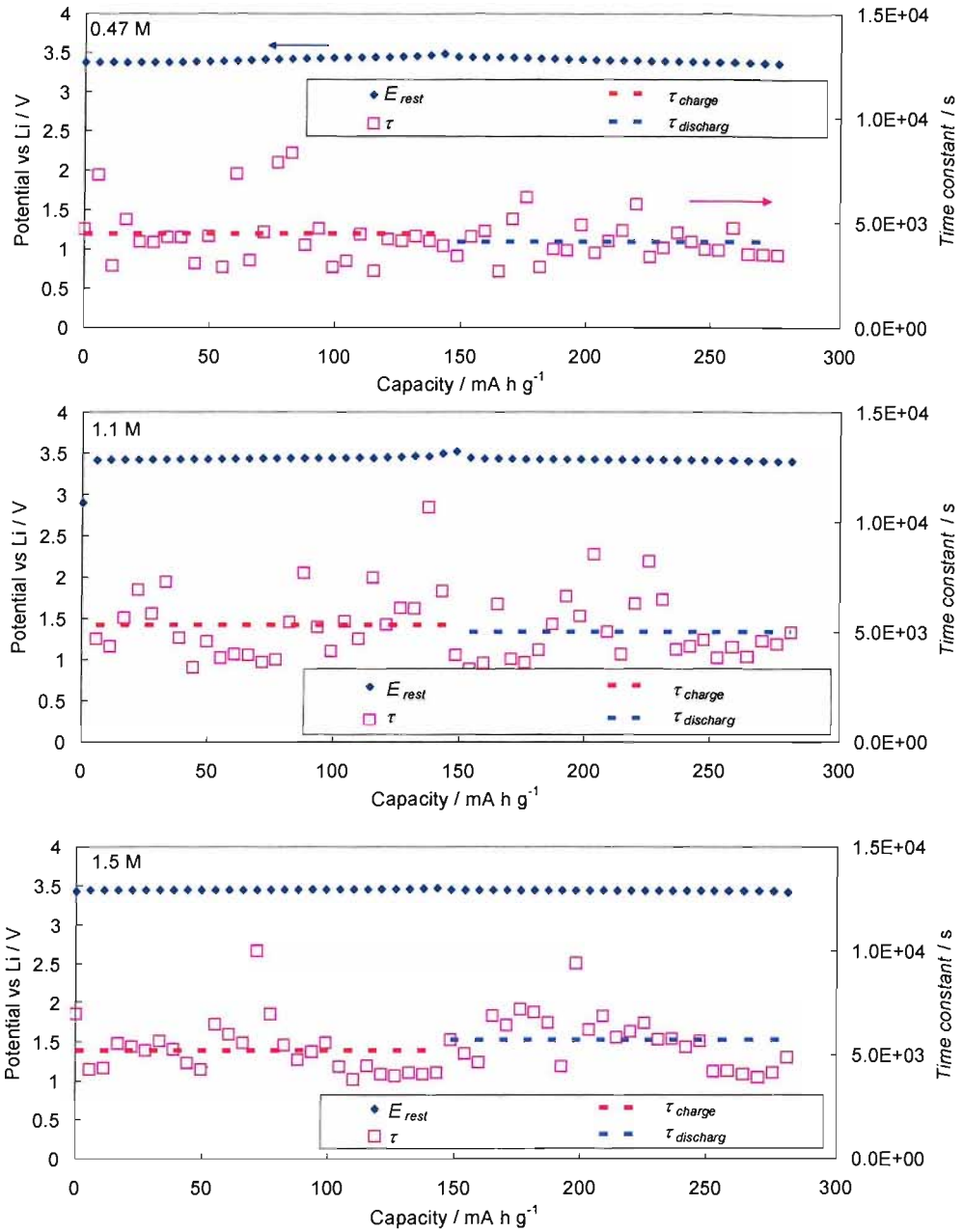

Fig. 4.25 Rest potentials and time constants of a cell using 20 μm $LiFePO_4$ composite electrodes and LiTFSI /EMITFSI, measured by the GITT method

The time constants obtained by the GITT method show scattering, which is larger than that for the time constants in bulk LiTFSI / EMITFSI. This may be due to the smaller exchange current of $LiFePO_4$ system than that of lithium metal; therefore the measured

potential could be affected by electric disturbance. A close inspection to a curve between 500 seconds to 700 seconds in Fig. 4.24 (a) presents us *ca* 50 second periodical noise. Although it is ideal to use late data and wide duration for measurement to investigate the $-\ln(E-E_0)$ profiles, the data later than 700 seconds were found to be not appropriate. Furthermore, as E_0 was not directly measured but predicted from the profile fitting, the error affects the value of the time constants more.

Hence, the time constants during charge or discharge were averaged and shown as broken lines. In the case of each concentration, it was found that the difference between the time constants measured by the GITT technique during charge and that during discharge is insignificant. By contrast, it was shown in 4.3.8 that the effective diffusion coefficients during charge were significantly different from those during discharge.

4.4. Discussion: Models for Mass Transport limitations

The results given above have shown that the most important rate limitation is due to a diffusion process along the thickness of the composite electrode, from the separator side to the current collector. The nature of the diffusion has not been specified, in particular the species has not been identified. Two models will be presented below, referring to diffusion of neutral lithium via coupled diffusion of lithium ions with electrons, and salt diffusion.

4.4.1. The transmission line model

The circuit diagram of

Fig. 4.26 illustrates the model proposed by de Levie [3] to explain the behaviour of porous electrodes in which ion transport in the pores is coupled with electron transport in the electrode metal. The model has been applied to the impedance of composite electrodes by Owen *et al.* [4] and time domain behaviour of the electrodes by West *et al.* [5]. In the simplest case of the electrolyte and electrode resistance coupled with the electrode pseudo-capacitance, the model reduces to a mathematically equivalent situation of a homogeneous material whose diffusion coefficient is given by equation [4]

$$D = \sigma / C_v \qquad \text{eq. 4.3}$$

where σ is the effective conductivity, C_v is the pseudo-capacitance per unit volume.

One difficulty with this model is its poor description of the constant potential region found in the 2-phase discharge of materials such as $LiFePO_4$, which would require an infinite pseudocapacitance over an infinitesimally small voltage range.

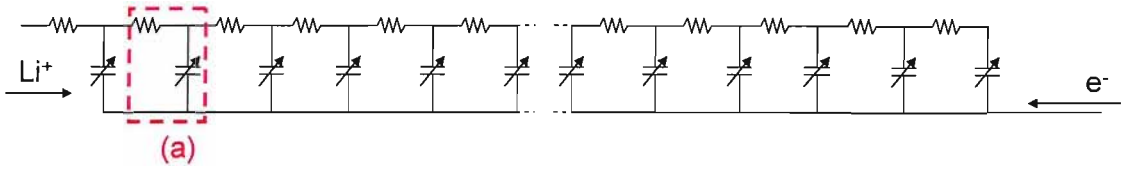

Fig. 4.26 RC model circuit

The experiments shown above can alternatively be modelled by Fick's law in a one-dimensional material with a constant diffusion coefficient. The diffusion equation may be solved by assuming a constant diffusion flux of lithium ions to compensate the consumption of lithium ions during galvanostatic discharge. A boundary condition may be derived from the fact that the lithium flux is zero at the current collector – *i.e.* at a finite distance from the interface.

4.4.2. Compact discharge front model

As observed in Fig. 4.17, the dependence of the discharge capacities at high rates are inversely proportional to the c-rates. The phenomena may be explained by the migration of the boundary between lithium inserted phase in the composite electrode and the other phase.

With the following assumptions, a model as shown in Fig. 4.27 is proposed.

- The amount of lithium ions already present in the electrolyte penetrating into the composite electrode is insignificant compared with the amount of lithium to be inserted.
- The concentration of salt at the interface between the electrolyte and electrode is constant.
- The diffusion coefficients of lithium ions in the electrolyte are not affected by the lithium salt concentration change in the electrolyte during charge / discharge.
- The lithium diffusion time in active material is faster than the time scale of the model.
- The discharge front is sharp – i.e. all material is in either the charged or discharged form.

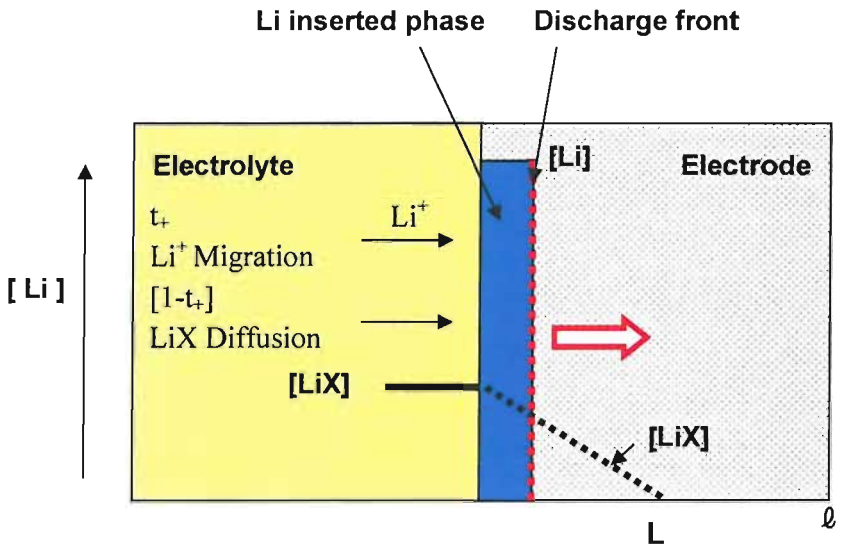

Fig. 4.27 Compact discharge front model

When discharge is galvanostatic, the system is in a steady state and the concentration profile of lithium ions in the composite electrode is proportional to the current density and the diffusion coefficient of lithium ions. Therefore, the thickness L, which lithium ions can reach from the bulk electrolyte, is function of these and the lithium salt

concentration in the electrolyte as shown in eq. 4.4, being derived from Fick's First Law and Faraday's Law.

$$dc/dx = it_- / FD_{LiX} = [\mathrm{LiX}]_0 / L \qquad \text{eq. 4.4}$$

Where i is the current density, F is the Faraday constant, D_{LiX} is the diffusion coefficient of lithium ions, $[\mathrm{LiX}]_0$ is the concentration of the electrolyte, L is the thickness to be discharged.

Hence,

$$i_A = \frac{FD_{LiX}[LiX]_o}{L(1-t_+)} \qquad \text{eq. 4.5}$$

The charge per area to be stored in the electrode q_A is proportional to the amount of lithium to be inserted in the active material (Faraday's Law) and therefore to L.

$$q_A = LF[\mathrm{Li}]_0 \qquad \text{eq. 4.6}$$

Where q_A is the charge to be stored per electrode area.

The duration to charge is the charge divided by current.

$$\tau = \frac{q_A}{i_A} = \frac{L^2(1-t_+)[Li]_o}{D_{LiX}[LiX]_o} \qquad \text{eq. 4.7}$$

$$\frac{L^2}{\tau} = \frac{D_{LiX}[LiX]_o}{(1-t_+)[Li]_o} \qquad \text{eq. 4.8}$$

The transition time τ_0 for each electrode, of which thickness is L, was measured in 4.3.9. The situation corresponds to $L = \ell$; *i.e.* the thickness which lithium ions diffuse is equal to the thickness of the electrode.

$$\frac{\ell^2}{\tau_o} = \frac{D_{LiX}[LiX]_o}{(1-t_+)[Li]_o} = D_{eff} \qquad \text{eq. 4.9}$$

Therefore, D_{eff} is a function of diffusion coefficient of lithium ions, the concentration of lithium ions in the electrolyte, the transference number and lithium concentration in the active material.

The eq. 4.9 explains a trend observed in Fig. 4.21; the effective diffusion coefficient is almost proportional to the concentration of the electrolytes.
The diffusion of lithium ions in composite electrodes is hindered by geometric factors; therefore, D_{LiX} in eq. 4.9 is a function of electrode porosity and electrode tortuosity.

$$D_{LiX} = \frac{\rho}{k^2} D_{Li\_in\_bulk} \qquad \text{eq. 4.10}$$

Where k is the tortuosity factor and ρ is the porosity of the electrode.
All the other parameters in eq. 4.9 and eq. 4.10 are known; hence, we can evaluate the tortuosity factor. In the case of the 0.47 mol dm^{-3} electrolyte, k was calculated as 2.

Table 4.2 Parameters based on the compact discharge front model

C_{Li} in electrolyte	mol dm^{-3}	0.47	1.1	1.5
C_{Li} in electrode	mol dm^{-3}	5.4	5.4	5.4
D_{eff}	$cm^2\ s^{-1}$	1.6E-09	6.7E-09	1.1E-08
D_{Li} in bulk	$cm^2\ s^{-1}$	1.1E-07	6.4E-08	5.0E-08
t_-	no unit	0.96	0.91	0.85
Porosity	no unit	0.65	0.65	0.65
tortuosity factor	no unit	4.0	1.4	1.0

In the same way, tortuosity factors in the different concentration of electrolytes were calculated based on parameters above. Although the tortuosity factors should be identical, calculated values are varied with the concentration of electrolytes. The low tortuosity factor calculated in the high concentration suggests, the rate capability of the electrode with the high concentration electrolyte is higher than expected with the compact discharge front model.
The problem is attributable to the incompleteness in one of the assumptions for the model. We ascribed that the amount of lithium ions in the voids of the composite electrode is insignificant to the amount which is required to discharge the $LiFePO_4$;

however, in the case of the 0.47 mol dm^{-3} electrolyte, 6 % of lithium ions required are already in the voids. The amount rises to 18 % in the case of the 1.5 dm^{-3} electrolyte; therefore, the lithium ions allow faster discharge and the effective diffusion coefficients appear to be larger than the model.

Although the compact discharge front model did not precisely fit the effect of salt concentration on electrode rate capability, the model can explain the linear trend between discharge capacities and $(C\text{-rates})^{-1}$ at high rates as shown in Fig. 4.16 and Fig. 4.17. Furthermore, we can expect the accumulation of lithium ions less affects the rate capability of the electrodes because the front is not formed and does not restrict the rate performance in the case of fast charge.

Therefore, the discharge front which is similar to what we modelled here may exist at high discharge rate.

4.4.3. Diffusion model for GITT measurements

As seen in Fig. 4.25 the time constants of cells evaluated by GITT method did not show a significant difference between charge and discharge; whereas the transition times shown in Fig. 4.18. were clearly different from charge and discharge. An explanation of the apparent discrepancy is given below.

As discussed in 4.3.8, the transition times observed during charge and discharge at constant current are due to accumulation and depletion of lithium ions to the point where the conductivity cannot support the applied current. On the other hand, in the GITT method, the time constant was measured for the final stage of a potential relaxation profile for the cell. The latter is a complex process, involving diffusion in the electrode and separator sections of the cell, and the final stage is probably a redistribution of the salt across the relatively thick separator, from the most concentrated region at one electrode to the most depleted at the other. The geometry should be almost symmetrical about a central point where the mean concentration is maintained, so that the actual diffusion distance is only half the separator thickness, i.e. 300 μm.

The above analysis results in a calculated diffusion coefficient as an order of 1 x 10^{-7} cm^2 s^{-1}, which is close to that found for the bulk electrolyte in Chapter 3. However, this must be regarded as interesting speculation, because at the time of the conclusion of this work, we did not have a certainly suitable simulation model to examine the progress of the concentration profile during a GITT experiment.

Nevertheless, the diffusion coefficients values obtained show interesting correlation between charge and discharge and also decreased with the concentration of the lithium salt, showing a similar trend as the diffusion coefficients in bulk electrolytes.

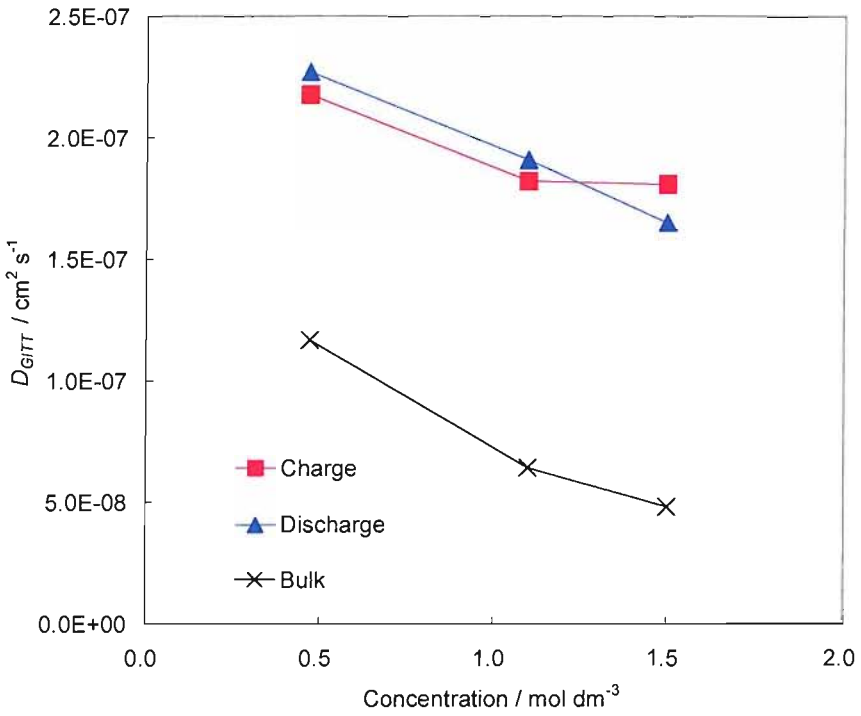

Fig. 4.28 Diffusion coefficients of lithium ions in a cell using a 20 μm thick $LiFePO_4$ electrode, depending on concentrations of LiTFSI in EMITFSI in comparison with the diffusion coefficients of lithium ions in bulk LiTFSI / EMITFSI.

4.5. Conclusion of the chapter

The charge / discharge rate performance of $LiFePO_4$ carbon composite electrodes with various thicknesses in different concentrations of LiTFSI / EMITFSI electrolytes was studied. To implement the investigations effectively, the homogeneity of the electrodes was confirmed by plotting the thickness against the weight. Moreover, it was shown that glass filter separators used to assemble the cells did not hinder the diffusion of lithium ions significantly.

Initially 2 electrode cells were used for the investigations, in order to achieve perfect seals for experimental cells. Lithium metal and $Li_4Ti_5O_{12}$ were applied to the common counter / reference electrode and a 100 mA h g^{-1} of discharge capacity was obtained from a 6 μm $LiFePO_4$ composite electrode at 10 C-rate; however, it was suspected that polarisation at the counter electrode distorted the potential profiles of the working electrode. Therefore, a 3 electrode system was introduced to study the rate capability of electrodes accurately. A mixture of $LiMnO_4$ and Li_2MnO_4 carbon ink was coated on a copper wire and used as a reference electrode. With a reference electrode, it was shown that lithium metal electrode formed a non-conductive layer under a high current density; hence, a $Li_4Ti_5O_{12}$ composite was adopted as the counter electrode for the following studies.

The effects of thickness on the rate capability of electrodes were shown clearly with 3 electrode cells. Discharge capacities were reduced with increases in the thickness of electrodes or fast discharge and the results were attributed to an electrolyte depletion effect in the composite electrode. At fast charge or discharge rates, discharge capacities were almost proportional to $(\text{C-rate})^{-1}$, suggesting that the capacities were simply controlled by lithium ion diffusion in the pores of the composite electrode. To analyse the phenomena, discharge capacities at high rates were extrapolated into the finite capacity and a transition time, τ_0, was obtained. The transition time showed a proportional trend against a square of thickness, ℓ^2; therefore, effective diffusion coefficients D_{eff} were defined for the gradient of ℓ^2 / τ_0. With a 0.47 mol dm^{-3} LiTFSI / EMITFSI electrolyte, the effective diffusion coefficient for charge is 5 times larger than

that for discharge. On the other hand, the effective diffusion coefficient for charge was smaller than that for discharge, implying an electrolyte accumulation effect.

A compact discharge front model was proposed to explain the rate capability of electrodes. The effects of salt concentration on the rate capability of cells can be explained qualitatively. The model also corresponds to the linear trend of discharge capacities on C-rates in the actual cases. The difference between effective diffusion coefficients for charge and discharge is attributable to formation or non-formation of the charge / discharge front. The simple discharge front model did not show perfect agreement with the measured rate capability data, however presented a similar trend.

Lithium diffusion coefficients in cell containing the ionic liquid were also studied by the GITT method. It is supposed that the potential relaxation mainly represents a redistribution of the lithium salt across the separator. The coefficients show a similar trend as those in bulk electrolyte.

Reference

1. Y. Kobayashi, Y. Mita, S. Seki, Y. Ohno, H. Miyashiro and N. Terada, *J. Electrochem. Soc.*, **154**, A677 (2007).

2. T. Le Gall, K. H. Reiman, M. C. Grossel and J. R. Owen, *J. Power Sources*, **119**, 316 (2003).

3. De Levie, *Adv. Electrochem. Electrochem. Eng.*, **6** 329 (1967)

4. J. R. Owen, J. Drennan, G. E. Lagos, P. C. Spurdens and B. C. H. Steele, *Solid State Ionics*, **5**, 343 (1981).

5. K. West, T. Jacobsen and S. Atlung, *J. Electrochem. Soc.*, **129**, 1480 (1982).

Chapter 5. Applications

5.1. Introduction

In previous chapters, the potentials of EMITFSI as an electrolyte for lithium batteries were studied in the aspect of stabilities and ion transfer. It was found that the ionic liquid can be used for lithium rechargeable batteries when the cell design, especially thickness of electrodes is carefully selected.

In this chapter, more practical aspects of lithium batteries containing ionic liquid electrolytes will be discussed, such as a cycle life of the lithium batteries and cells comprising a polymer electrolyte plasticised by EMITFSI.

5.2. Experimental

5.2.1. Synthesis of EMITFSI and LiTFSI/EMITFSI

1-Ethyl-3-methylimidazolium bis-(trifluoromethylsulfonyl)-imide (EMITFSI) and LiTFSI / EMITFSI were prepared as mentioned in Chapter 2.

5.2.2. Firing test

The ionic liquid electrolyte and $LiPF_6$ / EC : DMC were ignited with a cigarette lighter.

5.2.3. Lithium rechargeable cell

a) test cell preparation

$LiFePO_4$ and $LiCoO_2$ were made into inks and electrodes were prepared from them as detailed in Chapter 4. Cells were assembled with lithium counter electrodes.

b) Polymer electrolyte (a melt casting method)

0.47 mol dm^{-3} LiTFSI / EMITFSI and PVdF-HFP copolymer (Solvay 2080) were directly mixed at 180 °C in a glove box. The molten polymer electrolyte was cast on a

$LiFePO_4$ composite electrodes and cooled to room temperature. The formed polymer electrolyte and positive electrode were assembled with a lithium counter electrode into a test cell without glass filter separators.

5.2.4. Electrochemical measurements

a) Effects of concentration of lithium ions on the behaviour of a lithium electrode

To investigate the passivation at the surface of the lithium electrode, 3 electrode cells with various concentrations of electrolytes described in Chapter 4 were used. The cells were charged at a constant current, 0.25 C and discharged at 2.0 C. The effects of concentration of lithium salt in the electrolyte on the behaviour of the lithium counter electrode were studied.

b) Lithium batteries containing the ionic liquid electrolyte; cycling life

For measurements of long duration cycling, 2 electrode cells comprised $LiCoO_2$ and $LiFePO_4$ composite electrodes as the positive electrode and lithium metal as the negative electrode were assembled. Both charge and discharge were implemented at 0.5 C.

c) Lithium batteries composed of a polymer electrolyte plasticised by EMITFSI

Cells composed of polymer electrolytes were discharged at the rate from 0.25 C to 30 C while a charge rate was kept 0.25 C. Subsequently, the charge rates were varied while a discharge rate was kept 0.25 C.

5.3. Results and discussion

5.3.1. Electrode porosity and uniformity of electrode

The $LiPF_6$ / EC : DMC electrolyte took the fire instantly from the lighter and burnt continuously as shown in Fig. 5.1 (b). By contrast, a mixture of LiTFSI and EMITFSI did not catch the fire but resisted and reflected the flame (Fig. 5.1 (a))

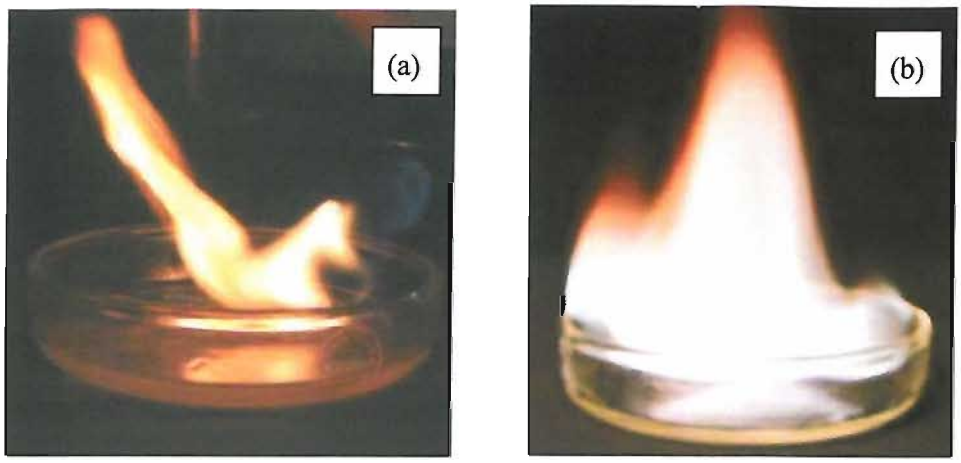

Fig. 5.1 Pictures showing non-flammability of a LiTFSI / EMITFSI electrolyte (a) and flammability of $LiPF_6$ / EC : DMC (b)

5.3.2. The effect of lithium salt concentration on behaviour of lithium electrodes

In Chapter 4, it was found that electrolytes with high lithium concentration allowed high rates discharge because more lithium ions were provided into the porous structure. To consider the total performance of lithium batteries, it is also necessary to know the behaviour of counter electrodes.

Lithium metal and $Li_4Ti_5O_{12}$ composite electrodes were studied as the counter electrode previously. Lithium is preferable for negative electrodes due to a lower potential; however, the formation of passivation films was suggested in Chapter 4 and this might degrade the performance of the batteries.

The discharge profiles of 18 μm $LiFePO_4$ composite electrodes containing different concentrations of LiTFSI / EMITFSI at 2.0 C (ca 0.5 mA cm^{-2}) were shown in Fig. 5.2 (a). With the 0.47 mol dm^{-3} LiTFSI / EMITFSI electrolyte, the profile of the counter electrode presents a shift of potential from 0 to 0.6 V vs lithium while a 120 mA h g^{-1} of capacity was discharged from the $LiFePO_4$ composite electrode. In contrast, in the case of the 1.5 mol dm^{-3} electrolyte, the potential of the lithium counter electrode rose greatly after a 50 mA h g^{-1} of capacity was discharged and elevated to 10 V, which was over the range limitation of the equipment. The potential of the $LiFePO_4$ composite electrode

was distorted on the plateau Fig. 5.2 (b), suggesting the counter electrode affected the behaviour of the working electrode even before reaching over potential.

As discussed in Chapter 4, the passivation on lithium electrodes only occurs during cell discharge; i.e. the counter electrode releases lithium ions and these may be accumulated in the neighbourhood of the surface of the lithium electrode. By comparison between the cases of 0.47 mol dm^{-3} and 1.5 mol dm^{-3}, it was shown that this accumulation was enhanced by the high concentration of lithium ions in the electrolyte. The mechanism of passivation is unknown, however, suggested to be due to precipitation of lithium salt from the electrolyte.

This problem of accumulation is more serious for the plane electrodes than composite electrodes because the electrolyte was more concentrated in thin space and the surface area was small; whereas depletion of lithium ions was significant for composite electrodes. Therefore, for 2 electrode lithium batteries, it is not preferable to use electrolytes with excessively high lithium concentration, which allow fast discharge from $LiFePO_4$ composite electrodes but also hinder the fast reaction at the lithium counter electrode.

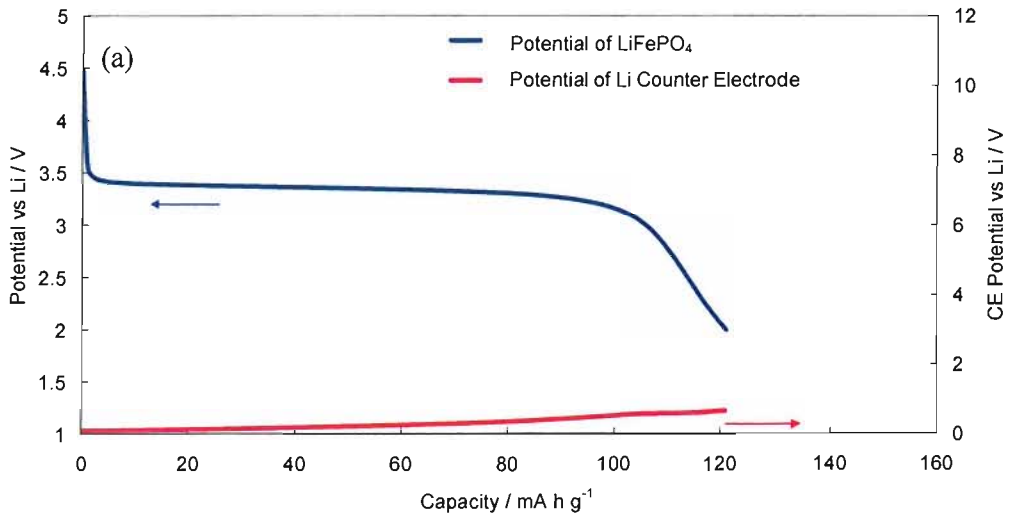

Fig. 5.2 (a) Potential profiles of a 18 μm $LiFePO_4$ electrode and a lithium counter electrode. The electrolyte was 0.47 mol dm^{-3}. The charge rate was 0.25 C and the discharge rate was 2.0 C. The potentials were measured by the 3 electrode method.

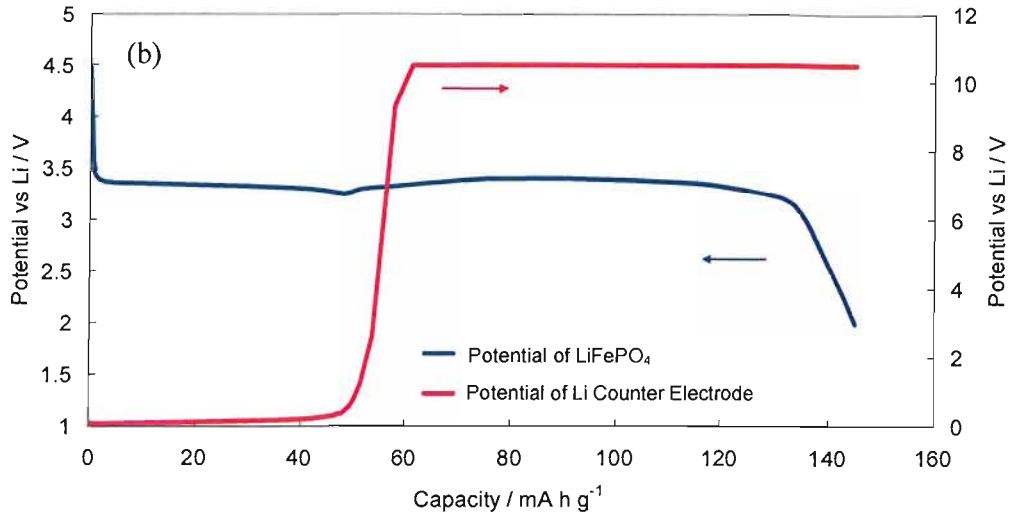

Fig. 5.2 (b) Potential profiles of a 18 μm $LiFePO_4$ electrode and a lithium counter electrode. The electrolyte was 1.5 mol dm^{-3} LiTFSI / EMITFSI. The charge rate was 0.25 C and the discharge rate was 2.0 C. The potentials were measured by the 3 electrode method.

5.3.3. Cycle life of lithium batteries containing the ionic liquid electrolyte

A lithium cell composed of a 10 μm $LiFePO_4$ composite electrode, a 0.47 mol dm^{-3} LiTFSI /EMITFSI electrolyte and a lithium metal electrode showed reasonable discharge capacities over 700 cycles at 0.5 C. For initial 50 cycles (ca 6 days), discharge capacities show 30 % increase, suggesting that ionic liquid electrolyte gradually penetrates into the pores of composite electrodes for days after the assembly of the cell. A similar trend can be seen with $LiPF_6$ / EC : DMC when $LiFePO_4$ is applied to the active material but not significant as the case of the ionic liquid.

Unlike the case of $LiFePO_4$, the capacity of $LiCoO_2$ faded quickly even at a slow rate, 0.1 C. The result was not expected because some reports for reversible lithium insertion into $LiCoO_2$ [1][2] in the ionic liquid have been published. With the $LiCoO_2$, the same configuration cell with an electrolyte of $LiPF_6$ / EC:DMC was assembled and showed a capacity of 140 mAh g^{-1} retained for more than 30 cycles.

Therefore, at least it was shown that the lithium insertion in the ionic liquid electrolyte is more reversible with the $LiFePO_4$ than the $LiCoO_2$ used in the experiment. Properties such as the surface characteristics of the $LiCoO_2$ used here may be different from that used in literature; accordingly, a poor retention of capacity may have been due to oxidation of the electrolyte. Also, it has been reported that aluminium corrodes in solutions of TFSI salts at high potentials [3]. The electrolyte decomposition and the corrosion of the current collector were prevented in the presence PF_6^-, suggesting that cycling of high voltage positive electrodes such as $LiCoO_2$ depend on protection behaviour of anions. It may be suggested that PF_6^- is required for SEI formation, and that $TFSI^-$ in the presence of EMI^+ results in a non-conductive passivation layer.

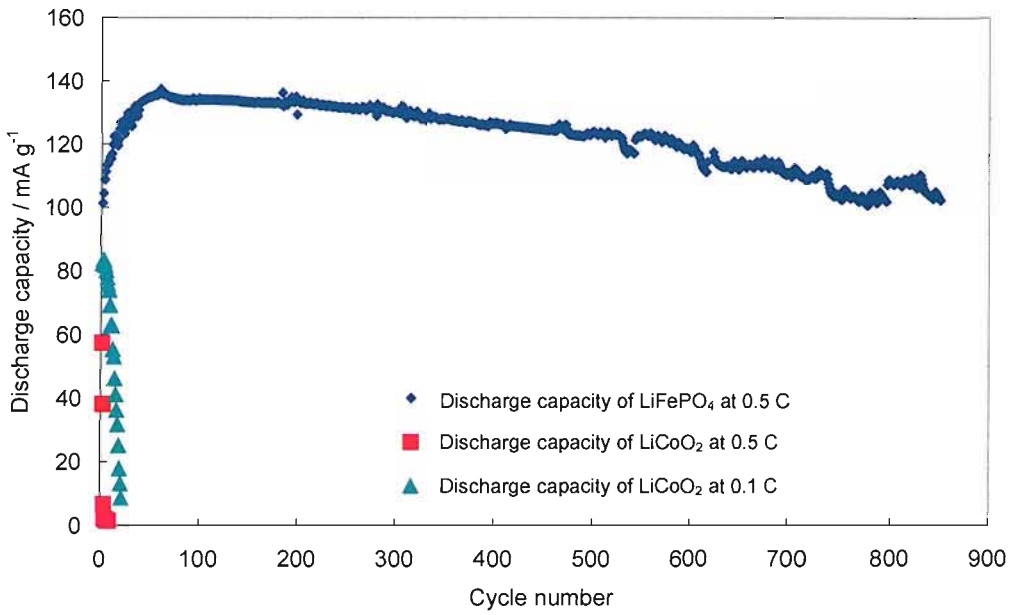

Fig. 5.3 Discharge capacities of a 10 μm $LiFePO_4$ electrode and a 10 μm $LiCoO_2$ electrode. The electrolyte was a 0.47 mol dm^{-3} LiTFSI / EMITFSI. Both charge and discharge rate were 0.5 C. Capacity profiles for $LiCoO_2$ were also shown at 0.1 C.

5.3.4. Lithium batteries with a polymer electrolyte plasticised by EMITFSI

The potential profiles of a battery composed of a 6 μm electrode, 0.47 mol dm^{-3} and a lithium counter electrode at various discharge rates were shown in Fig. 5.4. Plateaus are stable and almost a full capacity was obtained from $LiFePO_4$ composite electrode at a lower rate than 1.0 C. However, unlike the case of the cells containing the electrolyte without polymer as in Chapter 4, the profiles show significant IR drop at the start of discharge. The discharge capacity is affected by lithium ion diffusion but also the IR drop.

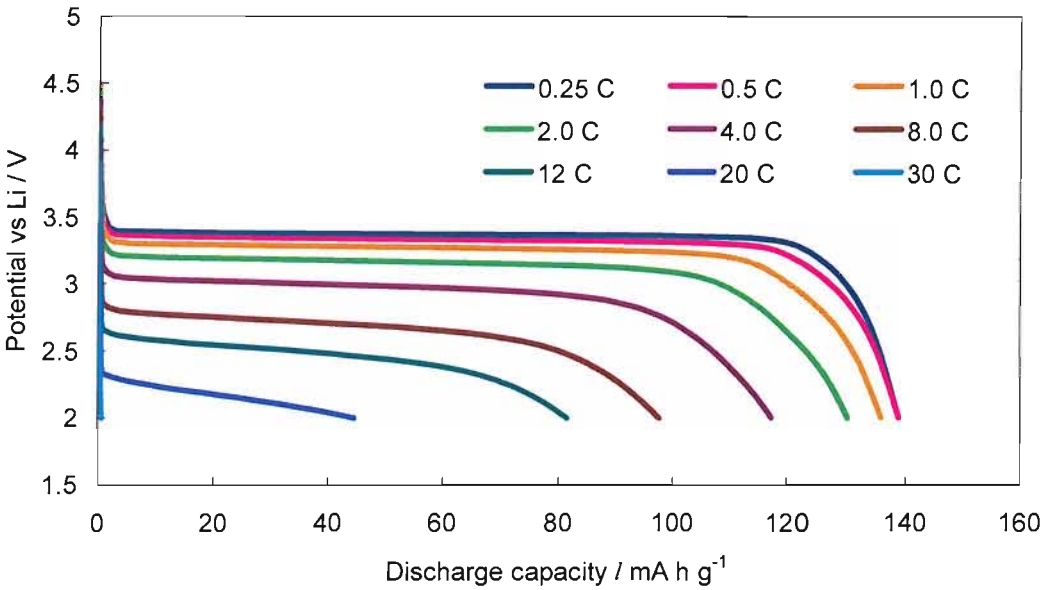

Fig. 5.4 Discharge potential profiles of a cell comprised of a 6 μm $LiFePO_4$ electrode, 0.47 mol dm^{-3} LiTFSI / EMITFSI + 20 wt% PVdF-HFP and a lithium counter electrode. The charge rate was 0.25 C and the discharge rates were varied. The potentials were measured the common counter / reference electrode.

To explain the resistive factor, an impedance measurement was implemented for the cell with the ionic liquid electrolyte and the polymer electrolyte as shown in Fig. 5.5. The extrapolation into the highest frequency shows the resistance of the liquid and polymer

electrolyte, showing a few times difference Fig. 5.5 (a). This corresponds to the results for bulk electrolyte measurements with stainless steel blocking electrodes. However, the contribution of this resistance to the IR drop is only 30 mV at 12 C. The significant IR drop is attributed to the interfacial resistance shown at slow rates Fig. 5.5 (b). Therefore, in the case of the polymer electrolyte, it was suggested that the capacity at high rates is limited by lithium ion transfer between the electrolyte and $LiFePO_4$ composite electrode or lithium metal electrode.

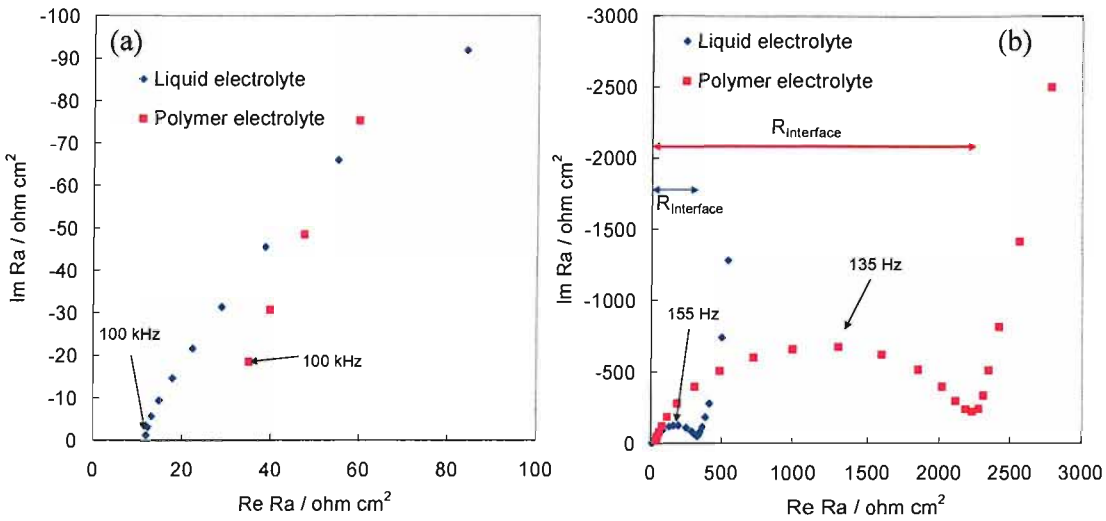

Fig. 5.5 Impedance spectra of a cell comprised of a 6 μm $LiFePO_4$ electrode, 0.47 mol dm^{-3} LiTFSI / EMITFSI or this + 20 wt% PVdF-HFP and a lithium counter electrode.

The dependence of discharge capacity of the $LiFePO_4$ electrode with the polymer electrolyte on charge / discharge rates shows a sharpe drop at high rates, due to the IR drop as described above. Therefore, no difference was observed between the dependence on charge rates and discharge rates.

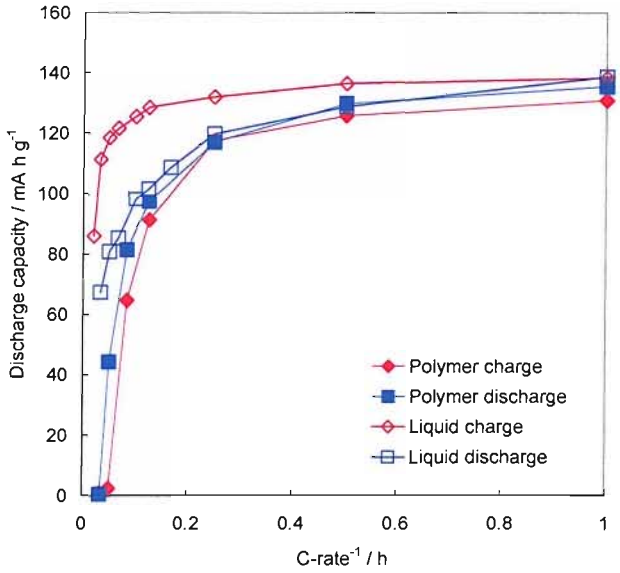

Fig. 5.6 Discharge capacities of a cell comprised of a 6 μm $LiFePO_4$ electrode, 0.47 mol dm^{-3} LiTFSI / EMITFSI or this + 20 wt% PVdF-HFP and a lithium counter electrode.

5.4. Conclusion of the chapter

The LiTFSI / EMITFSI electrolyte did not take the fire but resisted and reflected the flame; on the other hand, $LiPF_6$ / EC : DMC ignited easily.

It was shown that the passivation at lithium counter electrodes was enhanced by high concentrations of lithium ions in an ionic liquid electrolyte. The problem of accumulation is more serious for the plane electrodes than composite electrodes; whereas the problem of lithium ion depletion was significant for composite electrodes. Therefore, we must consider the behaviour of the counter electrode to optimise the concentration of lithium salt in the ionic liquid electrolyte.

A lithium cell composed of a $LiFePO_4$ electrode, a LiTFSI /EMITFSI electrolyte and a lithium metal electrode showed reasonable discharge capacities over 700 cycles at 0.5 C. The capacity of a $LiCoO_2$ electrode degraded quickly, suggesting a lack of a Solid Electrolyte Interface on the high potential cathode in the ionic liquid electrolyte.

The potential profiles of a battery composed of a polymer electrolyte plasticised by EMITFSI showed almost a full capacity of $LiFePO_4$ at a lower rate than 1.0 C. At high rates, the capacity appeared as limited by lithium ion transfer at the interface between the polymer electrolyte and $LiFePO_4$ composite electrode or lithium metal electrode.

Reference

1. S. Seki, Y. Kobayashi, H. Miyashiro, Y. Ohno, A. Usami, Y. Mita, N. Kihara, M. Watanabe and N. Terada, *J. Phys. Chem. B*, **110**, 10228 (2006).

2. M. Holzapfel, C. Jost, A. Prodi-Schwab, F. Krumeich, A. Wursig, H. Buqa and P. Novak, *Carbon*, **43**, 1488 (2005)

3. K. Xu, *Chem. Rev.*, **104**, 4303 (2004)

Conclusion of the thesis

As the fire accidents due to lithium batteries have been a serious concern for users and makers, non-flammable ionic liquids have aroused an interest as alternative electrolytes. EMITFSI (1-Ethyl-3-methylimidazolium bis-(trifluoromethylsulfonyl) -imide) was chosen among the ionic liquids for this study.

The ionic liquid was synthesised and purified until Br < 40 wtppm, H_2O < 2 ppm. Effects of water on the cathodic stability limit were studied using a platinum microdisc electrode and a gold microdisc electrode array. The current was found to increase exponentially with increasing overpotential according to a Tafel slope of 93 mV per decade. For current densities below 10 mA cm^{-2}, the current density was found to increase exponentially with the square root of the water concentration, suggesting catalytic decomposition of EMI^+ with moisture. However, at higher currents, corresponding to overpotentials and high water contents, the decomposition current increased linearly with water concentration as expected from direct, diffusion limited, reduction of water.

The cathodic potential limit shifted negative with addition of lithium salt; especially on a nickel microelectrode, so that deposition and stripping current for lithium was observed. This is attributed to the formation of a solid electrolyte interface (SEI). On a lithium metal electrode, evidence for the formation of a SEI is also found from cyclic voltammograms, impedance spectra and open circuit potentials. Preliminary results show that tin can be used as a lithium insertion electrode in LiTFSI / EMITFSI.

The conductivity was found to decrease with an increase in lithium salt concentration but is still relatively high for a non-aqueous electrolytes, e.g. 5.6 mS s^{-1} for 0.47 mol dm^{-3} LiTFSI / EMITFSI at 298 K. The diffusion coefficient obtained for the same electrolyte was 1.2 x 10^{-7} cm^2 s^{-1} by the restricted diffusion method and 1.4 x 10^{-7} cm^2 s^{-1} by the microelectrode technique. Even though conductivities are several times

smaller than those of $LiBF_4$ / $EMIBF_4$, the diffusion coefficients of lithium ions in both ionic liquid systems were essentially the same. It was found that the coefficients in the ionic liquids are ca. 100 times smaller than the value for 1 mol dm^{-3} $LiPF_6$ / EC:DMC, 1.2×10^{-5} cm^2 s^{-1}.

The transference numbers for lithium ions in LiTFSI / EMITFSI were found to be proportional to the concentration of the lithium salt and show small dependence on temperature. As compared to the transference number of $LiBF_4$ / $EMIBF_4$, the numbers of LiTFSI / EMITFSI are higher at the same concentrations of lithium salt and the same temperatures. This may be explained with two factors; the differences in size and dissociation level of anions.

The charge / discharge rate performance of $LiFePO_4$ carbon composite electrodes with various thicknesses in different concentrations of LiTFSI / EMITFSI electrolytes was studied using 3 electrode systems. At fast charge or discharge rates, discharge capacities were almost inversely proportional to C-rate, suggesting that the capacities were simply controlled by lithium ion diffusion in the pores of the composite electrode. Rate performance of cells is different for charge and discharge and the difference is varied by the concentration of lithium salt in the ionic liquid.

A compact discharge front model was proposed to explain above phenomena and can explain the rate performance partly; however, the presence of lithium salt in the composite electrode gives a deviation from the model.

Preliminary GITT measurements were implemented and the results suggested the redistribution of lithium salt in the separator.

The effects of the accumulation of lithium salt at the lithium metal electrode are significant and lithium salt may be precipitated and passivate the surface of the electrode. More than 100 mAh g^{-1} was retained as discharge capacity for 850 cycles using an optimised cell configuration; a 14 μm $LiFePO_4$ electrode, 0.47 mol dm^{-3} LiTFSI / EMITFSI and lithium electrode.

The potential profiles of a battery composed of a polymer electrolyte plasticised by EMITFSI showed almost a full capacity of $LiFePO_4$ at a lower rate than 1.0 C. At high

rates, the capacity appeared as limited by lithium ion transfer at the interface between the polymer electrolyte and $LiFePO_4$ composite electrode or lithium metal electrode.